Microfibrillated Cellulose and High-value Chemicals from Orange Peel Residues

Eduardo Macedo de Melo

PhD

University of York

Chemistry

November 2018

"We should be able to change the world just as we change matter."

(Anonymous)

DEDICATION

I dedicate this work to my dear mother and father, Tereza and Francisco.

ABSTRACT

Recent studies have applied orange peel waste for the extraction of essential oil and pectin but neglected the cellulosic residues. This thesis presents a sustainable approach for the production of microfibrillated cellulose (MFC) and high-value chemicals from depectinated orange peel residue (DOPR) in the context of a *zero-waste* orange peel biorefinery.

The methodology applied was based on an *acid-free* hydrothermal microwave treatment of DOPR undertaken at several temperatures (120–220 °C). This valorisation approach formed two fractions: a solid fraction, giving MFC, and a hydrolysate, which was potentially rich in pectin and other molecules. To evaluate the green and sustainable credentials of the process, energy efficiency calculations, E-factor and green star metrics were carried out.

MFC was successfully characterised as a nanostructured material with properties highly dependent on the treatment temperature. MFC produced at 120 °C presented excellent hydrogel formation and improved rheological performance against conventional food rheology modifiers. The hydrolysate produced residual pectin, lignin microparticles, sugars, soluble organic acids and furans. The process greenness assessment showed that microwave can be up to 50% more economic than conventional heating, and solvent use in MFC work-up has major role in the environmental impact of the process.

In conclusion, the presented valorisation of orange peel cellulosic residues confirmed its potential as a valuable bioresource for the production of bio-based materials with tunable properties and numerous potential applications, as well as other high-value chemicals which can be further explored.

LIST OF CONTENTS

LIST OF FIGURES

LIST OF TABLES

ACKNOWLEDGEMENTS

First and foremost, I'd like to thank my two supervisors, Dr. Avtar Matharu and Prof. James Clark for the fruitful guidance, patience and support that they gave me throughout my PhD training.

A special thanks go to the Brazilian National Council for Scientific and Technological Development (CNPq) for funding my PhD through the Science without Borders Program.

I would also like to thank Dr. Hannah Briers, Dr. Thomas Dugmore, Dr. Julen Bustamante, Dr. Joseph Houghton and Dr. Javier Remón for the introduction to the orange peel exploitation company (OPEC) and their help during my time in that project. Also, my thanks to all green chemistry fellows and technicians for promoting a pleasant working atmosphere. Special thanks go to these folks: Allyn, Andy, Roxana, Long, Tom Attard, Hao, Yang, James Shannon and Jenny.

I'd like to acknowledge the helpful support I received during my research from these amazing staff members that brought many contributions to my work thanks to their expertise: Meg Stark, Joanne Marrison, Amanda Dixon, Heather Fish, Karl Heaton and Maria Garcia Gallarreta.

Finally, I'd like to thank my family, which has always supported me even from afar and to my beloved partner Ross Agar, which has been my best friend and has given an amazing support to me for the last two years. Also, a big thanks to my dear friends Douglas, Allan, Stephany, Henrique, Emily, Szonja and Barry which were always people I could count with and have always supported me through this journey.

AUTHOR'S DECLARATION

I declare that this thesis is a presentation of original work and except where stated, I am the sole author. This work has not previously been presented for an award at this, or any other, University. All sources are acknowledged as *References*. Selected parts of my work were developed in collaboration with other researchers, which I hereby acknowledge.

Collaboration	Section	Collaborator(s)	Institute
Pilot-scale extraction of pectin for DOPR production	2.1.2	Dr. Thomas Dugmore Dr. Hannah Briers Dr. Rob McElroy Dr. Joseph Houghton Hao Xia	Biorenewables Development Centre, University of York
Conventional Hydrothermal Treatment of DOPR	2.1.7	Dr. Gang Luo Nan Zhou Hao Xia	Fudan University, China
Electron microscopy	2.2.6 2.2.7	Meg Stark	University of York
Confocal microscopy	2.2.8	Joanne Marrison	University of York
CHN Analysis	2.2.9	Dr. Graeme McAllister	University of York
HPLC Analysis	2.2.11	Dr. Hannah Briers	University of York
ICP-IOS	2.2.12	Lancrop Laboratories	York, UK
GPC Analysis	2.2.15	Dr. Kontturi Eero	University of Aalto, Finland
Rheology Analysis	2.2.16	Dr. Vincenzo di Bari	University of Nottingham

LIST OF PUBLICATIONS

Original publications resulted from this work are listed as follows:

1 A. S. Matharu, E. M. de Melo and J. A. Houghton, Opportunity for high value-added chemicals from food supply chain wastes, *Bioresour. Technol.*, 2016, **215**, 123–130.

2 E. M. de Melo, J. H. Clark and A. S. Matharu, The Hy-MASS concept: hydrothermal microwave assisted selective scissoring of cellulose for in situ production of (meso)porous nanocellulose fibrils and crystals, *Green Chem.*, 2017, **19**, 3408–3417.

3 M.-J. Chen, X.-Q. Zhang, A. Matharu, E. Melo, R.-M. Li, C.-F. Liu and Q.-S. Shi, Monitoring the Crystalline Structure of Sugar Cane Bagasse in Aqueous Ionic Liquids, *ACS Sustain. Chem. Eng.*, 2017, **5**, 7278–7283.

4 A. S. Matharu, E. M. de Melo and J. A. Houghton, Green Chemistry: Opportunities, waste and food supply chains, in *Routledge Handbook of the Resource Nexus*, eds. R. Bleischwitz, H. Hoff, C. Spataru, E. van der Voet and S. D. VanDeveer, Routledge, 2017, pp. 457–467.

5 A. S. Matharu, E. M. de Melo and J. A. Houghton, Food Supply Chain Waste: A Functional Periodic Table of Biobased Resources, in *Waste biorefinery: potential and perspectives*, eds. T. Bhaskar, A. Pandey, S. V. Mohan, D. J. Lee and S. K. Khanal, Elsevier, 1st edn., 2018, pp. 219–233.

6 A. S. Matharu, E. M. de Melo, J. Remón, S. Wang, A. Abdulina and E. Kontturi, Processing of Citrus Nanostructured Cellulose: A Rigorous Design-of-Experiment Study of the Hydrothermal Microwave-

Assisted Selective Scissoring Process, *ChemSusChem*, 2018, **11**, 1344–1353.

7 V. Andritsou, E. M. de Melo, E. Tsouko, D. Ladakis, S. Maragkoudaki, A. A. Koutinas and A. S. Matharu, Synthesis and Characterization of Bacterial Cellulose from Citrus-Based Sustainable Resources, *ACS Omega*, 2018, **3**, 10365–10373.

8 Y. Luo, J. Fan, V. L. Budarin, C. Hu, J. H. Clark, A. Matharu and E. M. de Melo, Toward a Zero-Waste Biorefinery: Confocal Microscopy as a Tool for the Analysis of Lignocellulosic Biomass, *ACS Sustain. Chem. Eng.*, 2018, **6**, 13185–13191.

9 A. Grudniewska, E. M. de Melo, A. Chan, R. Gniłka, F. Boratyński and A. S. Matharu, Enhanced Protein Extraction from Oilseed Cakes Using Glycerol–Choline Chloride Deep Eutectic Solvents: A Biorefinery Approach, *ACS Sustain. Chem. Eng.*, 2018, **6**, 15791–15800.

LIST OF ORAL PRESENTATIONS

1. *Porous nanocellulose from citrus peel: Production and characterisation*. Graduate Research Seminar — Dept. of Chemistry, University of York (04/07/2018)
2. *Nanocellulose from citrus peel waste*. Finalist of the 2018 KMS Memorial Prize (for excellence in research) — Dept. of Chemistry, University of York (25/06/2018)
3. *Microfibrillated cellulose from citrus peel waste: A sustainable biorefinery approach*. 3rd International EPNOE Junior Scientists Meeting — Maribor, Slovenia (15/05/2018)
4. *Introducing the Hy-MASS concept: New insights for an orange peel biorefinery*. 3rd EuCheMS Congress on Green and Sustainable Chemistry (EuGSC) — University of York (03/07/2017)
5. *Towards a zero-waste orange peel biorefinery*. XI ABEP-UK Conference 2017 — London (20/06/2017)
6. *Food waste valorisation*. VIII ABEP-UK Conference 2016 — London (14/05/2016)
7. *Food waste valorisation: Drivers and opportunities*. Brazil-UK Newton Fund Workshop — Rio de Janeiro, Brazil (14/04/2016)

THESIS STRUCTURE

This thesis is aimed at, but not limited to, undergraduate students and research fellows in green chemistry, environmental studies and biomass and food waste valorisation research.

This thesis is structured into four chapters:

Chapter 1 includes a general introduction to the thesis presenting the major global drivers, a literature review on the traditional use and new opportunities from orange peel waste, including the use of the cellulosic residues to yield microfibrillated cellulose, green chemistry context, and the thesis aim and objectives.

Chapter 2 reports the materials, methods and instruments used to carry out the experiments reported in this thesis.

Chapter 3 presents results and discussion with an emphasis on the characterisation and application of the extracted biomolecules, namely: microfibrillated cellulose, pectin, lignin and soluble molecules (sugars, organic acids and furans). It also discusses the overall process greenness.

Chapter 4 closes the thesis with conclusions drawn from the obtained results, their limitations, future work, recommendations and final remarks.

Post-textual matter includes *references*, *appendices* and a list of *abbreviations*.

Chapter 1

1 INTRODUCTION

- A. S. Matharu, E. M. de Melo and J. A. Houghton, Opportunity for high value-added chemicals from food supply chain wastes, *Bioresour. Technol.*, 2016, **215**, 123–130.
- A. S. Matharu, E. M. de Melo and J. A. Houghton, Green Chemistry: Opportunities, waste and food supply chains, in *Routledge Handbook of the Resource Nexus*, Routledge, 2017, pp. 457–467.
- A. S. Matharu, E. M. de Melo and J. A. Houghton, Food Supply Chain Waste: A Functional Periodic Table of Biobased Resources, in *Waste biorefinery: potential and perspectives*, 2018, pp. 219–233.

1.1 Global Drivers

1.1.1 Moving from a linear to a circular bioeconomy

We live in a linear economy that takes from planet Earth, makes, uses and abuses, *i.e.* from "cradle-to-grave" [a].[1] The global population is expected to reach over 9 billion by 2050 from 7.5 billion today (2018).[2] Concomitantly, global GDP is expected to increase steadily at 3% per annum (*p.a.*) and material consumption is expected to reach 100 Gt *p.a.* by 2030 (40% increase in relation to 2013).[3] The World Bank reported that 2.2 billion tonnes of solid waste will be generated every year by 2025, which is 70% more than in 2013. This waste predominantly comprises plastics, which are now increasingly making their way into oceans.[4] Currently, about 5 to 12 million tonnes of plastics reach the oceans every year, disturbing the natural environment and causing the death of many types of marine and birds species.[4,5] Our current linear economy is based on crude oil, which is the cornerstone of our chemical, material and energy needs.

Despite the oil price has been forecasted to increase by 3.7% annually up to 2024,[6] global oil consumption is not decreasing. In fact, by 2040 113 million barrels/day are expected be consumed (18% more than 2015), mainly due to increasing demands from fast-growing economies like China and India.[7] The industrial sector contributes to 36% of total oil consumption and a considerable share of that will serve as feedstock for producing chemicals and materials in addition to energy and heat.[7] In fact, 96% of all manufactured organic compounds are derived from fossil fuels.[8]

[a] *Cradle-to-grave* is an expression used in life-cycle analysis of materials denoting a linear economy approach: from extraction of resources (cradle) to use and disposal (grave).

However, petroleum and other fossil fuels are finite resources. There are only *ca.* 50 years left of known reserves of oil and gas, and 114 years of coal.[9,10] Additionally, in order to prevent the global temperature from rising above the 1.5 °C target set by the UN in 2015,[11] 80% of coal, 50% of gas and 33% of oil reserves must remain untouched (known as *unburnable carbon*).[12,13] In 2018, the International Panel on Climate Change (IPCC) reaffirmed the crucial task of limiting global warming to 1.5 °C in the next 12 years in order to prevent any further environmental and social catastrophes (*e.g.* floods, droughts, ice sheet melting, sea-level rise, poverty and hunger) related to climate change.[14] According to CICERO (Centre for International Climate Research), at our current CO_2 emission rates, by 2021, the 1.5 °C temperature rise limit will be exceeded.[15] Controversially, if policy makers keep investing in unburnable carbon, this could lead to an economic loss of up to US$ 6.74 trillion (almost 3 times the UK's GDP of 2017) otherwise known as "stranded assets".[13]

In this context, as a "global nation", we need to move away from oil-based economies associated with climate change and adopt circular bioeconomies,[b] based on biomass, both terrestrial and marine, to produce chemicals, materials and, to some extent, energy. Developing a circular bioeconomy based on biomass, particularly in waste biomass, has been strongly encouraged by specialists because biomass is renewable, biodegradable and an abundant resource with several socioeconomic and environmental advantages.[16] For instance, the recycle timescale (renewability) of agricultural/food waste biomass

[b] According to Nova Institute[31], circular bioeconomy can be defined as an intersection between circular economy (efficient use of resources to reduce waste generation) and bioeconomy (replacement of fossil carbon by renewable carbon from biomass).

(3–12 months) is up to 80 times better than wood biomass (25–80 years) and 280 million times that of oil, gas and coal (more than 280 million years).[17]

1.1.2 Sustainable development goals

In 2015, the United Nations Sustainable Development Summit launched 17 Sustainable Development Goals (SDG, see **Figure 1.1**) as part of the resolution *''Transforming our world: the 2030 Agenda for Sustainable Development"*,[c] aimed at protecting people and, the planet, stimulating global prosperity and peace, and developing global partnerships.[18]

Figure 1.1: The 17 Sustainable Development Goals to be addressed by 2030 (Ref. 18). SDG in green are directly related to the scope of this thesis. Original in colour.

The scope of this thesis directly impacts the following SDG:

> ***SDG 2: End hunger, achieve food security and improved nutrition and promote sustainable agriculture***
>
> *Target 2.3. By 2030, double the agricultural productivity and* ***incomes of small-scale food producers****, in particular women, indigenous peoples,*

[c] This resolution (A/RES/70/1), and in special SDG 13 — Climate Action, was adopted by the *Paris Agreement*[11] where 195 nations agreed to mitigate climate change and hold the increase in the global average temperature to below 2 °C by 2020.

family farmers, pastoralists and fishers, including through secure and equal access to land, ***other productive resources and inputs****, knowledge, financial services,* ***markets and opportunities for value addition*** *and non-farm employment.*

Impact: By using food supply chain (FSC) waste as resource, value from waste is automatically created, benefiting small producers and local economy.

SDG 6: Ensure availability and sustainable management of water and sanitation for all

Target 6.3. By 2030, improve water quality by ***reducing pollution, eliminating dumping and minimizing release of hazardous chemicals and materials****, halving the proportion of untreated wastewater and substantially increasing recycling and safe reuse globally.*

Impact: Valorisation of food waste diverts it from being landfilled, burned or dumped in water streams which could lead to the release of phytotoxic chemicals like oils present in the fruit peels.

SDG 12: Ensure sustainable consumption and production patterns

*Target 12.3. By 2030****, halve per capita global food waste*** *at the retail and consumer levels and reduce food losses along production and supply chains, including post-harvest losses.*

Target 12.4. By 2020, ***achieve the environmentally sound management of chemicals and all wastes*** *throughout their life cycle, in accordance with agreed international frameworks, and* ***significantly reduce their release to air, water and soil*** *in order to minimize their adverse impacts on human health and the environment.*

Target 12.5. By 2030, ***substantially reduce waste generation*** *through prevention, reduction, recycling and reuse.*

Impact: Transforming unavoidable food waste into a resource, reduces waste generation and environmental burden. Valorisation of food

waste is also interlinked with the principles of green chemistry, which advocates for the non-generation of waste in all chemical processes.

SDG 13: Take urgent action to combat climate change and its impacts

Target 13.3. Improve education, ***awareness-raising and human and institutional capacity on climate change mitigation****, adaptation, impact reduction and early warning*

Impact: Global food waste has a great impact on climate change, where emission of greenhouse gases (GHG) reached 3.3 billion tonnes of CO_2 equivalents in 2007.[19] Incorporating this waste into the bioeconomy circular chain will certainly mitigate its impact on the climate change.

1.1.3 Food waste as a bioresource

We live in controversial times, especially regarding food production, supply and consumption. Today, close to 1 billion people are chronically undernourished,[20] whilst 1.2 billion have no access to clean drinking water.[21] Yet, according to the Food and Agriculture Organization (FAO), 1.6 billion tonnes of food (1/3 of all food produced in the world) is wasted every year, corresponding to an economic loss of *ca.* US$ 1 trillion.[22] In the UK alone, 15 million tonnes of food is wasted every year, equating to an economic loss of £11.8 billion.[23] **Figure 1.2** illustrates typical food losses at different phases of the FSC.

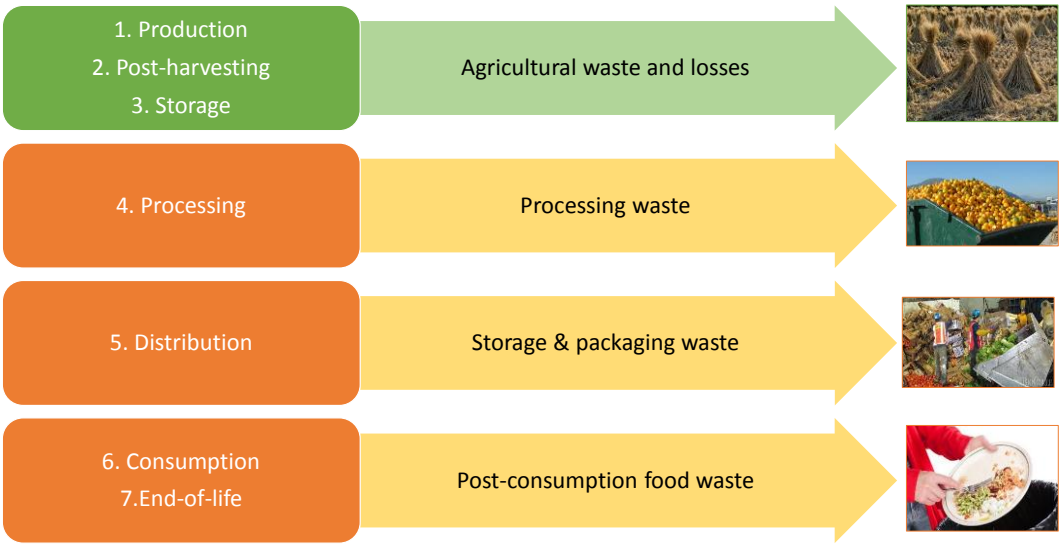

Figure 1.2: The different phases of the food supply chain and their respective waste (Ref. 19). The first 3 phases compose the upstream waste and phases 4 to 7 compose downstream waste. Original in colour.

Although developed and developing regions produce almost the same volume of food waste (630 and 670 million tonnes, respectively), its origin within the FSC varies significantly.[19] As shown in **Figure 1.3**, low-income developing regions produce more upstream waste, especially at postharvest and storage, due to poor infrastructure, limited technology and climate conditions fit for food spoilage. In developed regions, downstream food waste is higher, especially at the consumer level. This is caused by restrictive regulations on food quality standards, miscommunication between producers, retailers and consumers, marketing and consumer behaviour.[19]

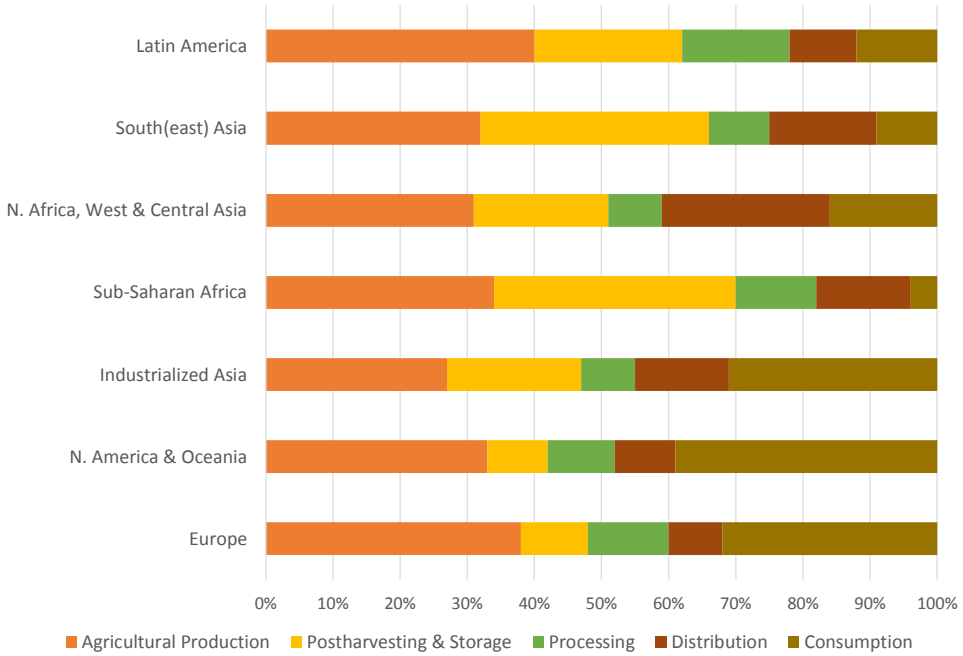

Figure 1.3: Distribution of food waste by region and by phase of the supply chain (adapted from ref. 19). Original in colour.

Food loss seriously compromises our global food security, natural resources, environment and economy. Therefore, addressing the food waste problem and improving FSC efficiency should follow a strategic approach led by priorities, as suggested by FAO[19] and other authoritative literature.[16,24,25]

Firstly, as shown in **Figure 1.4**, prevention and reduction of food waste and losses across the FSC should be prioritised. Secondly, in view of the food scarcity present in many countries, redistribution of food suitable for consumption should be encouraged. For instance, a recent study identified 15 potential edible food recovery points across the FSC, which could feed millions of people.[26] Thirdly, the recovery and recycling of food waste should be sought, but here, special attention should be given to *unavoidable food supply chain waste* (UFSCW). The last and least wanted approach to food waste is, for obvious reasons, irrational disposal or landfill.

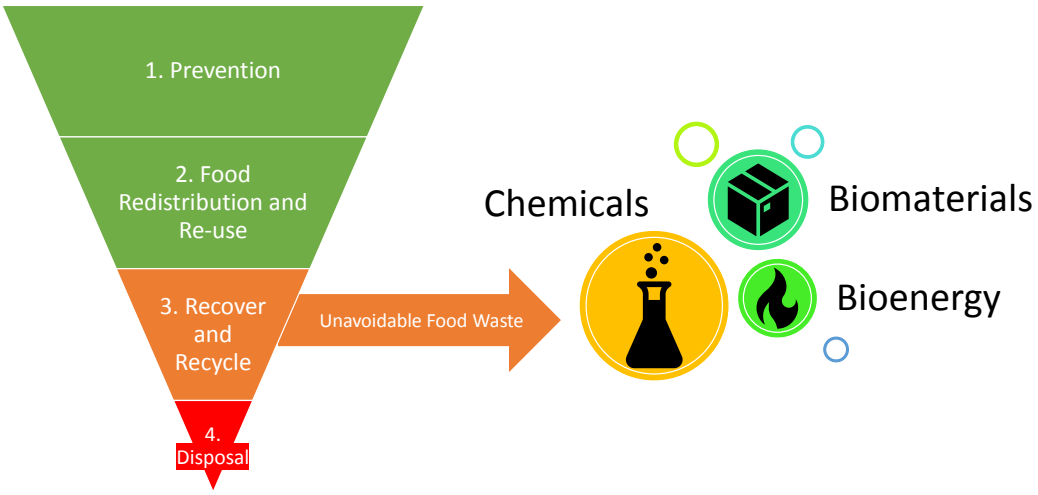

Figure 1.4: A strategic approach towards food waste (sourced from ref. 16). Original in colour.

UFSCW is a high-volume fraction of food waste, usually inedible, resulting from the post-harvesting and processing phases of the FSC. This category includes agroindustrial by-products such as straws, husks, peels, seeds, pulps and bagasse.[16] Currently, UFSCW is used in animal feed, composting or biogas generation (anaerobic digestion). Otherwise, this type of waste is burned or dumped in waterways or landfill, negatively impacting the environment.[16,27,28] The problem with the above "sensible approaches" (animal feed, anaerobic digestion and composting) is that they overlook the potential of UFSCW as a bioresource. Indeed, UFSCW can be considered as the "periodic table of fit for purpose biobased chemicals",[16] bearing an unique profile of extractable functionalised biomolecules, such as fibres, fats and oils, enzymes, flavours and aromas, pigments, proteins, polysaccharides and antioxidants.[16,25,27] Moreover, UFSCW does not compete with food or natural forests. This unique source of functionalized chemicals actually requires less energy to be upgraded to high-value chemicals and materials when compared to crude oil, because it already contains heteroatom functionality (*e.g.* N, O, S), making it a valuable renewable

feedstock for biorefineries,[d] as seen in **Figure 1.5**. A highly developed biorefinery should primarily focus on the production of chemicals and materials from biomass, since energy can be (and has been) efficiently produced by other renewable resources.[7] Nevertheless, the use of biomass for chemicals and materials still have some challenges to be overcome, such as turning pre-treatment (drying, neutralisation, etc) economically viable, creating processes that are insensitive to inherent biomass heterogeneity and finding efficient separation methods for complex mixtures.

In a biorefinery context, by retaining the biomass' inherent chemical complexity and convertibility to high-tonnage output,[29] UFSCW can be an economically viable and greener alternative to oil-based chemicals and materials. For example, Scott *et al.*[30] reported that using a bio-derived amino acid such as serine, instead of the oil-based ethylene in the synthesis of 1,2-ethanediamine can save up to 41.5 GJ/tonne of the total process energy. Vandamme *et al.*[24] reported an extensive list

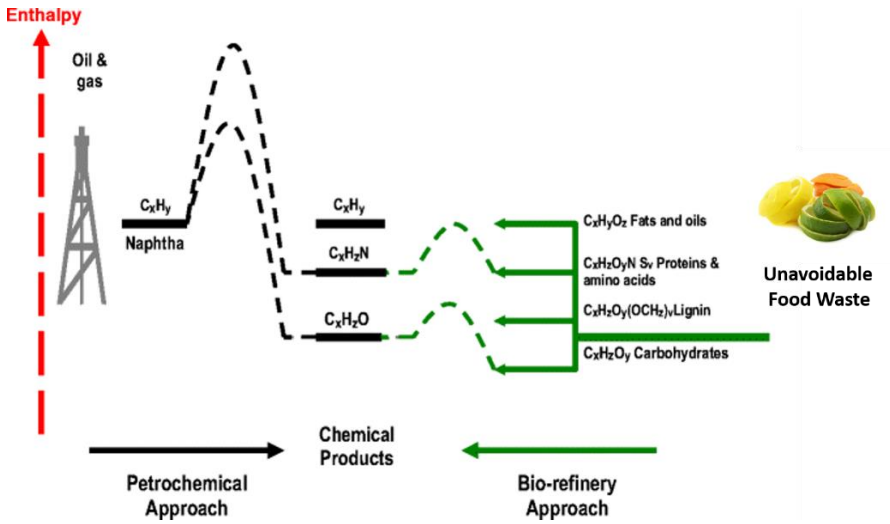

Figure 1.5: Unavoidable food waste can be a more energy-efficient feedstock for platform molecules conversion than fossil fuels (adapted from ref. 30). Original in colour.

[d] The biorefinery concept regards the conversion of low-value bioderived resources (biomass) into a variety of high-value platform molecules, materials and fuels, imitating the oil refinery concept but using renewable resources instead.[25]

of building blocks molecules derived from biomass via biotechnological processes, including small organic acids, alcohols and aminoacids. Some building blocks such as lactic acid, glycerol, butenodiol, succinic acid are important for the synthesis of bioderived polymers which can replace oil-derived plastics.[27] Moreover, most bio-based materials (bioplastics, biofoams, biocomposites) are biodegradable while most oil-based materials are not, and that is an important factor within any circular bioeconomy.[31]

In developing countries, which are usually highly agricultural, high volumes of agricultural waste are burned, contributing to air, water and land pollution.[28] Typically, waste is burned at the source field, primarily because it is not economically feasible to transport it to a processing plant. Such transportation could almost double the cost of production.[32] If all agricultural biomass that is currently burned was instead converted into high-value outputs, it would create economic value equivalent to US$120 billion/year.[32] Thus, the creation of local or *in-situ* biorefineries should be encouraged.

In the EU, 19% of all biomass produced is used for energy purposes and 15% is used for chemical and biomaterials production.[31] Converting more UFSCW to non-energy products will accelerate the development of a circular bioeconomy.[31] The choice of specific waste streams to be used in early-stage biorefineries must take into account both, the volume of waste and the potential value of products. Orange peel waste (OPW) is a good example of a high-volume UFSCW that could supply a potential non-energy biorefinery.

1.2 Opportunities from orange peel waste

The citrus genus is an important fruit cultivar,[33] both for its economic value as fruit and juice, and for its peel waste, which is a source of valuable products.[34] Citrus represents an important commodity for major emerging economies like Brazil, India and China, which are the top three global producers, respectively.[35] In 2016, the global market value of citrus fruits was *ca.* US$ 6 billion,[36] equating to more than 124 million tonnes. By volume, sweet oranges (*Citrus* × *sinensis*) are the most dominant (67 million tonnes), corresponding to *ca.* 54% of total production (**Table 1.1**).[35] Approximately, 20–30% of all citrus and 30–40% of oranges go into the juice processing industry.[35,37]

Table 1.1: 2015 and 2016 volumes of citrus production and processing (FAO, 2017).

Type	Year	
	2015 (Mt)	2016 (Mt)
World citrus production	**131.0**	**124.3**
Oranges	68.6	67.0
Mandarins/Tangerines	38.3	33.0
Acid citrus	15.5	16.0
Grapefruits	8.5	8.3
Total citrus for processing	**25.0**	**23.6**
Oranges	20.0	18.5
Mandarins/Tangerines	1.8	1.8
Acid citrus	2.4	2.5
Grapefruits	0.8	0.8

Using modern extraction technologies, from 1000 kg of oranges it is possible to produce on average: 553 kg of fresh juice (or 100 kg of concentrate juice and 1.2 kg of essences from the evaporation process), 413 kg of peel, seeds and rags, 30

kg of pulp and 3 kg of essential peel oil.[38] Thus, roughly 50 wt.% of the fruit is under-utilised in the process, including peel, pulp and seeds,[27,39] which accounts for at least 10–15 million tonnes/year of traceable OPW being globally produced.[16] In fact, if all OPW produced worldwide could be tracked these numbers would be much higher.

1.2.1 Conventional uses of orange peel waste

To date, large-scale utilisation of OPW and other citrus wastes has been limited to *low-value* direct uses, *i.e.* animal feed (mainly for ruminants) or energy recovery by bioprocessing, *eg.* anaerobic digestions or fermentation. Animal feed is the most common destination of fresh and dried OPW/citrus waste deriving from large juice processing plants.[38,40–42] However, using the latter in feed is limited to a maximum of 5–30% dry matter (DM) due to its potential toxicity to some species and its potential to decrease the yield of animal products (**Table 1.2**).[43,44] Moreover, several pre-treatments (alkalinisation with CaO, milling, drying and pelletisation) and supplementation are required to render OPW safe, palatable and nutritive for most animals,[44] making its utilisation for animal feed nearly non-profitable.[45]

Table 1.2: Maximum recommended concentration of dried orange peel on animal feed by species. Remarks on risks involved in higher intakes are also presented. Data from Feedpedia (by INRA, CIRAD, AFZ and FAO, 2018).

Animal species	Maximum safe concentration on total daily intake (wt.%, DM)	Remarks on levels above recommended
Dairy cattle	20	Reduces milk production, DM intake, digestibility and can cause milk fever.
Beef cattle	30	Can cause urinary calculi and reduces backfat thickness
Sheep (caprines)	30	Reduces digestibility, performance and can cause rumen parakeratosis
Pigs & sows	5–10	Increases toxicity due to limonin, affects growth rate and requires supplementation (P and vit. D)
Poultry	5–10	Lowers feed efficiency, alters fatty acid ratio on meat, darkens yolk
Rabbits	25–30	Can replace other feeds (*e.g.* alfalfa meal)
Horses & donkeys	28	
Fish	10–25	Might need co-mixing with probiotics

In contrast, some characteristics of OPW,[39] *e.g.*, high water content (*ca.* 80%), high content of fermentable and biodegradable organic matter (>97%), mild acidity (pH ~4), low lignin content (*ca.* 7%) and low protein content (7–9%) make it a suitable substrate for anaerobic digestion and fermentation.[45,46] However, the use of OPW for biogas or bioethanol production is hampered by the presence of residual essential oils in the peel, which are known microbial activity inhibitors.[45,46] Hence, purification of the peel is required to bring limonene levels to below 0.05%, which can be costly.[40]

Thermochemical processing of OPW for energy recovery (incineration, pyrolysis, gasification) is believed to be economically unfeasible because the high-water content of orange peel makes pre-drying very expensive. OPW also has a relatively low calorific value (*ca.* 18–19 MJ/kg).[47,48] Moreover, approaches like incineration are not seen as environmentally-friendly, since they can contribute to climate change and air pollution by generating GHG.[27,45,49] The major advantages and drawbacks of conventional valorisation approaches for OPW are summarised in **Figure 1.6**.

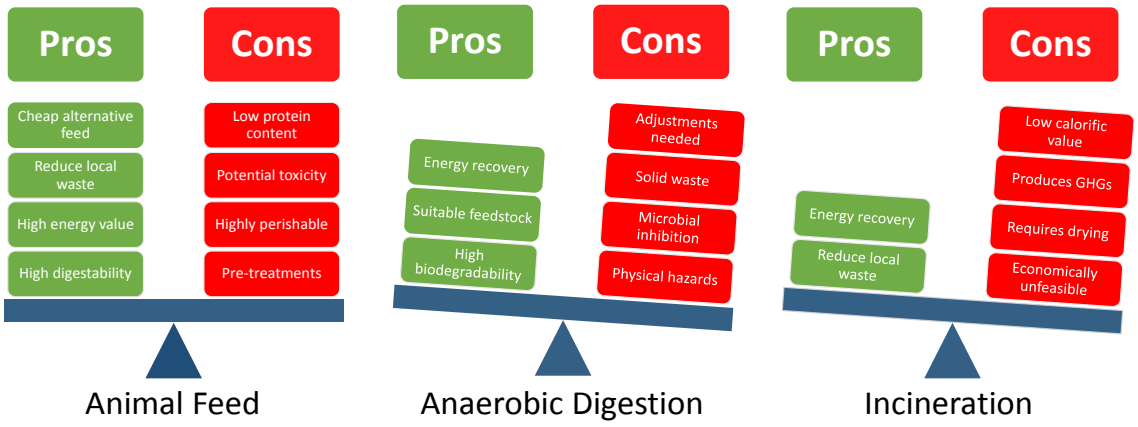

Figure 1.6: Pros and cons of conventional valorisation approaches of orange peel waste (wet basis). Original in colour.

Despite reuse opportunities like animal feed and energy recovery, landfill of smaller volumes of highly biodegradable agroindustrial waste like citrus peel is still legal in some regions. In Europe, for instance, citrus waste is only allowed to landfill after being processed (energy recovery, thermochemical treatment, etc).[45] In a similar way, Brazilian legislation declares that the food supply chain is responsible for the correct and safe disposal of its waste, prioritising recycling and reutilisation.[50] In the USA, citrus waste is not allowed into landfill at all.[49] Although direct disposal of untreated citrus waste can cause severe

environmental pollution and even explosions (due to methane build-up),[39,43,45] correct disposal of treated citrus waste can be beneficial in some cases.

An experimental reforestation project between the Costa Rican government and a local orange juice company successfully demonstrated forest restoration on damaged land and consequential carbon sequestration by using high tonnage of *oil-free* orange peel waste (12,000 tonnes) as a low-cost, natural fertilizer.[51] It is worth mentioning that the authors do stress the importance of carefully considering social, political and environmental implications when using agricultural waste for reforestation to avoid any potential harm to the local environment and community.

1.2.2 Orange peel composition and commercial value

OPW is rich in biomolecules of economic interest (see **Table 1.3**) such as d-limonene, carotenoids, flavonoids, sugars, proteins and lignocellulosic matter (pectin, hemicellulose, cellulose and lignin).[52] Lignocellulosic matter alone makes up to *ca.* 60–65% of OPW total dry matter.[40,44,53,54]

Table 1.3: Average reported composition of orange peel.[40,44,53,54]

Components	Reported Content (%, DM)
Cellulose	22–37
Hemicellulose	5–17
Pectin	14–23
Lignin	1.4–9
Protein	7–9
Sugars (mono/disaccharides)	9.5–24.5
Oil/fats/ether extract	2–4
Flavonoids/Pigments	4.5–11
Ash	2.5–3.7

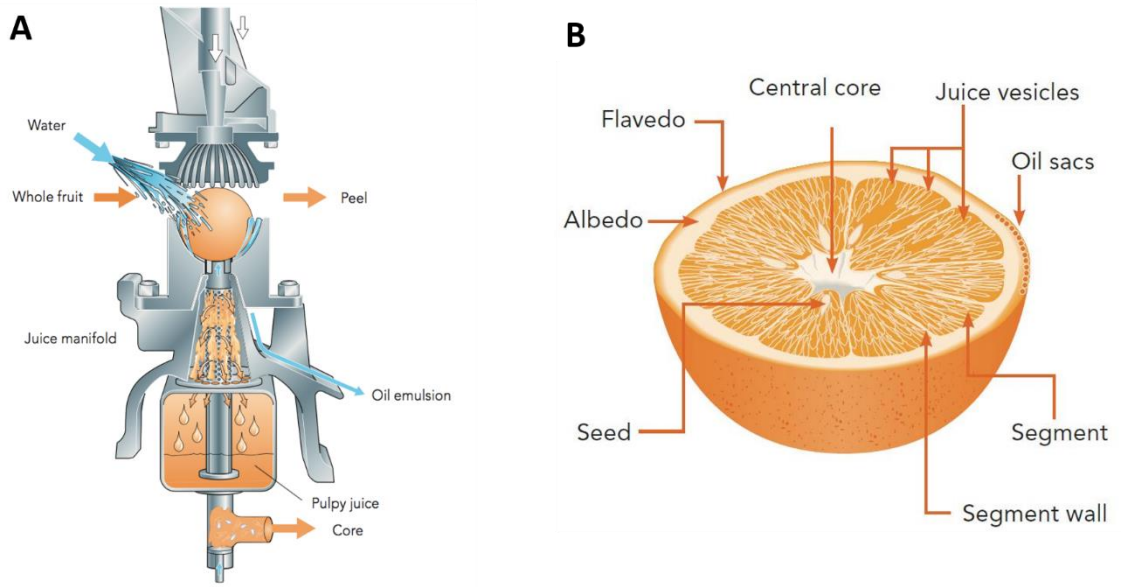

Figure 1.7: A squeezer-type juice extractor (A) where essential oil is co-extracted along with the juice and the anatomy of an orange (B) (adapted from ref. 38). Original in colour.

1.2.2.1 Essential Oil

Orange peel essential oil is a well-established co-product in the juicing industry, being concomitantly extracted with the juice (**Figure 1.7A**) or extracted prior/after juicing (*e.g.* cold press, peel perforation or distillation).[38,41,43,55] Essential oil is present in oil sacs found in the outer layer of the peel (see *flavedo* in **Figure 1.7B**). Essential oil comprises a complex mixture of several volatile compounds and a minor fraction of waxes and phenolics. The volatile fraction is rich in terpenoids, with d-limonene as the major component (>90%).[39,40] As an example, **Figure 1.8** presents the major composition of essential oil extracted from navel oranges.[56] As can be seen, 99.3% of the oil is composed of monoterpenes, of which 97% are d-limonene.[56] Crude orange essential oil or purified d-limonene (extracted from the crude oil or OPW "press liquor") are valuable products for several industrial applications, such as natural flavouring and fragrances, alternative green solvents, antioxidant or antimicrobial agents, bio-pesticides and resins & adhesives.[38,40,43,53] The price of essential oil is increasing due to increased

demand; US$ 5/kg in 2014 to US$ 7/kg in 2015.[57] The price of d-limonene has also been affected by increasing demand (45,000 tonnes in 2015 and 65,000 tonnes by 2023) and market volatility, causing recent sales price to vary between US$ 2–8/kg (2013 reference)[49] or even as high as US$ 14/kg (2015 reference).[58] By 2022, the global market for d-limonene is forecast to yield revenues close to US$ 451.8 million.[40]

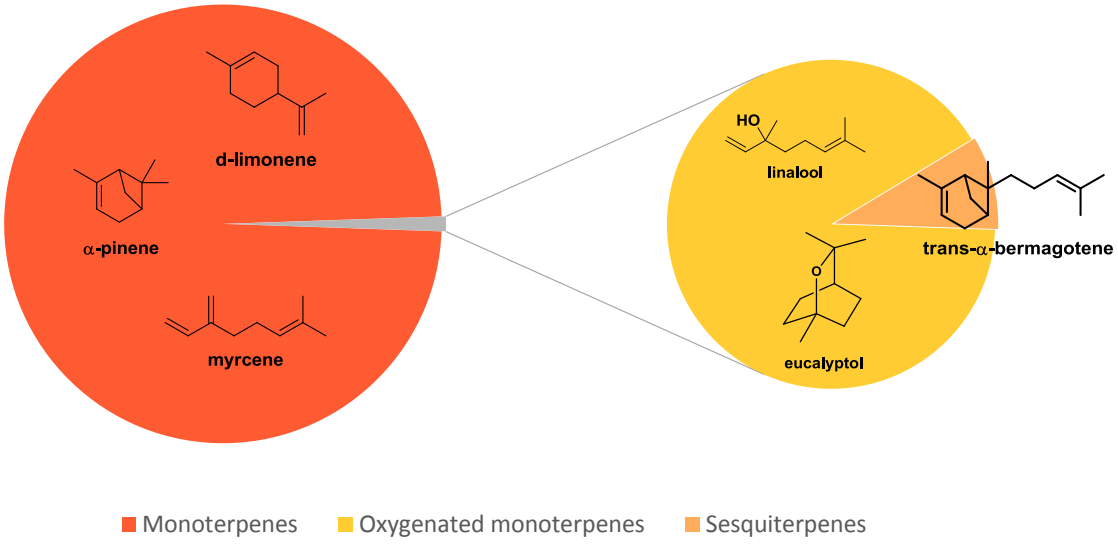

Figure 1.8: Chemical composition of navel oranges essential oil (99.3% monoterpenes, 0.14% oxygenated monoterpenes and 0.01% sesquiterpenes). Original in colour.

1.2.2.2 Pectin

Pectin is a generic term used to describe several complex heteropolysaccharide (co-)polymers present in plant cell wall and middle lamella.[59] Pectin comprises different regions of galacturonic acid as backbone, such as homogalacturonan, xylogalacturonan, rhamnogalacturonan, as well as branched polymers composed of neutral sugars (also known as "hairy regions"),[58] such as galactans and arabinans (**Figure 1.9**).[59] In orange peel, pectin is mainly found in the inner layer (see *albedo* in **Figure 1.7B**). Pectin is probably the most valuable component of orange peel because of its importance in the food industry as a natural thickener, stabiliser of drinks, creams, desserts, yogurts, fillings and as a gelling agent in jellies and jams.[34,40] In the pharmaceutical sector, it is used as chelator, detoxifier and in drug delivery formulations.[39] In 2016, global pectin sales achieved 60,830 tonnes with an approximate price of US$ 18/kg (for all pectin grades), resulting in a remarkable global revenue of over US$ 1 billion.[60]

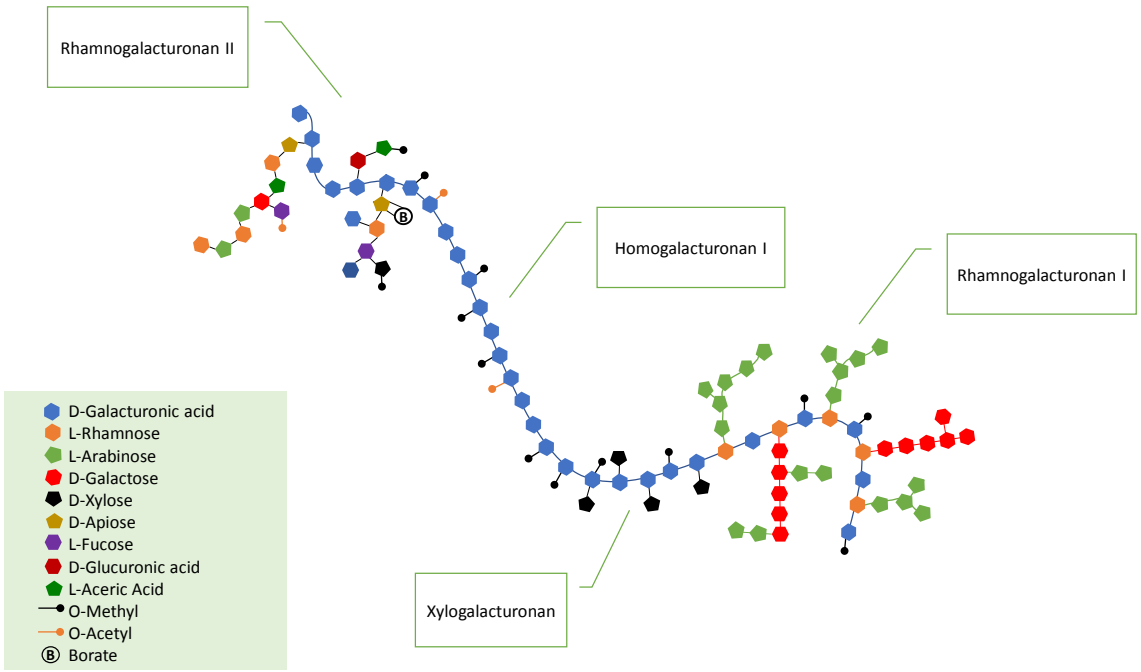

Figure 1.9: Representation of a complex pectin structure comprising different polymeric regions. Adapted from ref. 59. Original in colour.

Pectin is classified by its degree of esterification (DE) into high-methoxyl grade (HM, DE >50%) and low-methoxyl grade (LM, DE <50%).[58,61] HM pectin forms a gel in the presence of sugar (sucrose) at low pH, stabilised by hydrophobic interactions, whereas LM pectin gel formation depends on electrostatic stabilisation, usually involving the presence of divalent cations such as Ca^{2+}. Further de-esterification hydrolysis or amidation of HM pectins using ammonia is sometimes carried out to form an amidated LM pectin, which usually requires less calcium to gel and is less sensitive to precipitation as compared to conventional LM pectins.[58]

At present, industrial pectin production is monopolised by a few manufacturers in Europe (Germany, Denmark, Czech Republic, France and Italy), Mexico, Brazil and China.[58,60,62] Conventional extraction of pectin is carried out by acid hydrolysis of the OPW (pH 1–2, 60–100 °C and 1–4 h), followed by treatment of the resulting hydrolysate with ethanol or isopropanol for precipitation. Subsequent washing, filtration/centrifugation and drying affords pectin as an off-white powder.[41,43] However, acid hydrolysis is a polluting and expensive process partly due to the costs involved in treating the acid waste. Greener alternatives, like enzymatic or microwave extraction are currently been explored.[39,58]

1.2.2.3 Lignocellulosic fibres

Lignocellulosic fibre is insoluble matter derived from dead plant cell walls, where cellulose microfibrils are found embedded in a polymeric matrix of hemicellulose, lignin and other structural compounds like proteins and minerals (**Figure 1.10**).[63–65] Lignocellulose fibre comprises *ca.* 50% of orange peel, as shown in **Table 1.3**. As discussed previously, the commercialisation of citrus/orange peel fibres has mainly been focused on animal feed after essential oil extraction.[38,40,41] However, other products using the crude fibre or the purified cellulose fraction have been explored at lab and industrial scale. For example, physical and chemical pre-treatments of the crude fibre (from both pulp and peel) allows its conversion to useful pollutant biosorbents[66–68], dietary fibres[16] and even food rheology modifiers commercially known as *citrus fibres* (*e.g.* Fiberstar®, Herbacel® and Citritex®).[69–73] Alternatively, citrus peel fibres can be purified to yield a material claimed to be one of the top 10 technologies to change the world by 2025, *i.e.* nanocellulose.[74]

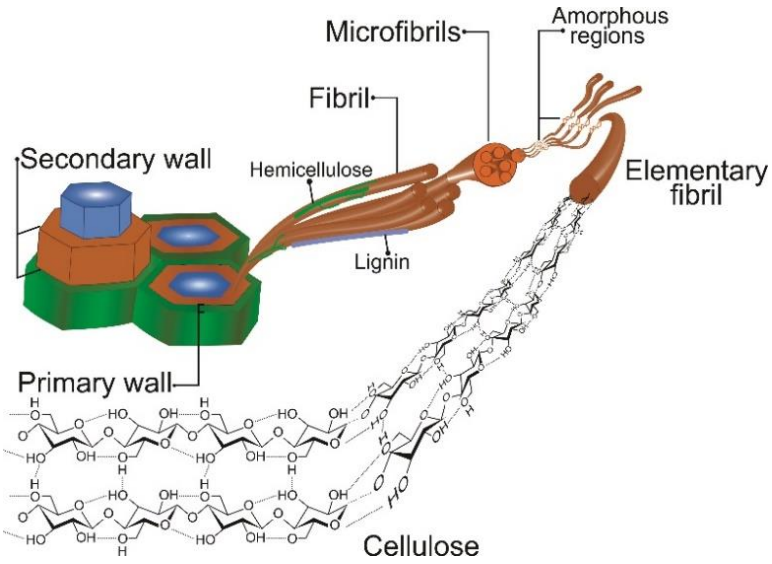

Figure 1.10: Hierarchical structure of lignocellulosic fibres (adapted from ref. 65). Original in colour.

1.2.2.3.1 Cellulose nanomaterials

Nanocellulose is a generic term used to describe two grades of cellulosic nanomaterials; nano-objects, and, nano-structured materials, depending on their morphology (**Figure 1.11**).[75,76] Cellulose nanocrystals (CNC) are conventionally produced by acid hydrolysis from lignocellulosic biomass (usually bleached wood pulp), whilst cellulose nanofibrils (CNF) and microfibrillated cellulose (MFC) are produced by mechanical disintegration of the fibres by means of high-pressure homogenisers, microfluidisers and micro-grinders.[77,78] A typical MFC/CNF manufacturing process is summarised in **Figure 1.12**.

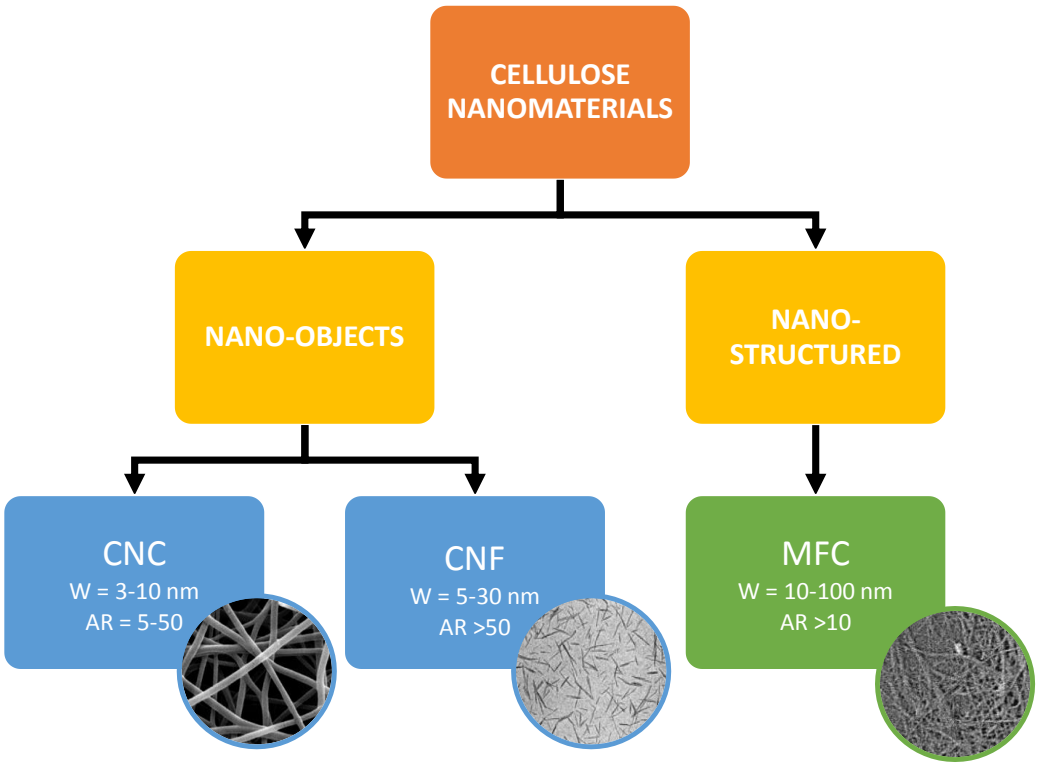

Figure 1.11: Suggested classification for cellulose nanomaterials from proposed TAPPI standard WI3021 (ref. 76). W = width, AR = aspect ratio. Original in colour.

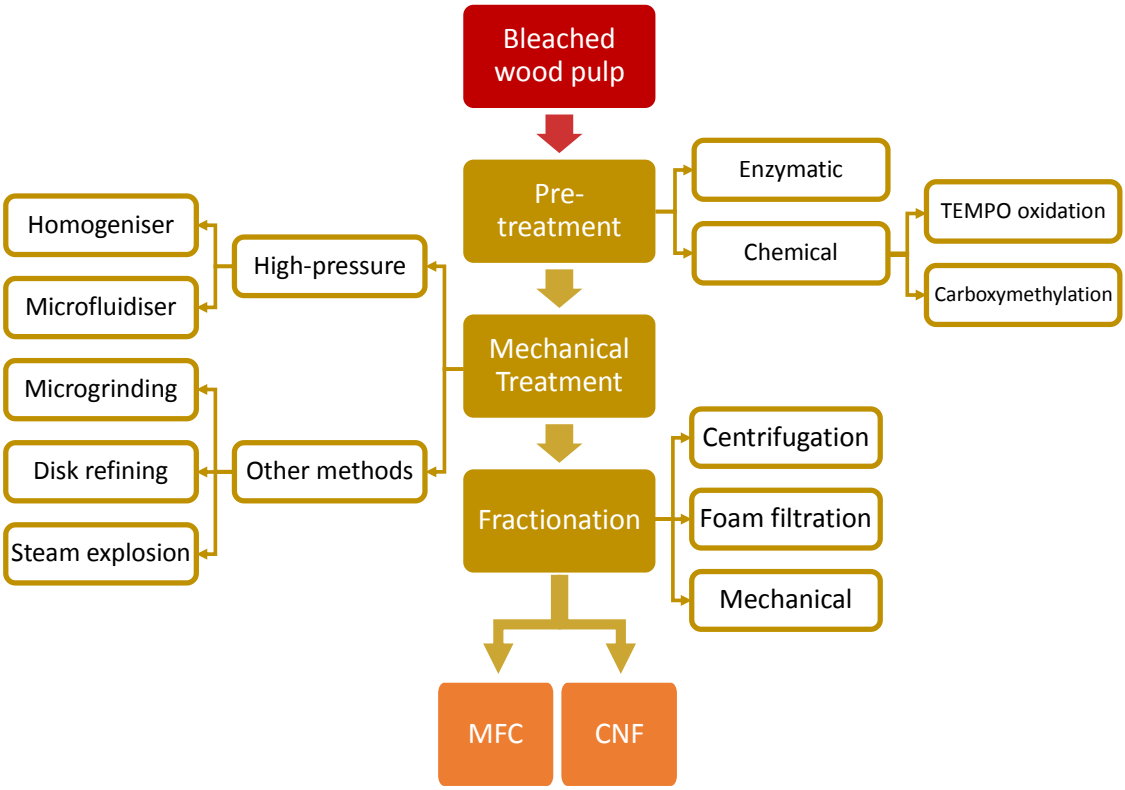

Figure 1.12: A typical example of a manufacturing process of MFC/CNF. Original in colour.

The main difference between CNF and MFC is that the former is more homogenous, *i.e.* fibrils are delaminated to their most elementary structure of only few nanometres wide and it is primarily comprised of nanofibrils (3–5 nm).[79] On the other hand, MFC is a heterogenous cellulosic material containing elementary fibrils (~3.5 nm wide), microfibrils (10–100 nm wide), fibres and cell wall fragments (1–50 μm wide).[79,80] Usually fractionation of CNF from MFC can be carried out by (ultra)centrifugation[81–83], mechanical fractionation[84] and more specific techniques like foam filtration.[85] However, in order to achieve high levels of fibrillation, pre-treatment of the fibres before mechanical processing is necessary.

The most common approaches are chemical oxidation, *eg.* carboxymethylation or 2,2,6,6-tetramethylpiperidine-1-oxyl (TEMPO)-mediated oxidation and enzymatic treatment.[76,79,86] These pre-treatments are known to ease delamination

or fibrillation of the fibres by increasing their surface charge, therefore drastically reducing energy consumption during mechanical disintegration.[77,86,87] However, it is important to take into account the economic and environmental implications of such pre-treatments; for instance, TEMPO is an expensive and toxic chemical that presents several issues when used on a large scale.[88] Nanocellulose experts in Japan, Europe and North America have expressed concern over the environmental impact of conventional methodologies, due to their dependence on catalysts, acids and other hazardous additives.[89] Although some processes are relatively energy-efficient, they still depend on the use of corrosive chemicals and solvents, adding to waste treatment costs and environmental impact. For instance, Graveson and English[87] patented a low-energy methodology for producing nanocellulose using organic and inorganic swelling agents (morpholine, piperidine, metal halides/hydroxides) followed by mechanical processing of the cellulosic biomass. Another patent uses sulfur dioxide and other additives in a mix of water and ethanol as pre-treatment for the isolation of nanocellulose fibrils and crystals.[90]

MFC is a particularly interesting material because its high surface area and aspect ratio gives it an outstanding water-binding ability. Hence, MFC readily forms hydrogels and films (upon drying).[91] MFC is also lightweight, translucent, strong and flexible.[92] Due to its properties, MFC is now found in cutting-edge applications in consolidated and innovative sectors,[93] including food & cosmetics (rheology modifier),[94,95] pharmaceutical & biomedical,[96] pulp & paper, electronics & sensors[96,97] and composites & packaging[92,98] (**Figure 1.13**). Due to the higher demand for biodegradable, lightweight and *eco-friendly* products, a global market growth of *ca.* 39% is expected for MFC by 2019, corresponding to revenues of

almost US$ 10 million.[93] The commercial price of MFC is quite variable and mainly dependent on costs (feedstock, electricity and labour) and supply.[99] At pilot scale, the price of unmodified MFC ranges between US$ 2–6/g.[100] For high-volume applications, estimated prices are between US$ 4–11/kg.[101,102]

Although MFC has mainly been produced from chemical wood pulp, alternative feedstocks that are able to reduce energy and inputs costs during processing have been also considered.[99,103] In this context, orange peel waste has also been deemed a suitable candidate for MFC production due to its "easy-to-fibrillate" biological structure (primary cell wall/parenchyma cell rich biomass with high pectin content),[80,95] high abundance and lower price (at least 10-fold cheaper than bleached wood pulp).[99] There are relatively few examples of MFC/nanocellulose production from orange peel waste in the literature, and these still rely on conventional methods of production, *i.e.* chemical/enzymatic pre-treatments combined with highly energy-intensive mechanical processing.[104,105]

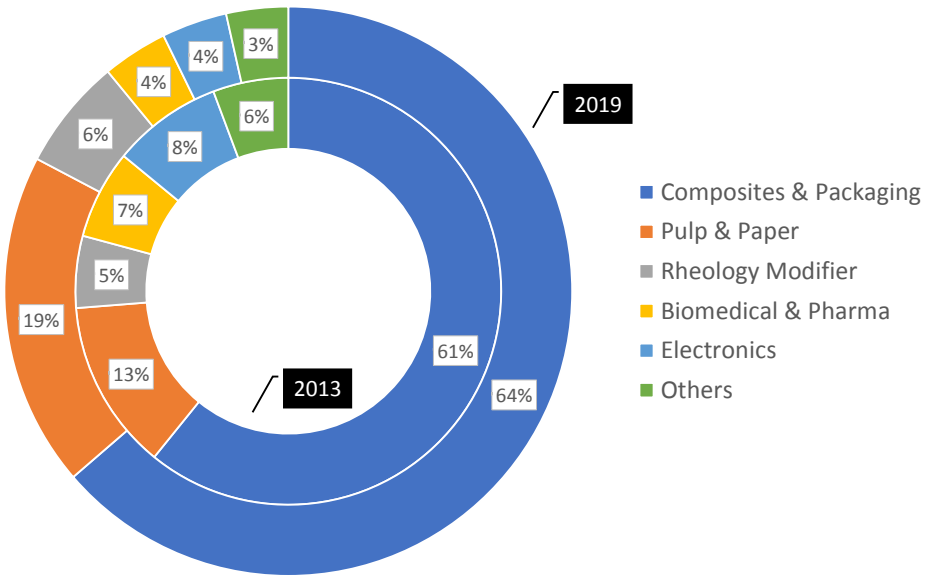

Figure 1.13: Assessed (2013) and estimated (2019) nanocellulose market share by application (data from ref. 93). Original in colour.

1.2.2.4 Orange peel waste biorefinery models for chemicals and materials

In a circular bioeconomy context, limiting the use of OPW to *low-value* approaches (energy, animal feed and composting) rather than exploring its value as a bioresource (pectin, cellulose, carbohydrates, proteins, etc) is a waste of opportunity, especially when 96% of all chemicals and materials are derived from petroleum[8]. The conversion of food waste to *high-value* chemicals is predicted to be up to 7.5 times more profitable than using it for animal feed or energy recovery.[53] Because of this potential value, several biorefinery models have been suggested in order to extract these chemicals from OPW.

Most of the reported OPW biorefinery models for chemicals focus on the extraction of volatiles (essential oil/d-limonene), pectin and small molecules (*e.g.* flavonoids, phenolics, sugars, organic acids) as part of a non-integrated[34,39] or integrated process.[40,106] As discussed before, although it is a common practice in the literature to include essential oil extraction on bench-scale biorefinery models, most of the oil is actually extracted in the juicing plant in a well-established process.[38,55] In a few cases, the final lignocellulosic residue is considered, usually being addressed as a feedstock for bioethanol or biogas production.[43,45] However, using lignocellulosic biomass as energy resource is not a suitable approach for developing a circular bioeconomy, since once burned, the lost carbon cannot be easily recovered or recycled.[31] Only a few bench-scale studies have suggested a more functional alternative use of post-extraction solid residues, such as mesoporous materials and nanomaterials.[107,108] However, most of these methodologies rely on the use of hazardous solvents and reactants (*e.g.* flammable, toxic solvents and acid/base treatments) combined with processing technologies that are outdated and wasteful (acid hydrolysis, distillations).[40,109] In

some cases the technologies are modern, but expensive and not easily scalable. Examples of these include enzymatic hydrolysis,[110] ultrasound-assisted treatment,[106,111,112] steam explosion[113] and supercritical fluid extraction.[34,45,114]

1.2.2.4.1 Microwave-based biorefineries

Microwave technology is one of the few novel technologies that is available at pilot[115] and industrial scales at capacities up to 150 tonnes/h (continuous process) or 1 tonne/h (batch process),[116,117] allowing green extraction of high-value biomolecules.[118] Microwaves are low-energy electromagnetic radiation with frequency between 0.3 GHz and 300 GHz (respective wavelengths of 1 m and 1 mm). Most microwave ovens and reactors (household, laboratory or industrial) operate at 2.45 GHz.[119,120] Microwave chemistry relies on the ability of ions and polar molecules to convert electromagnetic energy into heat by dipole polarisation and ionic conduction mechanisms (rapid and constant alignment of the electric field of ionic and polar species with that of the microwave), resulting in selective, fast and volumetric heating of the sample.[121] This direct and uniform sample heating is the major advantage of microwave over conventional conductive heating.[119,120,122] The recent interest in microwave technology for converting biomass to high-value chemicals can be attributed to its technical, environmental and economic advantages over other technologies.[120,123] The dielectric properties of a solvent or material (its ability to absorb electromagnetic energy and dissipate heat) defines how well it will interact with microwaves. For example, water molecules are excellent microwave absorbents (dielectric constant of 80.4 at r.t. and 2.45 GHz) but relatively poor heat dissipators (dielectric loss of 0.123 at r.t.).[120] The high water content and the presence of

natural microwave sensitisers[e] (salts, organic acids, etc.) in orange peel waste makes it a suitable biomass feedstock for green microwave processing, especially at hydrothermal conditions.[123]

In hydrothermal conditions water exists at subcritical state, meaning that the system is operated below the supercritical point of water (374 °C and 221 bar) but above its boiling point (100 °C). This system is also known as superheated water, pressurised hot water or pressurised low-polarity water.[120] The latter denomination is drawn from the fact that with increasing temperature the dielectric constant of water decreases corresponding to a drop in water polarity.[120] Also, with increasing temperature, the ionic product of water (hydronium and hydroxide ions) increases in the system, creating an "autocatalytic" environment.[119] Under these conditions, less polar and even non-polar biomolecules (lignin, phenolic compounds, polysaccharides) could be rapidly extracted from biomass using water as solvent, which would be more beneficial from a health & safety perspective in contrast to the use of traditional organic solvents.[120]

On microwave-assisted extraction, the physical properties of the different components of the biomass (molecular mobility, crystallinity, polarity, etc) also play an important role on the effective extraction of the interest compounds. Selective extraction and different extraction rates for different biomolecules are observed depending on how well they can interact with microwave energy and of the selected parameters of the experiment.[124]

[e] A substance that absorbs microwave energy strongly is called a *sensitiser*.

Although several microwave-based orange peel biorefineries have been suggested in literature,[39,40,43,106,125] very few have taken it to a complete zero-waste approach. One of the only examples of an integrated OPW biorefinery based on pilot-scale microwave technology was patented by the Green Chemistry Centre of Excellence (GCCE — York, UK).[126] The patent's claims included the sequential extraction of essential oil, pectin, flavonoids, sugars and, potentially, a mesoporous cellulosic material from orange peel residue, where the latter has opened up a new area to be explored on biomaterials research. Since the patent filing in 2015, valorisation of the *depectinated* cellulosic residue has remained relatively unexplored in the GCCE. For example, only Bagaria[127] further studied the characterisation of the crude mesoporous cellulosic material from orange and mango peels residues. Nevertheless, further investigation on the valorisation of cellulosic residues needs to be continued in order to convert the current approach into a profitable, integrated and sustainable *zero-waste* biorefinery model.

1.3 Green chemistry context

The term green chemistry started to appear in the 1990s as a new scientific and industrial praxis which envisioned the development and implementation of safe and environmentally-friendly chemistry. In 1998, Anastas and Warner coined the *12 principles of green chemistry*.[128] As shown in **Figure 1.14**, several of the green chemistry principles are aligned with the circular bioeconomy concept and, ultimately, with the scope of this thesis. In particular, principles 1, 7, 10 and 12 are important guides for a sustainable and clean approach towards the use of biomass as renewable resources for chemicals and materials manufacturing. Principle 6 reminds us that choosing an energy-efficient technology is crucial for maintaining the sustainability of the whole process. For instance, the use of

microwave reactors (currently, at lab and pilot-scale) has been shown to be more energy-efficient for many common organic reactions and biomass treatments when compared to conventional heating.[129–132] In a green chemistry philosophy, nature is both the supplier and the final customer, explaining the green chemists' quest for valuable bioresources, such as food waste, to yield sustainable bioproducts.

Figure 1.14: The 12 green chemistry principles. The principles in green are directly related to the scope of this thesis. Original in colour.

1.4 Aim and Objectives

Thus, the overall aim of this thesis is to contribute towards a complete orange peel biorefinery model by producing an in-depth study on the valorisation of the "depectinated" orange peel residue (DOPR). The latter can serve as a source of microfibrillated cellulose for potential applications in food, healthcare and biocomposites as well as yielding other high-value chemicals (residual pectin,

lignin, sugars and soluble organic molecules) based on a integrated *zero-waste* approach (**Figure 1.15**).

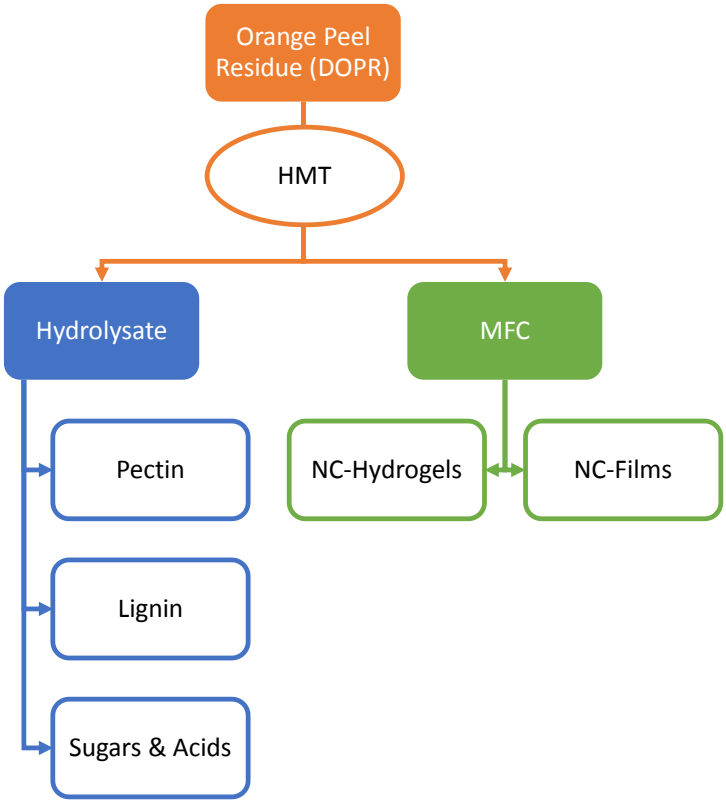

Figure 1.15: The general process of the hydrothermal microwave treatment (HMT) of DOPR to yield MFC and hydrolysate with their respective products. Original in colour.

In order to achieve the abovementioned aim, specific objectives were divided into three parts:

- **Part A:** *Characterisation and application of MFC materials produced from orange peel residue via acid-free hydrothermal microwave treatment at relatively low temperatures (120–220 °C).*

By studying the treatment at several temperatures, the interaction between the feedstock and the microwave as well as the changes in the properties of the product (MFC) driven by the applied processing temperature can be better understood. The techniques used for the characterization of MFC are

ATR-FTIR, TGA, SSNMR, XRD, SEM, TEM, CLSM, CHN, N_2 porosimetry, ICP, Py-GC/MS, WHC and GPC. Whenever relevant, comparison of MFC data with that of the starting material (DOPR) or a commercial cellulose sample will be carried out. Regarding application of MFC, hydrogels and films will be produced using conventional methods (homogenisation and solvent casting, respectively) and analysed by SEM and rheology (only for hydrogels).

- **Part B:** *Valorisation of the hydrolysates by recovering high-value chemicals (residual pectin, lignin, sugars and soluble organic molecules) and carrying out their characterisation*

The valorisation of the hydrolysates is a crucial step when developing a zero-waste biorefinery, especially when considering the economic value of pectin and the other molecules present in the hydrolysate (sugars, soluble organic acids and furans). The characterisation of these molecules, will also contribute to the further understanding of the mechanism behind the microwave-assisted hydrolysis of biomass, *i.e.* the *Hydrothermal Microwave-assisted Selective Scissoring* (Hy-MASS) concept.[133] The analysis of the hydrolysates' products includes ATR-FTIR, NMR, TGA, SSNMR, SEM, TEM, CLSM and HPLC. Also, proof-of -concept production of pectin gels was carried out.

Table 1.4 presents the major products of this thesis biorefinery model and their respective coding and processing temperature.

- **Part C:** *Greenness assessment of the biorefinery process*

In order to assess the sustainability and greenness of the suggested biorefinery process (**Figure 1.15**), green chemistry metrics will be applied. As quantitative metrics, energy efficiency and E-factor analysis of the hydrothermal microwave treatment against the conventional heating treatment (also known as superheated water treatment) of orange peel residue will be carried out. Green star analysis will be used as a qualitative metric to assess potential hazards and environmental impact of this thesis process scenario *versus* other possible greener scenarios.

Table 1.4: Orange peel derived materials produced and studied in this thesis.

Material	Coding	Temperature of MW treatment (°C)
Depectinated orange peel residue (precursor)	DOPR	95
Microfibrillated Cellulose	MFC-1	120
	MFC-2	140
	MFC-3	160
	MFC-4	180
	MFC-5	200
	MFC-6	220
Pectin	P-1	120
	P-2	140
	P-3	160
Lignin	L-4	180
	L-5	200
	L-6	220

Chapter 2

2 EXPERIMENTAL

2.1 Materials & Methods

All chemicals and reagents used in this work were purchased either from Sigma-Aldrich Chemical Company (now known as Merck) or VWR Chemicals and used without further purification unless otherwise specified. Deionised water was used throughout all experiments.

Sweet oranges (Spain) were purchased from a local supermarket (Morrisons, York), juiced on the day of purchase (ESPO 100 juicer) and the fresh orange peel (3 kg) was collected, macerated (Retsch, GM 300 food processor, 2500 rpm, 2 cycles of 30 seconds) and refrigerated (4 °C) until further use.

2.1.1 MFC composition

Relative composition of DOPR and MFC samples were calculated by combining several analyses. DTG (from TGA data, **Section 2.2.2**) was used to calculate proximate content of moisture (25–140 °C), pectin (140–270 °C), cellulose (270–400 °C) and residual char (693 °C) by their corresponding mass loss areas (in %).[134,135] Hemicellulose may contribute to the contents of cellulose and pectin due to overlapping decomposition (220–330 °C).[136,137] Residual char can be composed of both fixed carbon and ash.[137] Dry weight percent of all components were corrected based on the moisture content found for each sample.

Klason Lignin[138] was isolated following the standard biomass analytical method developed by National Renewable Energy Laboratory (NREL, USA).[139] Aqueous H_2SO_4 (72%, 3 mL) was added to the dry sample (300 mg) for 1 h (water bath, sparingly stirring the mixture every 10 minutes) followed by dilution of the acidic mixture to 4% concentration with deionised water (84 mL), heating to 121 °C (1 h), vacuum filtering (previously weighed filtering crucible) and drying at 105 °C

until constant weight was achieved (minimum of 4 h). Thereafter, each crucible was left to cool in a desiccator and the weight of the dry residue (Klason lignin) was calculated.

Protein content (%) was calculated from CHN analysis (**Appendix I**) by multiplying N content by the conversion factor for plant protein (4.64).[140] Finally, inorganic content was calculated from ICP-OES data (Section 2.2.12).

2.1.2 Depectinated orange peel residue

The starting material, depectinated orange peel residue (DOPR) was produced by processing fresh orange peel in a bespoke demonstrator microwave rig (Sairem Labotron, Pyro 60K microwave generator) based on University of York IP for pectin extraction (**Figure 2.1**).

A slurry comprising freshly milled orange peel (3 kg) and water (18 L) was charged in to the microwave rig and circulated for 10 minutes at a rate of 230 L min^{-1}. Microwave power was applied initially at 1 kW to test for any microwave leaks and then set to 6 kW until the target temperature of 95 °C was reached (~45 minutes). Thereafter, the aqueous orange peel slurry was recirculated at 95 °C for 1.5 h, cooled and filtered (cotton cloth). The aqueous filtrate was isolated for further treatment with ethanol to effect pectin precipitation whilst the pellet (DOPR) was frozen at -20 °C until further processing, i.e. DOPR was subjected

to hydrothermal microwave treatment (HMT) to yield microfibrillated cellulose (MFC). Experiments were carried out in duplicate.

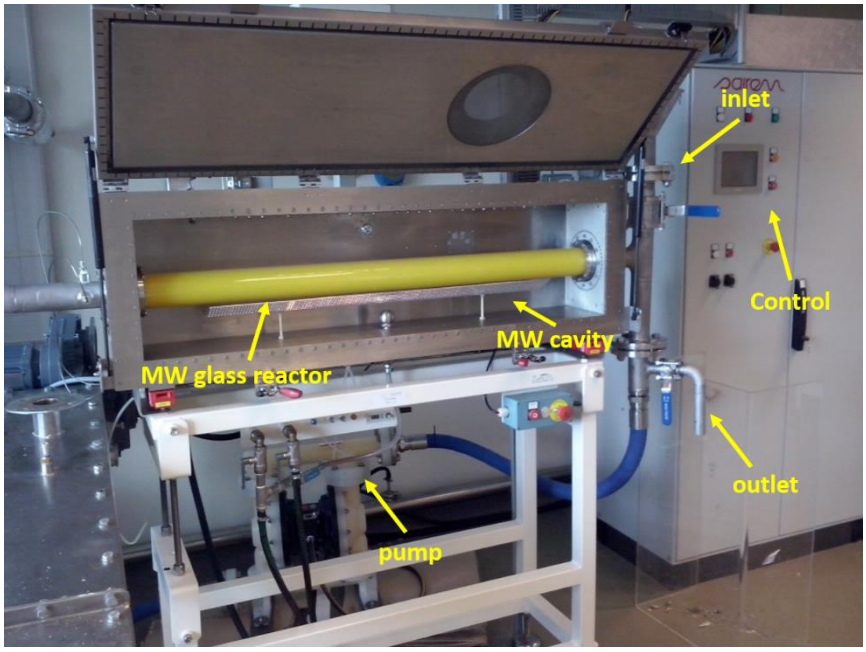

Figure 2.1: Modified microwave rig used for pectin extraction. Original in colour.

2.1.3 Hydrothermal microwave treatment of DOPR for microfibrillated cellulose production – General method

DOPR samples were treated in a closed vessel microwave (Synthwave Milestone, 2.45 GHz) to produce MFC and hydrolysate. Defrosted DOPR (120 g, wet basis with a water content of 93%) was mixed in a ratio of 1:5 (w/v) with deionised water (600 mL) contained in a PTFE closed vessel (1 L) purged with nitrogen gas (10 bar) and applied to HMT at different temperatures ranging from 120–220 °C with 20 °C intervals (operating at a maximum of 1500 W, ramping time of 15 min., holding time of 15 min. and 50% stirring power). Subsequently, the resulting slurry was filtered (Büchner) whilst hot and the solid residue was washed with hot ethanol (2x 300 mL, 15 min. each), ethanol (300 mL, 15 min.) and acetone (300 mL, 15 min.). Thereafter, the washed residue was dried (~40 °C, 48–72 h) to afford the desired MFCs, which were then ground (mortar and pestle) and stored in

glass vials for further use. Yield of MFC was calculated according to **Equation 2.1.**

$$Y\ (wt.\%) = \frac{dry\ MFC\ mass\ (g)}{dry\ DOPR\ mass\ (g)} \times 100 \qquad \text{(Equation 2.1)}$$

2.1.4 Hydrolysate work-up

Pectin and lignin were isolated from the hydrolysate using the following procedures. Sugars and the soluble organic molecules were not individually isolated from the hydrolysates, instead they were identified and quantified by HPLC based on known standards.

2.1.4.1 Pectin isolation

Pectin was isolated from hydrolysates produced at 120 °C, 140 °C and 160 °C as follows. An equal volume of ethanol (500–600 mL) was added to the hydrolysate to effect pectin precipitation and allowed to stand overnight. The resultant precipitate (pectin) was collected by centrifugation (2675 × g, 20 min.), washed with hot and room temperature ethanol (2 × 100 mL), dried in a vacuum-oven (40 °C, overnight) and ground (mortar and pestle) to afford pectin as an off-white powder. The pectin samples were coded as P-1 (isolated from 120 °C hydrolysate), P-2 (140 °C) and P-3 (160 °C). The yield of pectin was calculated according to **Equation 2.2**.

$$Y\ (wt.\%) = \frac{dry\ pectin\ mass\ (g)}{dry\ DOPR\ mass\ (g)} \times 100 \qquad \text{(Equation 2.2)}$$

2.1.4.1.1 Pectin sugar analysis

For sugar composition analysis of pectins, a sample of pectin (5.5 mg) was mixed with 1M aqueous H_2SO_4 (1.5 mL) for 2.5 h at 105 °C (magnetic stirrer plate). The

sample was then cooled, filtered (filter wheel, 20 μm pore) and the filtrate analysed by HPLC (instrumental details on **Section 2.2.11**).

2.1.4.1.2 Pectin degree of esterification (DE)

The DE of pectin samples were calculated from their respective ^{13}C SSNMR spectrum according to **Equation 2.3.**

$$DE_{\%} = \frac{I_{OCH_3}}{I_{COOR}} \times 100 \quad \text{(Equation 2.3)}$$

Where, I_{OCH3} is the integral of methoxyl signal at ~54 ppm and I_{COOR} the integral of carboxyl (ester and acid) at ~173–171 ppm.

2.1.4.1.3 Pectin gel formation

Pectin (0.5 g) and sucrose (15 g) were added to an AVS Titrinorm pH 3.0 buffer solution (19.5 ml), stirred (magnetic plate) and left overnight to ensure complete dissolution. The resultant clear solution was boiled, cooled to room temperature, upon which more sucrose (15 g) was added. The mixture was re-boiled and allowed to cool to room temperature prior to overnight refrigeration (4 °C) to effect gel formation.

2.1.4.2 Lignin-like material isolation

A lignin-like material (hereafter called lignin for simplification) was isolated as a brown powder precipitate from the hydrolysates produced at 180 °C, 200 °C and 220 °C, following overnight refrigeration of the hydrolysates (4 °C). The lignin sample was isolated by centrifugation (15 min., 2675 × g), filtered (vacuum filtration), rinsed at least 3 times with water and oven dried (~40 °C, 48 h). The lignin samples were coded as L-4 (isolated from the 180 °C hydrolysate), L-5 (200

°C) and L-6 (220 °C). The yield of lignin was calculated according to **Equation 2.4**.

$$Y\ (wt.\%) = \frac{dry\ lignin\ mass\ (g)}{dry\ DOPR\ mass\ (g)} \times 100 \qquad \text{(Equation 2.4)}$$

2.1.5 MFC-based hydrogels

MFC Hydrogels were produced at different concentrations (0.5–3.0%, w/v) by mixing an adequate amount of DOPR or MFC (50–300 mg) in deionised water (10 mL). The dispersion was then homogenised using a high-shear homogenisation (Ystral X10/20 E3 homogeniser, 2–3 min. at ~20000 rpm) to afford the hydrogel and refrigerated (4 °C). Gel formation was qualitatively assessed by the tube inversion test, where a sample is placed into a small vial which is then turned upside down to check for its flowability. A true gel is self-supportive, therefore it will not flow.[49,141,142]

2.1.6 MFC-based films

MFC films were produced at a concentration of 0.2% (w/v) by mixing MFC (10 mg) in deionised water (5 mL) and stirring the suspension overnight. Thereafter, the samples were also sonicated for *ca.* 15 min. to help break any large lumps and give a more homogenous dispersion. Subsequently, the suspensions were poured into a short-stem sintered glass filter (40–50 mm diameter, pore size 3) covered with a PTFE membrane (25 mm diameter) and air dried (~40 °C, 48 h). The resultant films were stored in petri dishes placed inside a desiccator.

2.1.7 Conventional hydrothermal (superheated water) treatment

The CHT of depectinated orange peel residue (DOPR) was performed in Fudan University (China) in a collaboration project. Dried DOPR (3 g) was mixed with water (177 mL) in a stainless-steel pressurised reactor vessel (250 mL). The reactor

vessel was enclosed in a thermal jacket, and before its closure, a stirrer bar was placed inside the reactor. The reactor was heated to the desired temperatures (120–220 °C) using a hot plate and the solid and liquid fractions were treated in the same way as for the HMT experiments.

2.1.8 Statistical analysis

Analysis of variance (ANOVA) with a confidence interval of 95% was used to analyse the data (JMP 10 software). In the data plots, the mean values are plotted along with the values obtained from the Fisher's least significant difference (LSD) test. To ensure significant difference between any pair of data or within the evolution of a response variable, the LSD bars must not overlap. For some points, the error bars would be shorter than the height of the symbol. In these cases, the plot does not contain error bars. All analyses were conducted in duplicate.

2.2 Instrumental Analysis

2.2.1 Attenuated Total Reflection Fourier-transform Infrared Spectroscopy (ATR-FTIR)

ATR-FTIR was carried out using a Perkin Elmer Spectrometer (Spectrum 400). Prior to recording a spectrum, a background scan (no sample) was run from 4000 cm^{-1} to 600 cm^{-1}, with a spectral resolution of 4 cm^{-1}. Thereafter, the appropriate sample was placed on the sapphire window and spectrum recorded (4 scans).

2.2.2 Thermogravimetric Analysis (TGA)

TGA was carried out under a flow of nitrogen (100 mL min^{-1}) using a NETZSCH STA 409 cell for MFC, pectin, lignin and references analysis (25–700 °C at 10 K min^{-1}). Roughly 50 mg of sample was used in each experiment.

2.2.3 Liquid state ^{13}C Nuclear Magnetic Resonance (NMR)

^{13}C NMR spectra were recorded at 125 MHz on a Bruker AV500 spectrometer and dimethyl sulfoxide (DMSO) was used as internal reference in order to elucidate the structure of the isolated pectins. Samples were dissolved in deuterated water (D_2O) at an approximate concentration of 4 wt.% and chemical shifts (δ) of the spectra were given in ppm based on tetramethylsilane (TMS) reference value (0.0 ppm). Experiments were run at 353 K (80 °C) with 30000 scans.

2.2.4 Solid state ^{13}C CP-MAS Nuclear Magnetic Resonance (SSNMR)

Solid State ^{13}C Cross Polarization Magic Angle Spinning (CP-MAS) NMR (SSNMR) spectra were acquired using a 400 MHz Bruker Avance III HD spectrometer equipped with a Bruker 4mm H(F)/X/Y triple-resonance probe and 9.4T Ascend® superconducting magnet. The CP experiments employed a 1 ms linearly-ramped contact pulse, spinning rates of 10000 ± 2 Hz, optimized recycle delays of 5 seconds, and numbers of scans varying from 200–300 for MFC and pectin and 1200 for lignin samples. Chemical shifts were reported with respect to TMS and were referenced using adamantane (29.5 ppm) as an external secondary reference.

2.2.5 X-Ray Diffraction (XRD)

XRD analysis was performed on a Bruker-AXS D8 Advance Diffractometer equipped with a Cu source producing a monochromatic K-α radiation at wavelength of 1.54184 Å and a PSD Lynx eye detector. Samples were ground to a fine powder prior to analysis. Samples were run with a rate of 2.0° min^{-1} over a 2θ range of 5–38° (cellulose does not present any diffraction pattern after this angle)[143] in a locked coupled theta–2θ scan mode. Generator voltage and current

were set to 40 kV and 40 mA respectively. Data processing included background subtraction and trace smoothing.

The crystalline index (CrI) of MFC samples was calculated according to Segal's equation[144] (**Equation 2.5**):

$$\mathrm{CrI}_{\%} = \frac{I_{200} - I_{am}}{I_{200}} \times 100 \qquad \text{(Equation 2.5)}$$

Where:

I_{200} = intensity of the (200) peak (at $2\theta = 22^{o} \pm 0.5$)

I_{am} = intensity of amorphous contributions (at $2\theta = 18.0^{o} \pm 0.5$)

2.2.6 Scanning Electron Microscopy (SEM)

SEM images were generated using a JEOL JSM-7600F SEM instrument. A diluted suspension of the sample (*ca.* 0.2% w/v) was either directly air-dried on the SEM grid or freeze-dried. When freeze-dried, a small amount of the gel or suspension was placed on a copper shim and excess liquid was removed with filter paper. The sample was then frozen in liquid nitrogen slush (-210 °C so it does not bubble, achieving better cooling rate and better preserving the original structure of the material).[145] The shim plus gel was transferred to the cooled Peltier stage in a Polaron coating unit and the air was pumped out. Temperature was kept at *ca.* -55 °C and the vacuum was maintained around 10^{-4} mBar. After a few hours the sample was warmed to room temperature and the gel was knocked off the shim. The remaining "scraps" of gel were imaged after mounting the shim plus scraps on a stub and coating with gold/palladium (*ca.* 4 nm thick). Analysis was performed by Meg Stark, Dept. of Biology, University of York.

2.2.7 Transmission Electron Microscopy (TEM)

TEM images of structured celluloses were acquired using a TEM Tecnai 12 BioTWIN (manufactured by FEI) coupled to a SIS Megaview 3 camera at an acceleration voltage of 120 kV. Prior to the analysis, diluted samples (0.2 wt.% aqueous) were sonicated for 30 minutes using an ice-cold ultrasound bath (output of 1200 W). Drops of the sample (about 8 μL) were left on the grid for five minutes then negatively stained with 1% uranyl acetate and finally glow discharged. Copper grids with a formvar/carbon support film were used.

2.2.8 Confocal Laser Scanning Microscopy (CLSM)

A Carl Zeiss LSM880 confocal microscope, fitted to an Axioimager and using a Plan Apochromat 20×/0.8 or 60×/1.4 oil objective with ZEN 2 software was used to capture the raw images. All samples were excited with a 405 nm laser using a 405 nm main beam splitter and emission collected from 410–695 nm in bins of 8.9 nm using the spectral detector. Reference spectra of citrus lignin, hemicellulose (both extracted from DOPR) and cellulose (Sigma-Aldrich) were collected independently and used to spectrally unmix the experimental images. Images were averaged to reduce noise and increase the precision of the spectral unmixing which was performed using the in-built application within ZEN 2 on a pixel-to-pixel basis. This processing resulted in the image being split into 2 individual images corresponding to the lignin and cellulose components present in the sample. Analysis was performed by Joanne Marrison, Dept. of Biology, University of York.

2.2.9 Elemental microanalysis (CHN)

Elemental analysis was performed in-house by Dr. Graeme McAllister. A CE-440 elemental analyser from Exeter Analytical was used, in conjunction with a

Sartorius S2 analytical balance. Samples were combusted at 975 °C in an oxygen atmosphere, and the combustion products analysed by a series of thermal conductivity detectors. Analysis were conducted in duplicate.

2.2.10 N_2 physisorption porosimetry

The porous structure of the DOPR, MFCs and lignins samples were analysed using a Micromeritics TriStar Surface Area and Porosity Analyser. A measured amount of dry (*ca.* 50 mg), powdered sample was put inside a clean, dry porosimetry tube and the mass was recorded. The samples were degassed at 90 °C for 4 h and the mass of the glassware and sample was re-measured. This value was used for the analysis. All analyses were conducted in triplicate. The data was processed using TriStar software, where specific surface areas were calculated using the Brunauer-Emmett-Teller (BET) equation, and desorption pore volume and average pore size were calculated using Barrett-Joyner-Halenda (BJH) equations.[146]

2.2.11 High-performance Liquid Chromatography (HPLC)

Sugars (levoglucosan, glucose, fructose/xylose, cellobiose and arabinose), sugar acids (glucuronic acid and galacturonic acid), soluble organic acids (lactic acid, formic acid, levulinic acid and acetic acid), furans (HMF and furfural) and levoglucosenone present in the hydrolysate were quantified by HPLC. Analysis was performed in-house by Dr. Hannah Briers.

Sugars and acids were analysed by using an Agilent 1260 equipped with a reverse-phase Hi-Plex H (300 × 7.7 mm, 8 μm particle size) column, using 0.005M H_2SO_4 as mobile phase, isocratic mode (no gradient), flow-rate of 0.4 mL min^{-1},

column temperature at 60 °C, refractive index detector (55 °C), injection volume of 5 μl and total run time of 35 minutes.

Furans were analysed by using an ACE C18 (250 × 4.6 mm, 5 μm particle size) column, acetonitrile : water (25/75) as mobile phase, isocratic mode, flow-rate of 0.8 mL/min., column temperature at 30 °C, diode-array detector (DAD) at 220 nm, injection volume of 5 μl and total run time of 22 minutes.

For all analytes, a small sample of each hydrolysate was collected, filtered through a disk filter (0.22 μm pore) and analysed in the HPLC.

2.2.12 Inductively Coupled Plasma Optical Emission Spectrometry (ICP-OES)

A weighed sample was placed in a microwavable digestion tube, and reverse aqua-regia was added (9 mL of conc. HNO_3 and 3 mL of conc. HCl). The sample was then digested (Mars Xpress microwave), diluted to 25 mL using deionised water and filtered. Samples were analysed on an axial Varian vista ICP-OES. Results were automatically corrected for dilution factor. Analysis was performed by Lancrop Laboratories, York, UK.

2.2.13 Pyrolysis Gas Chromatography–Mass Spectroscopy (Py-GC/MS)

Py-GC/MS data was acquired using a CDS Analytical 5250-T Trapping Pyrolysis Autosampler (UK), an Agilent Technologies 7890B GC System (USA) and an Agilent Technologies 5977A MSD (USA) mass spectrometer. The sample was loaded into the pyrolysis unit and pyrolysed at 600 °C for 10 s. The volatile materials released were carried into the GC/MS unit by nitrogen for analysis. The following GC/MS parameters were applied: GC inlet temperature at 350 °C, initial temperature at 40 °C for 2 min, ramp rate at 10 K min^{-1} till 300 °C, holding at 300 °C for 30 min, split ratio with 50:1. Volatile compounds were identified by

comparing the mass spectra with NIST Lab database. Analysis was performed at the Biorenewables Development Centre (BDC), University of York.

2.2.14 Water Holding Capacity (WHC)

Water holding capacity (WHC) of samples were estimated by the method described by Zain *et al*.[147] Weighted mass of the appropriate sample (*ca.* 0.20 g) was mixed with water (20 mL), stirred for 20 minutes and then centrifuged (2675 × g, 20°C, 20 minutes). After separating the supernatant from the centrifuge tube, the WHC (g of water/g dry sample) of the sample pellet was calculated according to **Equation 2.6**. Experiments were conducted in duplicate.

$$WHC = \frac{[(mass\ of\ tube+precipitate)-(mass\ of\ tube+sample\ mass)]}{mass\ of\ dry\ sample} \qquad \text{(Equation 2.6)}$$

2.2.15 Gel Permeation Chromatography (GPC)

Molar mass distribution of the MFC samples was determined by gel permeation chromatography (GPC) coupled with a multi-angle laser light scattering (MALLS) detector. First, the samples were activated by a water—acetone—*N, N*-dimethylacetamide (DMAc) sequence. The activated samples were then dissolved in DMAc containing 90 g L^{-1} LiCl at room temperature and under gentle stirring. The dissolved samples were diluted ten-fold to decrease the concentration of LiCl to 9 g L^{-1} in DMAc, filtered with 0.2 μm syringe filters, and analysed in a Dionex Ultimate 3000 system with a guard column (PL gel Mixed-A, 7.5 × 9 × 50 mm, Agilent Technologies, Santa Clara, CA, USA), four analytical columns (PL gel Mixed-A, 7.5 × 9 × 300 mm) and RI-detection (Shodex RI-101, Kawasaki, Kanagawa, Japan). Flow rate and temperature were 0.75 mL min^{-1} and 25 °C, respectively. Narrow pullulan standards (343 Da–708 kDa, Polymer Standard Service GmbH, Mainz, Germany; and 1,600 kDa, Fluka GmbH,

Germany) were used for calibration. The molar masses (MM) of the pullulan standards were modified to correspond to those of cellulose calculated by MALLS [$MM_{MALLS} = q \times (MM_{PULL})^p$] as validated by Berggren *et al.*[148], resulting in coefficients q = 12.19 and p = 0.78. Weight and number average molecular weight (M_w and M_n, respectively) were obtained. Dispersity (Đ) of the samples was calculated as $Đ = M_w/M_n$ and degree of polymerisation (DP) as $DP = M_w/M_g$, where M_g is the molecular weight of the monomeric unit of cellulose, anhydroglucose (162 g mol^{-1}). Analysis was performed at University of Aalto, Finland by Dr. Kontturi Eero.

2.2.16 Rheology of hydrogels

Oscillatory rheological behaviour of MFC hydrogels and commercial references (2.0%, w/v) were evaluated using a stress-controlled rheometer (Anton Paar Physica, MCR-301, Austria) equipped with a serrated parallel-plate measuring system (25 mm diameter). The rheometer was calibrated for torque and inertia and a 1 mm gap height was used for the analysis. Preliminary tests were carried out to identify the linear viscoelastic region (LVR) of each sample.

The rheological analysis of the samples included three steps: firstly, an equilibration step (20 °C, 2 min.) to ensure temperature homogeneity through the sample. Secondly, a frequency sweep test at a strain amplitude (γ) of 0.5% (i.e. within the LVR) over an angular frequency (ω) window ranging from 500 to 0.05 rad s^{-1}; data collection frequency was set at 6 points/decade and measuring point duration was kept at 30 s/point. Thirdly, an amplitude sweep test was carried out using angular frequency (ω) of 10 rad s^{-1} and progressively increasing the deformation strain (γ) from 0.001 to 1000%; data collection frequency was set at

6 points/decade and measuring point duration was kept at 45 s/point. Analysis was undertaken at the University of Nottingham, UK.

Chapter 3

3 RESULTS AND DISCUSSION

- E. M. de Melo, J. H. Clark and A. S. Matharu, The Hy-MASS concept: hydrothermal microwave assisted selective scissoring of cellulose for in situ production of (meso)porous nanocellulose fibrils and crystals, *Green Chem.*, 2017, **19**, 3408–3417.
- A. S. Matharu, E. M. de Melo, J. Remón, S. Wang, A. Abdulina and E. Kontturi, Processing of Citrus Nanostructured Cellulose: A Rigorous Design-of-Experiment Study of the Hydrothermal Microwave-Assisted Selective Scissoring Process, *ChemSusChem*, 2018, **11**, 1344–1353.

This chapter is divided in three parts mimicking the thesis objectives defined earlier (see **Section 1.4**), namely:

- **Part A:** Characterisation and Application of MFC
- **Part B:** Valorisation of Hydrolysate
- **Part C:** Process Greenness Assessment

3.1 Part A: Characterisation and Application of MFC

This section reports an in-depth characterisation of the produced microfibrillated cellulose (MFC) samples, discusses the mechanism behind its formation and explores some properties and performance of MFC-based hydrogels and films considered relevant for future applications in food, cosmetic and biomaterials.

The autohydrolytic environment created during the hydrothermal microwave treatment (HMT) of DOPR enabled the hydrolysis of residual pectin, hemicelluloses, proteins and lignin depending on the temperature applied (at 120–220 °C). It also allowed the formation of MFC by fibrillation of the cellulosic fibres via the *Hydrothermal Microwave-assisted Selective Scissoring* (Hy-MASS) mechanism described in this thesis. At high temperatures (>180 °C), structures similar to cellulose nanocrystals (CNC) aggregates were also formed. MFC produced at low temperatures (<180 °C) was found to be a highly hydrophilic with excellent water-binding capacity, able to form hydrogels and films at low concentrations (2–3%). The MFC hydrogels presented improved rheological performance against conventional food rheology modifiers (xanthan gum and wood pulp nanocellulose). Films were flexible and semi-transparent (in some cases), allowing possible application in biocomposites, packaging and biomedical scaffolds.

3.1.1 MFC composition, morphology and structure

3.1.1.1 Yield and proximate composition analysis

The proximate analysis described herein is derived from a mixture of analytical methods, namely, TGA, acid hydrolysis, CHN and ICP-OES. Therefore, these results are limited to a semi-quantitative interpretation.

The yield and proximate composition of DOPR and subsequent MFCs are summarised in **Table 3.1**. High to moderate yields of MFC were achieved at low-temperature (120–160 °C) HMT, ranging from 69% (MFC-1) to 46% (MFC-3). High temperature HMT (180–220 °C) resulted in moderate to low MFC yields (36–27%). Contrary to conventional MFC, *i.e.* composed of highly purified cellulose fibrils produced from chemical pulp,[77,92] the MFCs produced here are less refined cellulosic materials retaining some of the lignocellulosic components originally present in the starting material. With increasing HMT temperature, the cellulose, lignin and inorganic content increases while pectin and protein content decreases. Proteins can comprise structural proteins (bound to cell wall material)[123] and enzymes,[149,150] which are known to be present in fruit tissues. Cellulose is the major component of MFCs (52–68%), followed by variable ratios of pectin (1–14%), lignin (2.5–11%) and protein (4–1.7%). The MFCs also presented a small amount of residual moisture (4–8%) and inorganic species (1.7–2.3%). **Figure 3.1** shows the most abundant inorganic species present in the DOPR and MFC samples as determined by ICP-OES analysis. The relatively high content of species like copper and sulfur may be due to the presence of metalloenzymes[149], specialised metabolites (such as glucosinolates and allylsulfur compounds)[151] or even derive from inorganic pesticide residue (such as $CuSO_4$) in the orange peel.[152] Additionally, after pyrolysis of the MFCs (up to

700 °C), a considerable amount of char (*ca.* 20%) was formed, comprising minerals[39,153,154] and fixed carbon from decomposition products of carbohydrates, proteins and lignin.[137,155]

Interestingly, the Klason lignin content increased abruptly after 180 °C, probably due to the formation of recalcitrant lignin products (*e.g.* condensed lignin fragments) and *pseudo-lignin*, which is defined as "an aromatic material that yields a positive Klason lignin value that is not derived from native lignin."[156]

Pseudo-lignin (also known as *humins*)[157–159] is a complex material containing carbonyl, carboxylic, aromatic and aliphatic functional groups formed from the degradation of carbohydrates, pigments and proteins during acid-catalysed (auto)hydrolysis, such as HMT, of biomass.[158,160,161] Although *acid-free* treatment was used in this work, a gradual drop in pH of the hydrolysates (from 4.8 to 3.8) was observed with increasing temperature of treatment, as depicted in **Figure 3.2**. The latter supports the premise of organic acids being released from the biomass, catalysing hydrolysis of polysaccharides and leading to the formation of *pseudo*-lignin at higher temperatures. Several studies have shown that xylose and glucose hydrolysed from hemicellulose and cellulose are dehydrated to furfural and 5-hydroxymethylfurfural (HMF) and further converted into aromatic intermediates, 3,8-dihydroxy-2-methylchromone and 1,2,4-benzenetriol, respectively. The latter are responsible for *pseudo*-lignin formation via polymerisation/polycondensation (see **Figure 3.3**).[156–158,160]

Table 3.1: Yield and proximate composition analysis of DOPR and MFC samples. Contents of cellulose, pectin, moisture and char were calculated from TGA data, Klason lignin from acid hydrolysis, protein from CHN analysis and total inorganic species from ICP-OES (all methods are described in Chapter 2).

Sample	Process Temp. (°C)	Yield (% DM)	Moisture Content (%)	Cellulose[a] (%)*	Pectin[a] (%)*	Klason Lignin[b] (%)	Protein (%)	Char[c] (%)*	Total Inorganic Species (%)
DOPR	95	—	7.1±0.9	37.1±1.7	24.0±0.4	1.5±1.7	5.5±0.4	27.1±1.0	1.3
MFC-1	120	69±1.6	8.1±0.9	52.3±1.7	14.8±0.4	2.5±1.7	4.0±0.4	22.2±1.0	1.7
MFC-2	140	50±1.6	8.2±0.9	57.0±1.7	9.8±0.4	3.7±1.7	5.3±0.4	22.2±1.0	1.9
MFC-3	160	46±1.6	7.3±0.9	61.5±1.7	6.6±0.4	3.7±1.7	4.5±0.4	21.4±1.0	2.1
MFC-4	180	36±1.6	6.9±0.9	68.9±1.7	2.9±0.4	6.9±1.7	2.6±0.4	18.4±1.0	2.1
MFC-5	200	30±1.6	5.4±0.9	68.7±1.7	1.5±0.4	9.4±1.7	1.9±0.4	19.9±1.0	2.3
MFC-6	220	27±1.6	4.4±0.9	68.1±1.7	1.4±0.4	11.4±1.7	1.7±0.4	20.4±1.0	—

a: may comprise hemicellulose; **b:** comprises *pseudo*-lignin; **c:** comprises ash and fixed carbon; *moisture corrected.

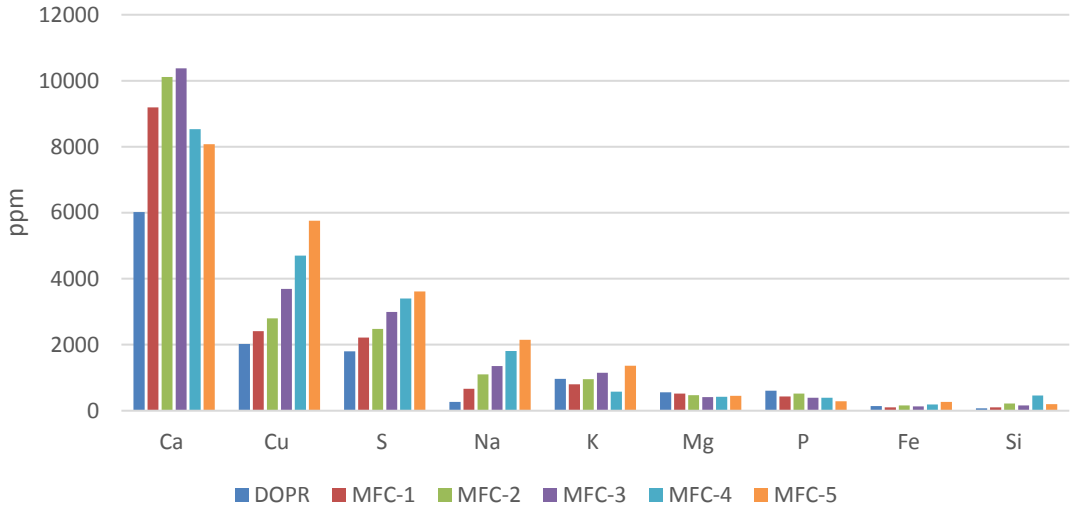

Figure 3.1: ICP-OES data showing the nine most abundant inorganic species present in DOPR and MFCs. Original in colour.

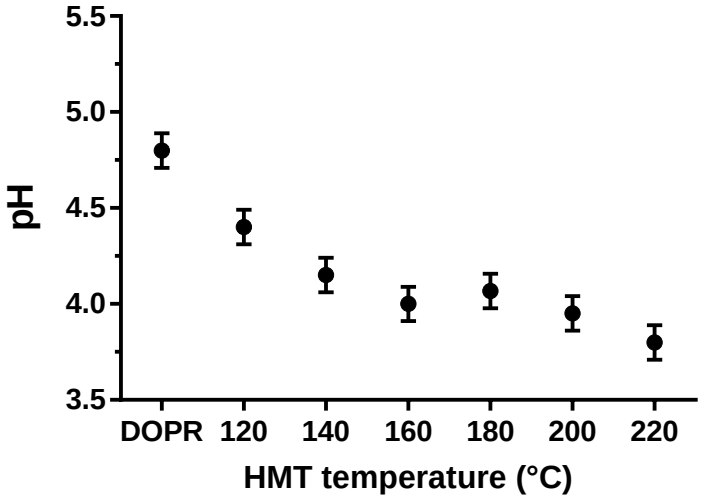

Figure 3.2: The pH of hydrolysates after HMT at different temperatures.

In fact, furfural, HMF and some trace aromatic species, such as 2-methoxy-4-vinylphenol (derived from ferulates present in carbohydrate-lignin complex)[137,159,162] and a benzenetriol isomer (possibly 1,2,4-benzenetriol), were identified in pyrolysed DOPR and MFC samples by Py-GC/MS, as shown in **Figure 3.4**. These findings further support the suggested mechanism for *pseudo*-lignin formation. Also, the lack of characteristic lignin phenolic units identified by Py-GC/MS[162–164] may be due to a low content of native lignin in the samples. As already shown in **Table 3.1**, low temperature HMT resulted in MFCs with lower content of Klason lignin, agreeing with the literature suggestion that in order to minimise *pseudo*-lignin formation, low severity treatments and an inert atmosphere should be used when treating biomass.[158,160] Also, since Klason lignin is not a direct measure of acid-insoluble lignin polymer in the sample, but instead a measure of an acid-insoluble "residue" of the sample,[157] its measurements can be easily corrupted by other acid-insoluble species present in the biomass or formed during the analysis, such as *pseudo*-lignin. Other lignin quantification analytical methods could be used to compare or complement the Klason lignin data, such as enzymatic hydrolysis or mild acidolysis treatments.[165]

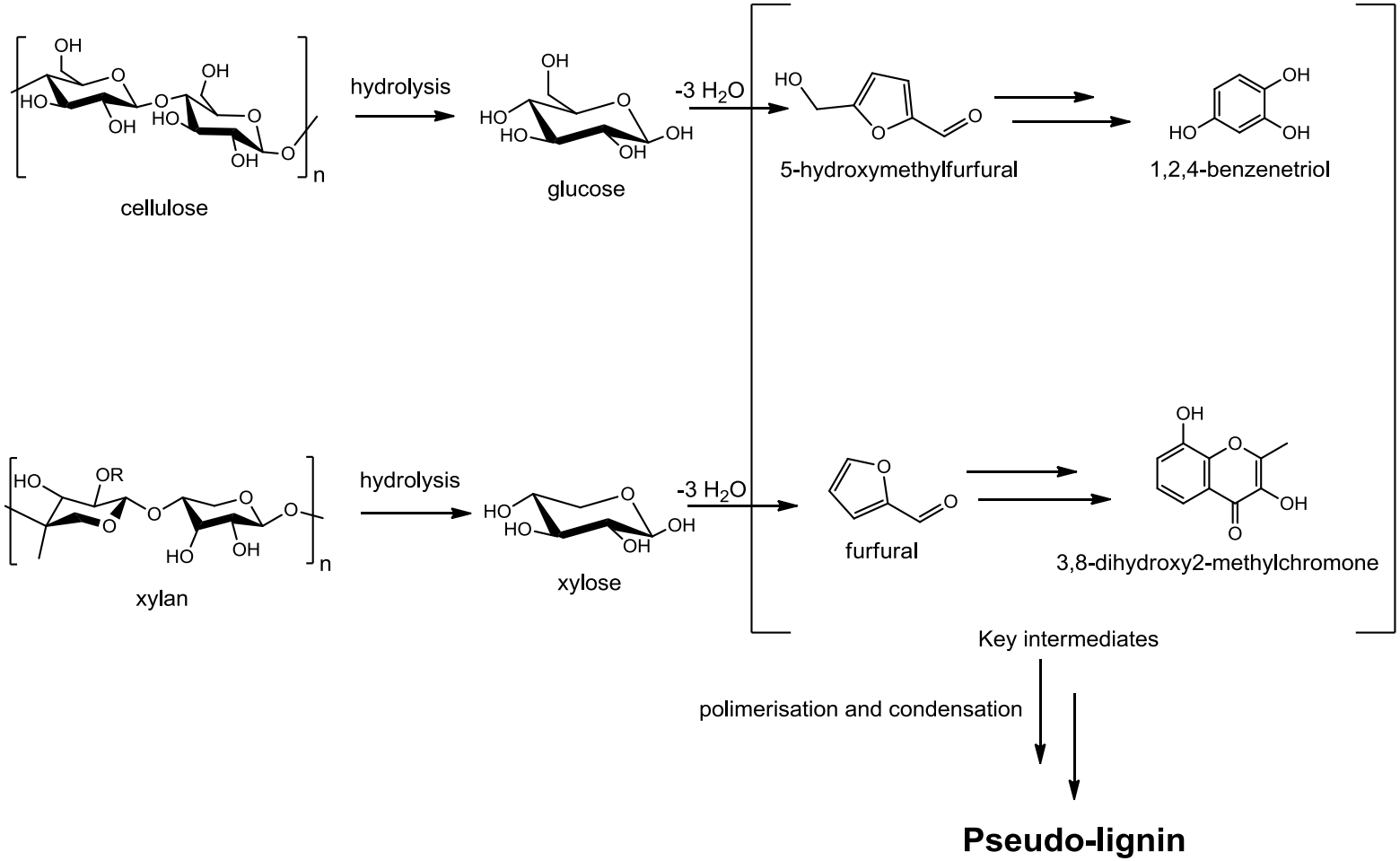

Figure 3.3: Proposed mechanism for *pseudo*-lignin formation (adapted from ref. 156).

Although hemicellulose is known to be present in orange peel biomass,[40,44,53] its typical temperature of degradation range (220–330 °C)[137,155,166] could not be easily distinguished from that of cellulose or/and pectin (see later in **Figure 3.13**), hence hemicellulose content is not reported. Therefore, cellulose and/or pectin content presented in **Table 3.1** might also include hemicellulose contribution. In fact, Py-GC/MS results suggested the presence of hemicellulose in DOPR and MFCs by the relative abundance of furfural (5–2%; see **Figure 3.4**), assuming that most furfural comes from the dehydration of xylose, which is most abundant in hemicellulose.[137,167,168]

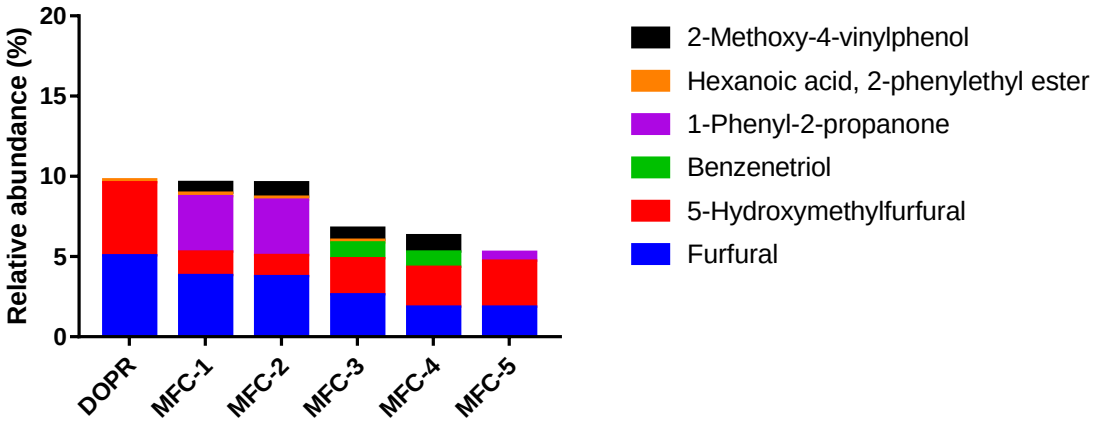

Figure 3.4: Relative abundance of major species identified from the Py-GC/MS analysis of DOPR and MFCs. Original in colour.

3.1.1.2 Electron microscopy analyses

The SEM analysis of the starting material (DOPR) revealed a dense and compacted morphology (**Figure 3.5A**), where plant cell wall structures like xylems (*ca.* 10 μm wide) and some macrofibres fragments and mineral crystals (inset in **Figure 3.5A**) were still visible amidst an amorphous matrix (possibly comprising residual pectin, hemicellulose and "lignin").[104,169] However, after treating DOPR under hydrothermal conditions, the resultant MFCs presented a

much more fibrillar morphology (**Figure 3.5C**), comprising microfibrils bundles of 40–120 nm wide, microfibrils (10–40 nm wide), elementary fibrils (3–5 nm) and some residual material (amorphous matrix and cell wall fragments).[169] The observed fibrils are similar to those reported in the literature for MFC derived from wood pulp.[79,92] Also, as the temperature of the treatment increased, more of the fibrillar moiety becomes apparent, leaving behind the dense and amorphous matrix covering the fibrils and fibres which is heavily present in the samples treated at temperatures below 180 °C (MFC-1 to MFC-3). For samples treated at 160 °C and above (MFC-3 to MFC-6), small pockets of amorphous aggregates (50–200 nm) could be observed on the surface of the fibrils (yellow arrows in **Figure 3.5C**), which could be due the presence of (*pseudo-*)lignin and/or Maillard products (derived from the degradation of carbohydrates and proteins at high temperatures).[158–160,170] Although sample preparation for SEM was carefully carried out to avoid aggregation of the individual fibrils upon drying, some aggregation was inevitable due to the hornification (irreversible aggregation) of fibrillated fibrils.[171,172] However, using a lyophilised (instead of oven dried)[171,173] sample prepared from a more diluted (*ca.* 0.2%) and well-dispersed (sonicated or homogenized) suspension prevented aggregation of fibrils on the SEM grid giving better evidence of fibrillation (see **Figure 3.6**).

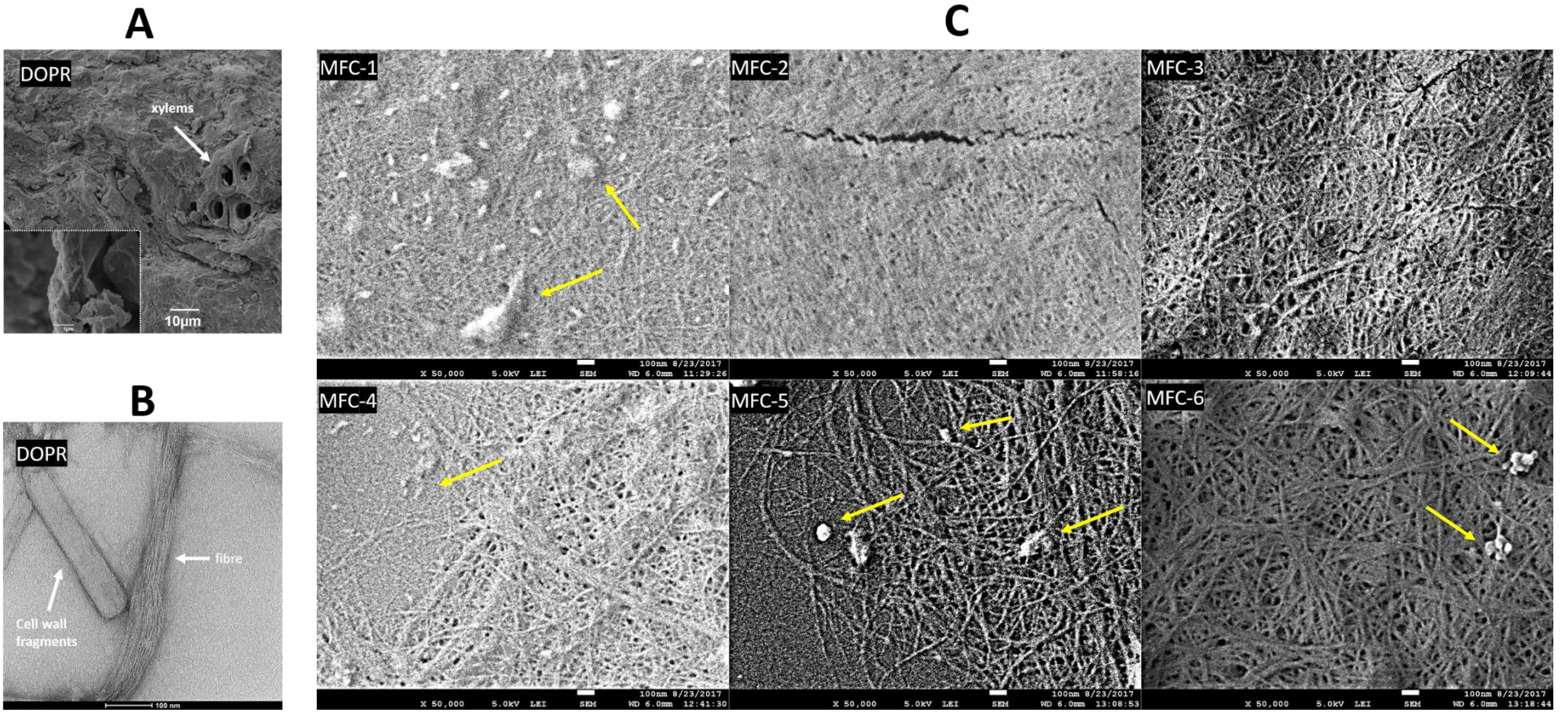
A
DOPR
xylems
10µm
B
DOPR
fibre
Cell wall fragments
100 nm
C
MFC-1
MFC-2
MFC-3
MFC-4
MFC-5
MFC-6

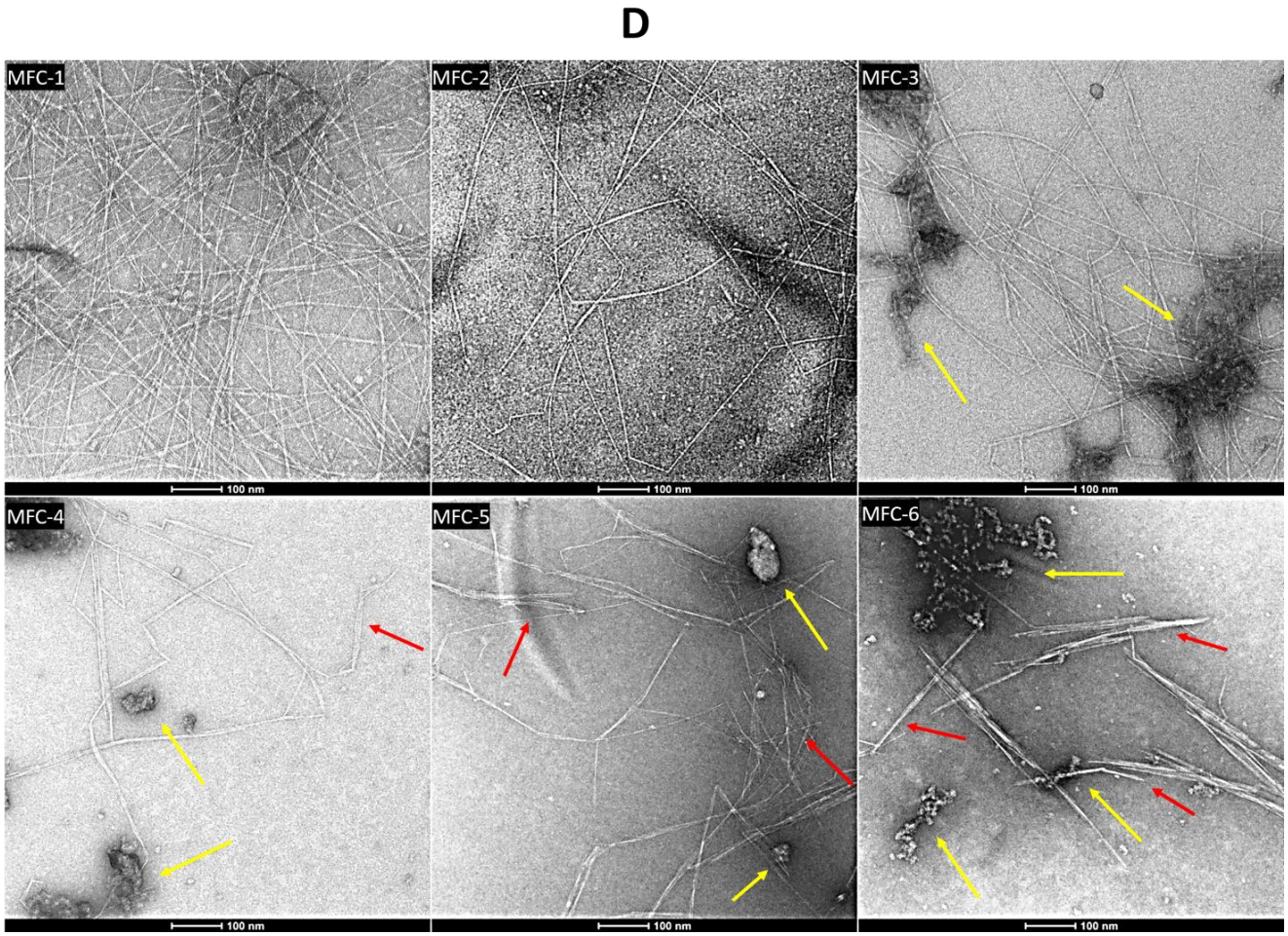

Figure 3.5: SEM (A and C) and TEM (B and D) of DOPR and MFC samples. Yellow arrows indicate degradation material deposited on cellulose fibrils surfaces, and red arrows show CNC bundles and aggregates. Scale bar in A = 10 µm and B, C and D = 100 nm. Original in colour.

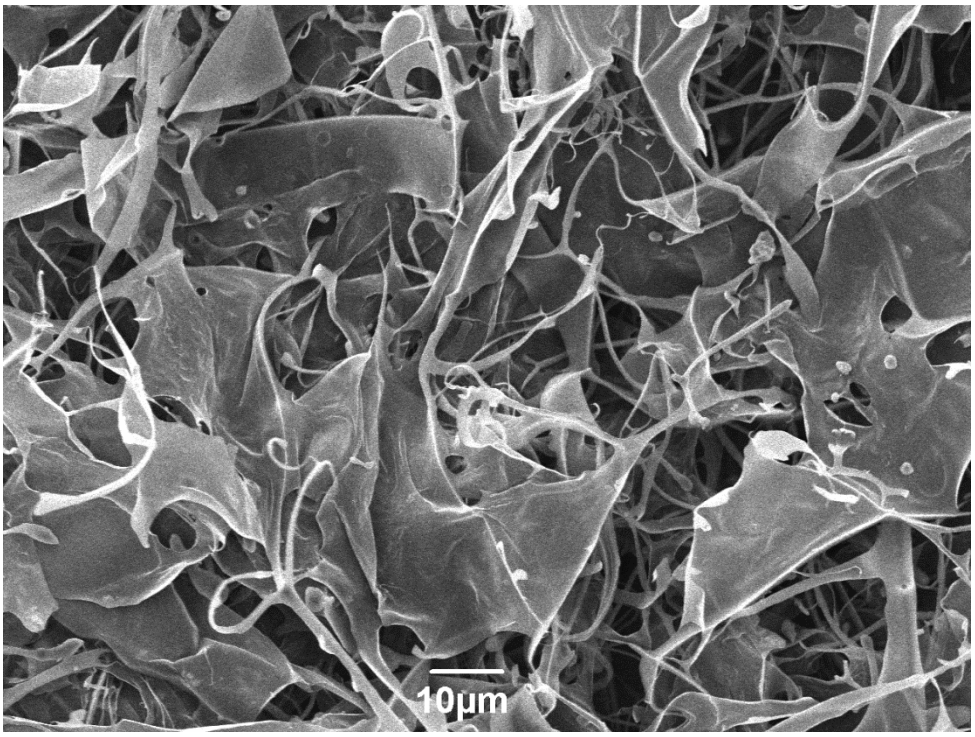

Figure 3.6: SEM of freeze-dried MFC-1. Scale bar = 10 µm.

The nanostructure of the fibrils become more evident using TEM because of its higher resolution, which by using the correct sample preparation, overlaying and aggregation of the individual fibrils are avoided.[174,175] The TEM image of DOPR fibres (**Figure 3.5B**) clearly shows non-fibrillated microfibrils and bulk cell wall fragments, indicating a poor level of fibrillation at this stage, as previously observed on its SEM image (**Figure 3.5A**). The TEM images of the MFCs (**Figure 3.5D**) present high levels of fibrillation, comprising individual microfibrils (10–40 nm wide), elementary fibrils (3–5 nm wide) and even CNC-like aggregates (5–40 nm wide and 200–500 nm long). Again, some amorphous "degradation matter" can be observed on the surface of fibrils from MFC-3 to MFC-6 (yellow arrows in **Figure 3.5D**), which might correspond to pseudo-lignin "aggregates" observed in the corresponding SEM images. The reason for their change in shape might be due to their dispersion and disaggregation during the sonication step of sample preparation. The presence of some CNC aggregates can also be

observed on samples treated ≥180 °C (red arrows in **Figure 3.5D**). The formation of CNC-like structures at higher temperatures can be explained by the *Hydrothermal Microwave-assisted Selective Scissoring*, *i.e.* the Hy-MASS concept, which can be translated as the hydrolysis (scissoring) of the labile disordered or "amorphous" domains of the cellulose chains, leaving behind its crystalline fraction that gives form to CNC structures.[133,176,177] Although the nature of these disordered regions is still not fully clear, it is known that they are located at cellulose chain ends and regions where the fibrils were mechanically damaged.[178] These can be identified as kinks and bends on the fibrils as previously suggested in the literature.[179,180] Furthermore, the formation of CNC aggregates can be a result of *denaturation* of cellulose fibrils when exposed to high temperatures or drying, wherein the native "twist" of the fibrils is shortened, creating disordered hydrolysable domains while crystalline domains becomes highly aggregated and more recalcitrant to hydrolytic attack (**Figure 3.7**).[181] Nevertheless, the above results suggest that having the microwave-assisted treatment of the biomass under *hydrothermal* conditions is crucial for the fibrillation of the cellulosic fibres and formation of nanocrystals.

The formation of MFC via additive-free hydrothermal microwave treatment is one of the great achievements of this thesis. Mainly because, as discussed before, conventional preparation of MFC involves the use of mechanical treatments requiring large amounts of energy to achieve fibrillation.[182] However, microwave treatment was able to achieve similar levels of fibrillation by catalysing the extraction of microfibrillar pectin and hemicelluloses which binds cellulose microfibrils together.[183] Direct visualisation of such polymeric matrix interlinking cellulose microfibrils has been previously reported.[184]

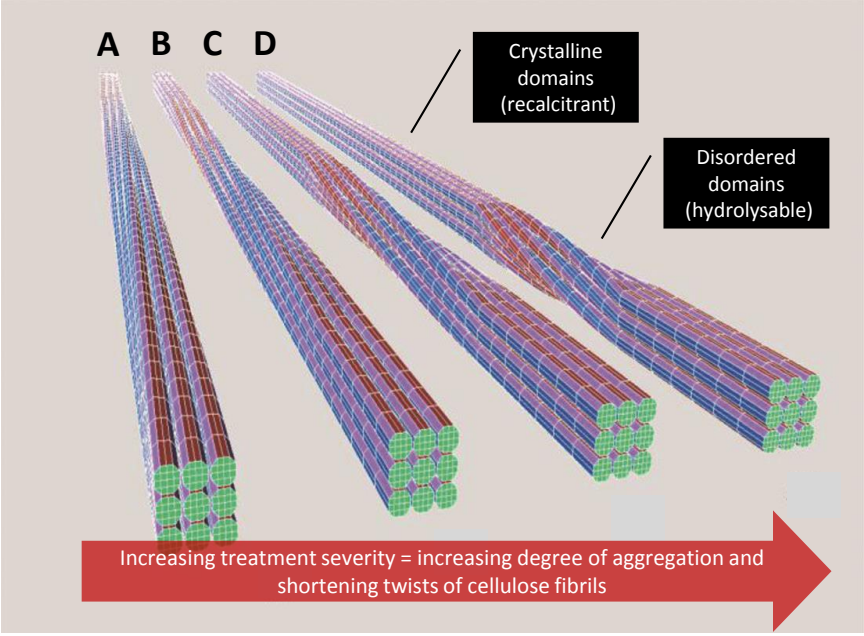

Figure 3.7: Models of cellulose microfibrils showing increasing degree of aggregation with increasing treatment severity. A: native fibrils, B: 35% aggregation, C: 65% aggregation and D: 85% aggregation. Adapted from ref. 181. Original in colour.

3.1.1.3 Confocal laser scanning microscopy

Confocal laser scanning microscopy (CLSM) was used for the identification and spatial distribution of fluorophores (*e.g.* cellulose, hemicellulose, lignin, proteins, phenolics)[64,185,186] in native and treated biomass.[187–192] Complementing electron microscopies, CLSM helps to identify and understand the distribution of recalcitrant degradation products (*i.e. pseudo*-lignin) on the surface of MFCs cellulose fibrils. The process involves the unmixing autofluorescence of *lignin-like* from that of *cellulose-like* components, respectively, based on referential autofluorescent emission (excitation at 405 nm) of lignin extracted from DOPR and commercial cellulose (see **Figure 3.8**).[188,189,193]

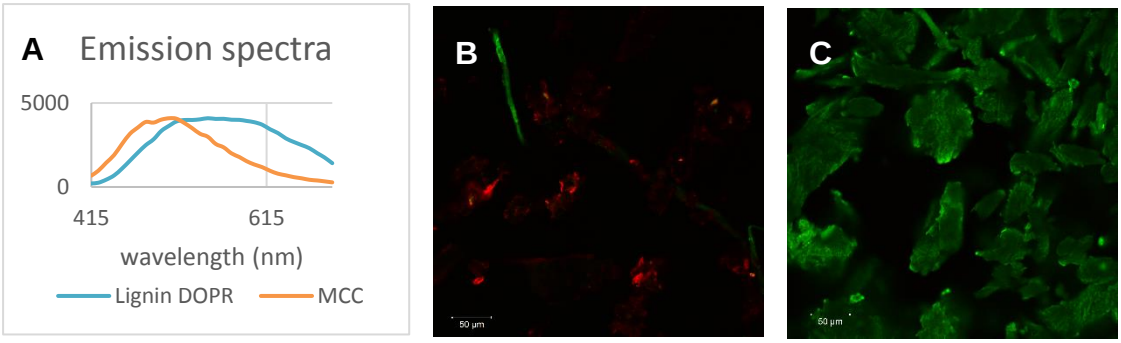

Figure 3.8: Fluorescence emission spectra (A) and confocal images of references, lignin from DOPR (B) and microcrystalline cellulose (C). The red colour refers to the lignin component and green to the cellulose component. Green fibres in lignin image (B) correspond to filter paper in order to show the efficiency of the method to unmix lignin from cellulose components. Original in colour.

The montage of the confocal fluorescence images (containing cellulose-like, lignin-like and both components combined) from DOPR and MFCs is presented in **Figure 3.9**. As can been seen in **Figure 3.9B**, the lignin-like component in DOPR is negligible whilst the cellulose-like component is dominant. However, with increasing temperature of HMT, more of the lignin-like component increases on the surface of MFCs, especially at ≥180 °C (MFC-4 to MFC-6, **Figure 3.9N**, **Q** and **T** respectively). This lignin-like matter was thought to be composed of re-condensed/re-polymerized native lignin,[133] but as discussed earlier, given the low content of native lignin in the starting material (*i.e.* DOPR, see **Table 3.1**), this lignin-like matter is more likely to be comprised of *pseudo*-lignin.[158–160] Chemically speaking, *pseudo*-lignin is quite similar to lignin (it can also contain lignin oligomers),[158,194] hence fluorescence emission similar to that of lignin can be expected.[161] In fact, the reference used for creating the lignin-like component is based on the emission spectrum of Klason lignin extracted from DOPR, which may contain contributions from *pseudo*-lignin fluorophores formed during the acid extraction.[195] Furthermore, cellulose autofluorescence, a debatable statement, since it is not clear if the latter derives from cellulose structure[186,196] or

from exogenous fluorophores formed during cellulose processing,[192] is believed to be quenched in the presence of lignin-like fluorophores,[186,189] which may also explain the gradual fading of cellulose-like component associated with the increasing temperature of treatment.

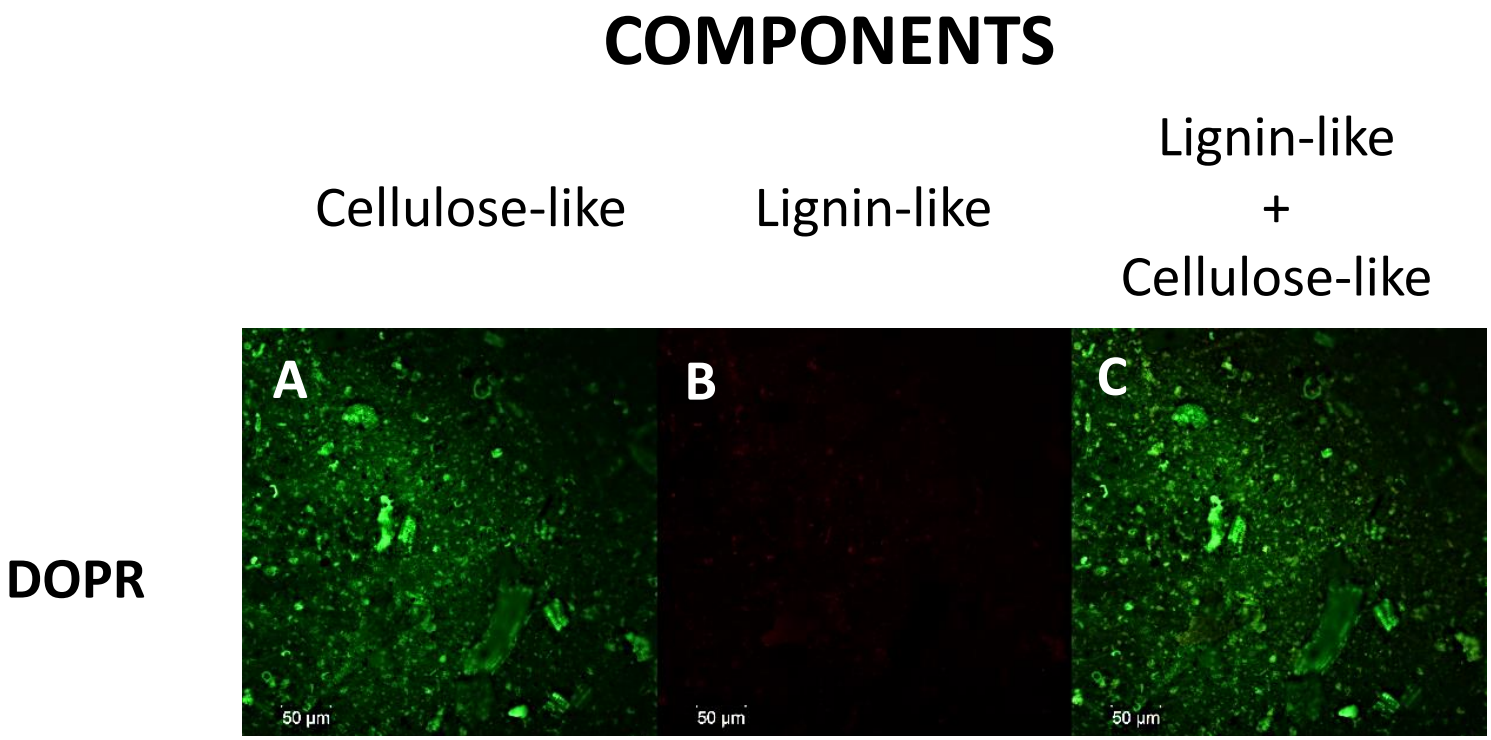

MFC-1

MFC-2

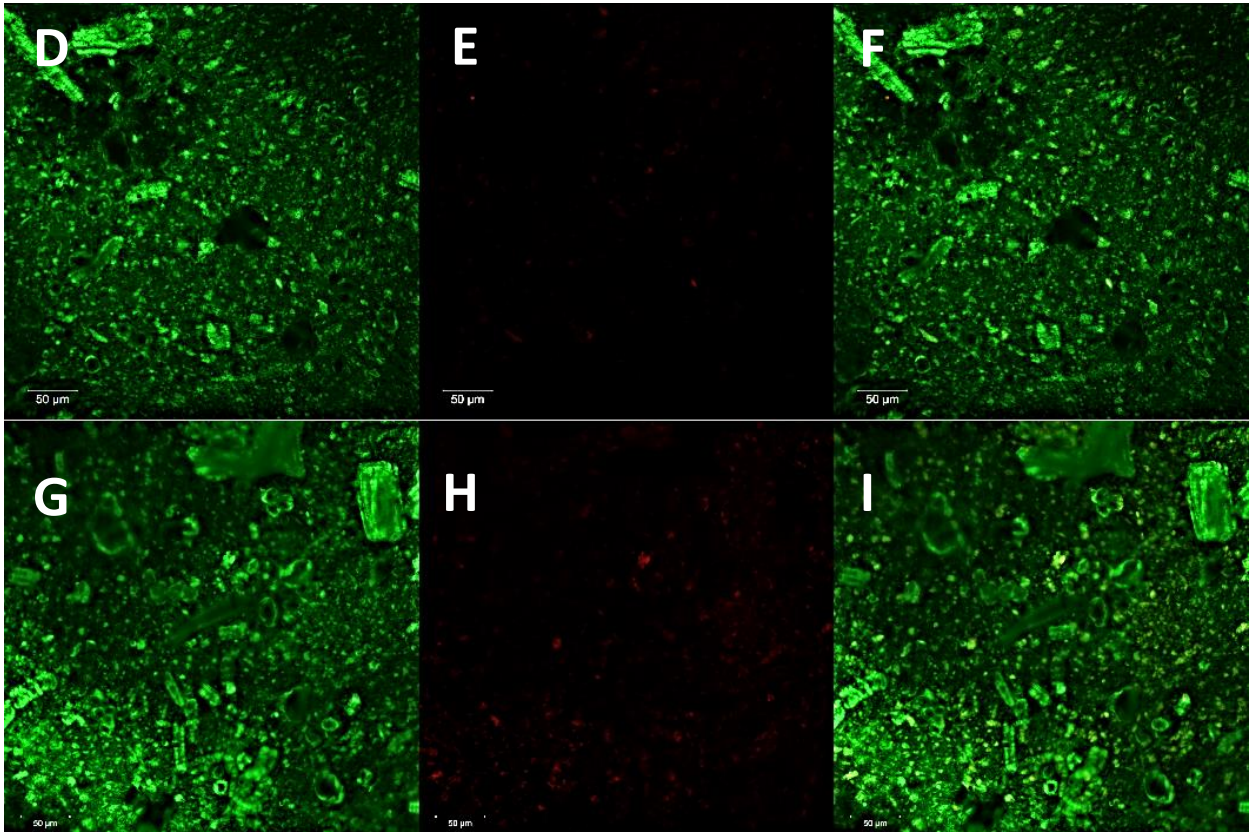

MFC-3

MFC-4

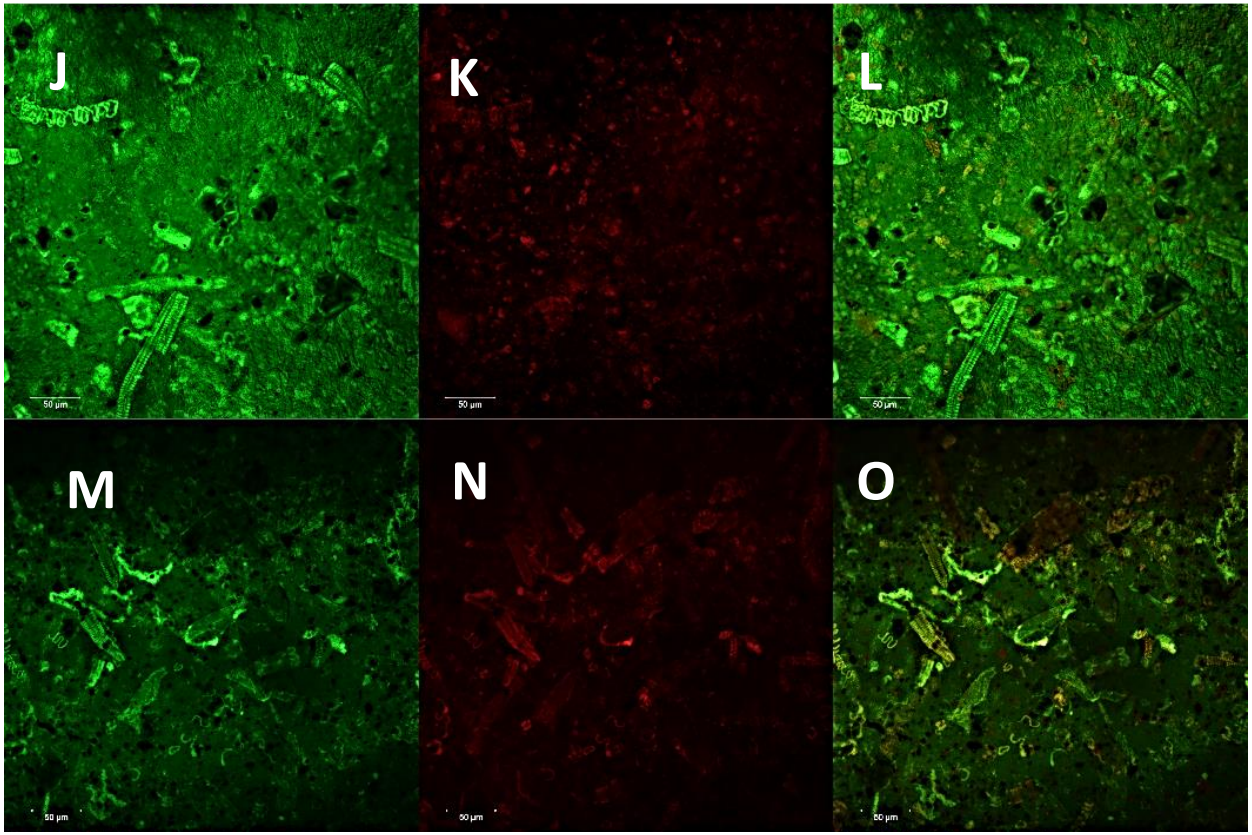

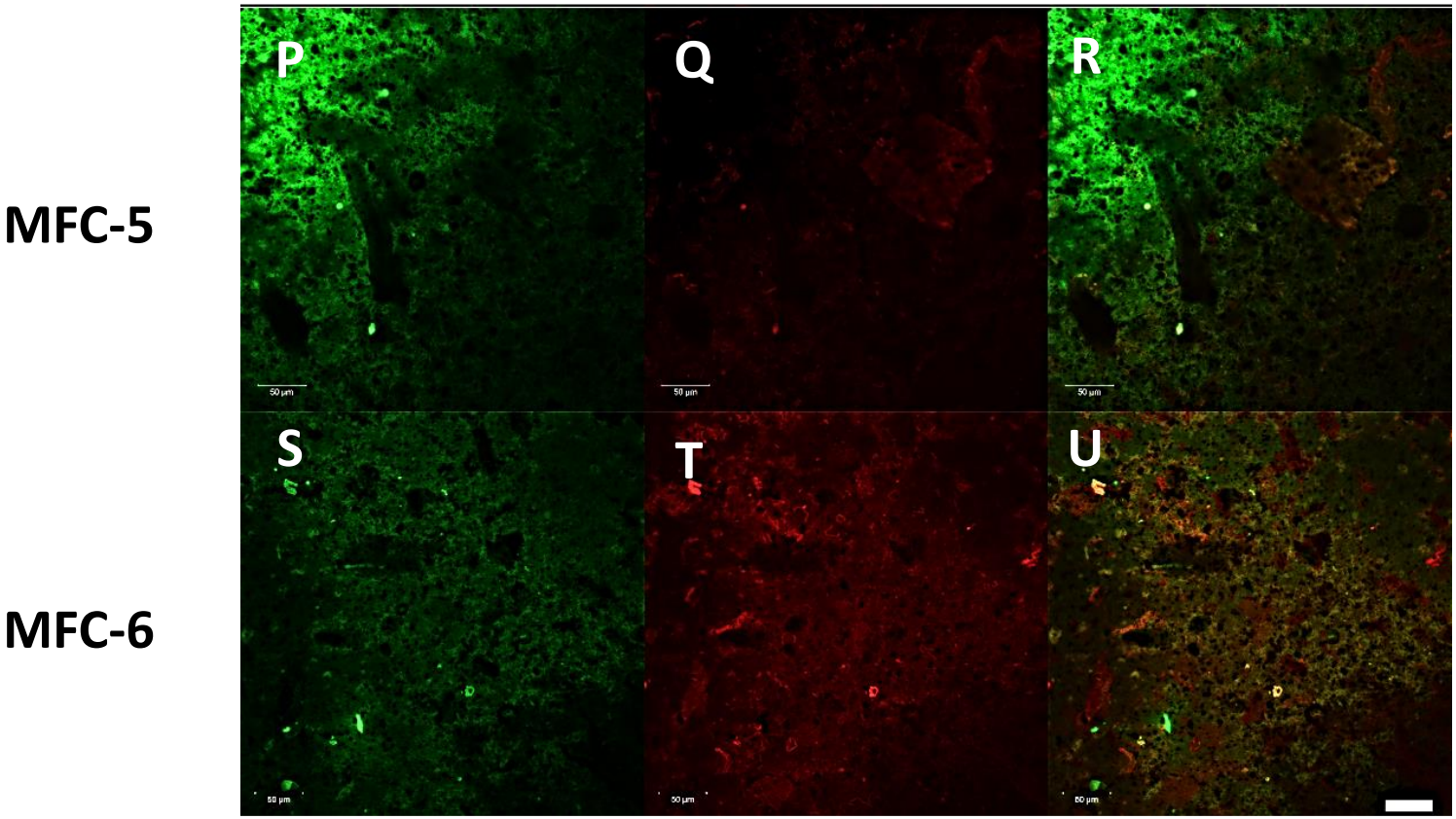

Figure 3.9: CLSM images of DOPR and MFC samples showing the unmixed cellulose-like component (first column), unmixed lignin-like component (second column) and the mixed component (third column). Original in colour.

3.1.1.4 Infrared spectroscopy

The infrared (ATR-FTIR) spectra of DOPR, MFCs and commercial cellulose (MCC) are presented in **Figure 3.10** and key assignments are summarised in **Table 3.2**. In general, it can be observed that DOPR and MFCs all presented strong absorptions typical of polysaccharides.[168,197,198] The inset in **Figure 3.10** clearly shows decreasing intensity of the uronic acid/ester absorbance band (*ca.* 1735 cm^{-1}) with increasing treatment temperature, confirming the gradual removal of pectin by HMT.[133,176] Due to the low content of lignin in the MFC samples, characteristic lignin bands (1600–1500 cm^{-1}) are not as evident as for polysaccharides bands, which is the dominant components in DOPR and MFCs. Yet, the band at *ca.* 1520 cm^{-1} present in DOPR, could correspond to the aromatic structure of lignin[199,200] (or even an indication of amide bands of protein).[197] Since this band seems not to be present in MFC samples, it could be deduced that lignin (and/or protein) has been extracted to the liquid phase (hydrolysate analysis will

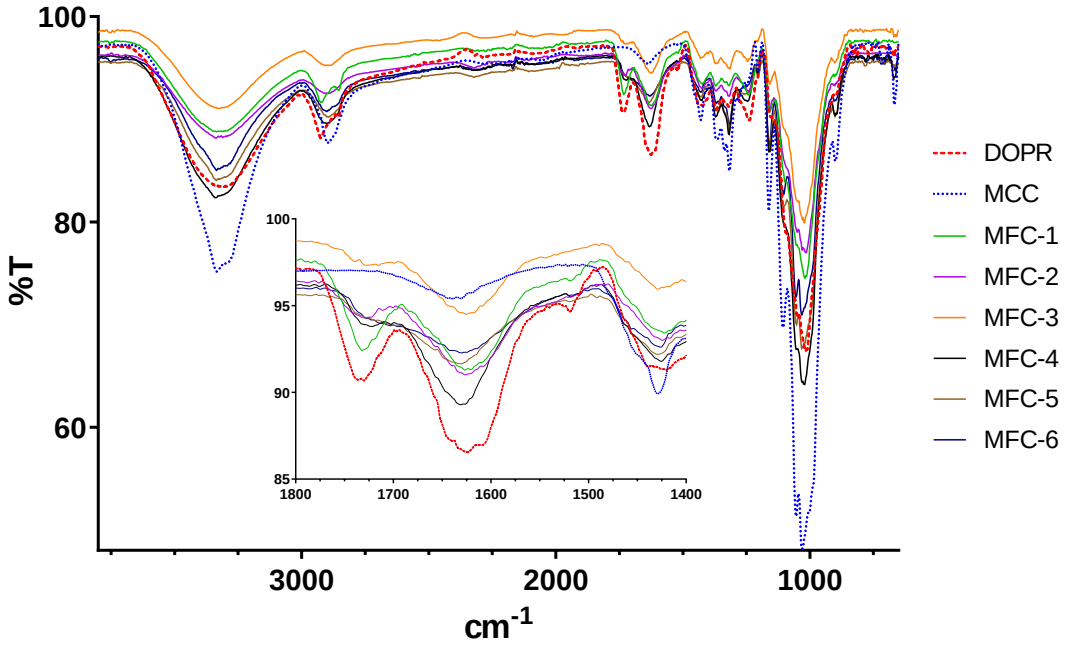

Figure 3.10: ATR-FTIR spectra of DOPR and MFCs. Inset expands ester and acids region. Original in colour.

be discussed later). Absorptions at *ca.* 1630–1620 cm^{-1} and *ca.* 1320 cm^{-1} could come from contributions of recalcitrant organic salts like calcium oxalate, previously identified in several biomasses,[201,202] cellulosic material from citrus[133] and bound water.

Table 3.2: Approximated assignment for major bands from ATR-FTIR spectra of DOPR, MFCs and MCC.[168,197,198,200,202,203]

Band (cm^{-1})	Assignment	Related compounds
3600–3200	$(O\text{-}H)_{\nu}$	all
2950–2850	$(C\text{-}H)_{\nu, \delta}$	C, P, H, L
1740–1710	$(C{=}O)_{\nu}$	P, H, L
1645–1630	(bound $H_2O)_{\delta}$	all
1640–1600	$(C{=}C, COO^{-})_{\nu}$	P, H, L, S
1600–1500	$(C{=}C)_{\nu}$	L
1400–1250	$(C\text{-}H, C\text{-}O, COO^{-}, C\text{-}C)_{\nu, \delta}$	all
1200–1000	(polysaccharides backbone)$_{\nu, \delta}$	C, P, H
920–880	$(C\text{-}O\text{-}C$ glycosidic bonds$)_{\delta}$	C, P, H

C: cellulose, **P:** pectin, **H:** hemicellulose, **L:** (*pseudo*-)lignin, **S:** organic salts, **ν:** stretching, **δ:** bending.

3.1.1.5 Solid state ^{13}C CP-MAS NMR

The solid state ^{13}C CP-MAS nuclear magnetic resonance (SSNMR) spectra of DOPR and MFCs are presented in **Figure 3.11**. The spectra were divided in four distinct regions for ease of interpretation, based on characteristic signals for: pectin (yellow); aromatics (red); polysaccharides (green), and; aliphatics (blue).[168,204–206] Overall, the most predominant regions are those related to the

structure of cellulose and pectin. Pectin signals (carbonyls at 176–170 ppm, methoxyl at 54 ppm and rhamnose residue at *ca.* 18 ppm), however, gradually reduce with the increasing of HMT temperature, until almost complete disappearance in MFC-4 to MFC-6 (≥180 °C), leaving those spectra even more similar to that of pure cellulose.[204,205] Interestingly, a change in the ratio of surface/amorphous cellulosic C4 and C6 (84 ppm and 62 ppm, respectively) to interior/crystalline C4 and C6 (89 ppm and 65 ppm, respectively)[207,208] with the increasing temperature of treatment can also be observed on MFCs spectra (black arrows in **Figure 3.11**). Apart from the removal of amorphous matter, such as pectin, from the cellulosic matrix, this also suggests that amorphous or disordered regions of cellulose microfibrils from MFC were also gradually hydrolysed during the treatment, which agrees well with the formation of cellulose nanocrystals at higher temperatures as evidenced by TEM (see earlier **Figure 3.5D**).These findings are in good agreement with the abovementioned results as well as with the previous literature.[133,176] Furthermore, some indication of lignin and/or protein structures (aromatic and aliphatic regions)[204,209–211] could be barely observed in DOPR and hardly evidenced in MFCs ^{13}C NMR spectra. This is probably due to the initial low concentration of these compounds in the starting material and their consecutive leaching or hydrolysation to the liquid phase during HMT, as anticipated by ATR-FTIR results. Also, lignin is a known to give weak signals in common CP-MAS ^{13}C NMR experiments due to its high molecular rigidity and lack of protons. Hence, optimized NMR experiments are required for quantitative data.[212,213]

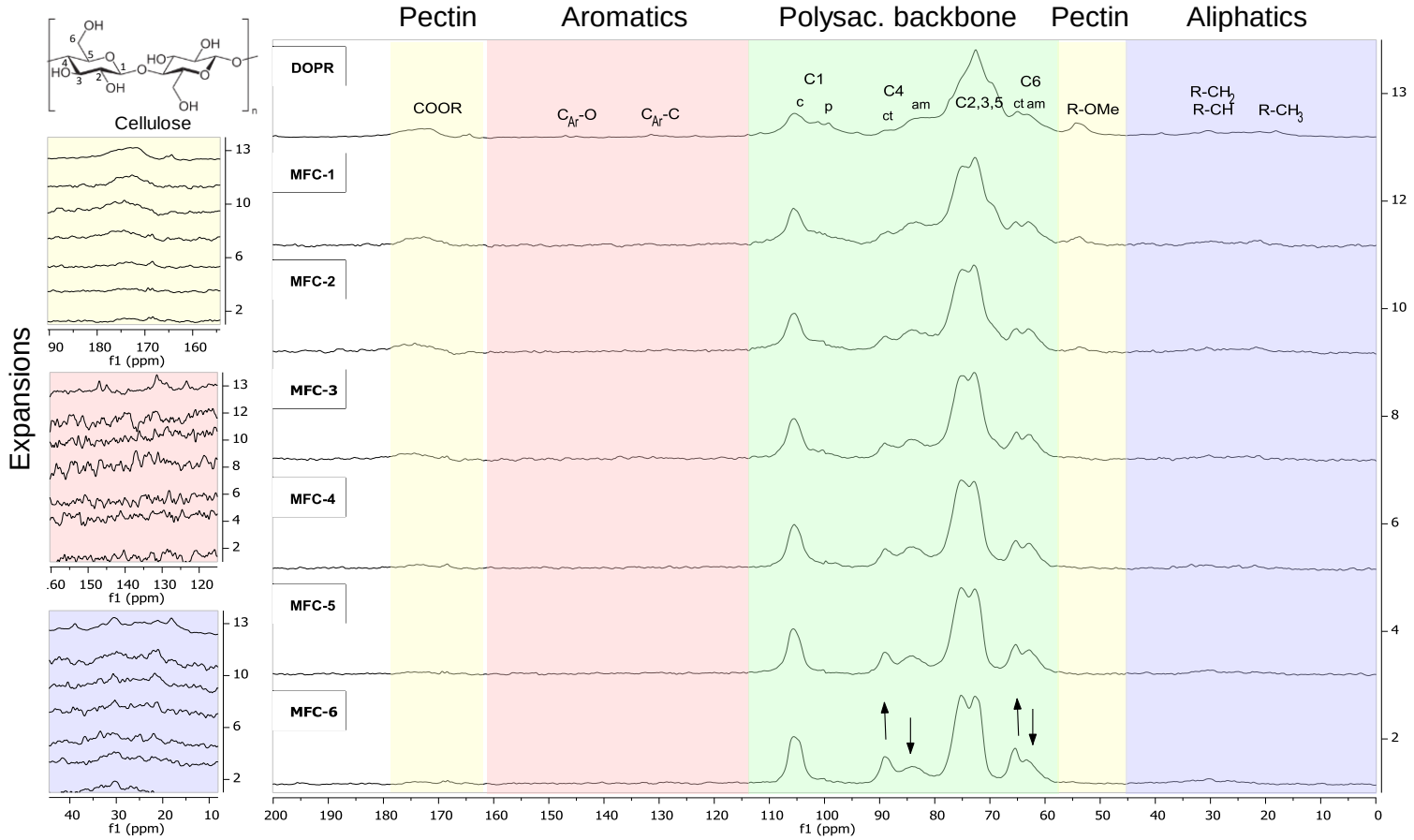

Figure 3.11: Solid state ^{13}C NMR spectra of DOPR and MFCs. Cellulose structure shown at the top left corner. Expansion of carbonyl, aromatic and aliphatic regions are shown on the left. Arrows indicate the change in the ratio of crystalline (cr) to amorphous (am) C4 and C6 of cellulose structure. C1 corresponding to anhydroglucose units of cellulose (c) and galacturonic acid units of pectin (p) is distinguished. Original in colour.

3.1.1.6 X-Ray diffraction and crystallinity index

The powder X-Ray diffraction (XRD) spectra of DOPR and MFCs and the respective calculated crystallinity indexes are presented in **Figure 3.12**. A diffraction pattern typical of semicrystalline cellulose type-I[143] containing crystalline regions, with main 2θ peaks at *ca.* 16°, 22° and 34.5°, and an amorphous contribution with a 2θ maximum *ca.* 18° can be observed in all samples (**Figure 3.12A**).[104,147,214,215] As the crystalline peaks of cellulose present in the samples become sharper with increasing treatment temperature, the amorphous contribution (initially quite strong in DOPR) becomes gradually less evident in the MFCs. This is consistent with the increasing removal of amorphous matter (mainly pectin) from the biomass with the increasing severity of treatment, as confirmed by above results and previous reports.[104,133,176] Interestingly, extra crystalline diffraction peaks (*ca.* 15°, 24.5°, 30°, 31.5° and 35.5°) are observed in the MFCs spectra (black arrows in **Figure 3.12A**), which are probably due to mineral salts[214] and calcium oxalate.[133,201,202] These biominerals are ubiquitous in plant biomass, and are usually stored in the vacuoles and cell walls.[201,214,216] They perform important functions in the plant, such as protection, growth regulation, physiological signalling and structure.[201,216] The presence of these biominerals in the samples can be further confirmed by previous discussed analyses, naming, ICP-OES (see earlier **Figure 3.1**) and ATR-FTIR (see earlier **Figure 3.10**). Although these biominerals were proved to be recalcitrant in the MFC cellulosic matrix even after treatment at 220 °C (MFC-6), by treating MFC with hydrochloric acid, the solubilisation of the biominerals can be achieved as previously reported by de Melo *et al*.[133]

Cellulose crystallinity is an important parameter for cellulose-based materials, affecting biodegradability, saccharification and thermal and mechanical properties of the materials.[143,214] Crystallinity index (CI) is a measure of the relative amount of crystallinity in cellulose materials, which can be measured by several methods.[143] Segal's method[144] based on XRD data was used in this study and the CI of the studied samples is presented in **Figure 3.12B**. The CI of MFC samples was as *ca.* 33% higher than in the corresponding starting material (DOPR). It also increased almost linearly in relation to the increasing temperature of HMT, going from 32% in MFC-1 to 61% in MFC-6, confirming the Hy-MASS concept of gradual removal of amorphous matter from the cellulosic matrix, including the amorphous domains from the cellulose microfibrils, with the increasing treatment temperature.[133] Although Segal's method is a convenient method to relatively compare CI values across cellulosic samples, it usually overestimates the figures, giving higher values than those found by other methods (NMR integration or XRD deconvolution).[104,143]

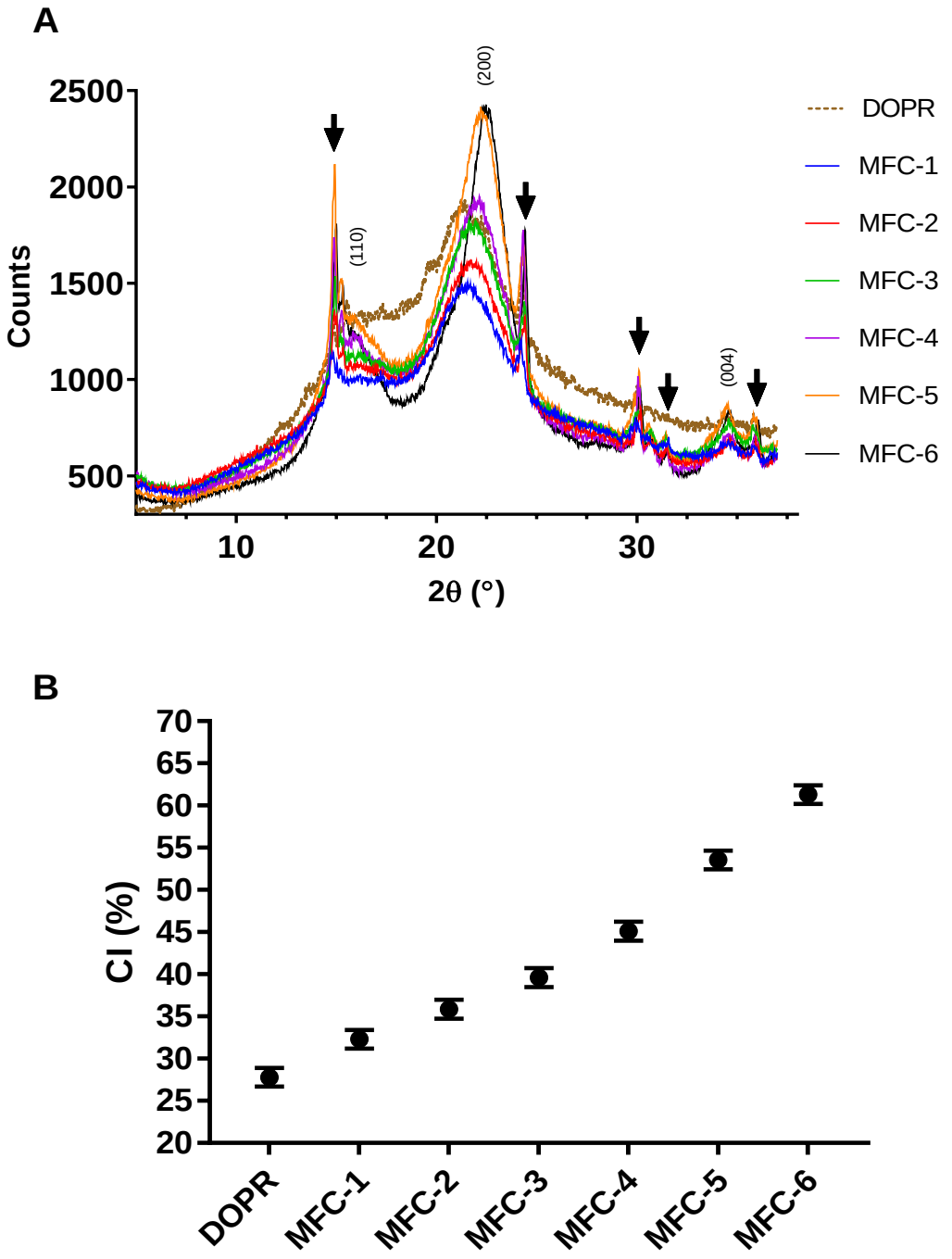

Figure 3.12: XRD spectra of DOPR and MFCs (A), highlighting calcium oxalate/biominerals peaks (arrows) and cellulose diffraction planes according to Miller index notation (hkl). Crystallinity index of DOPR and MFCs calculated from XRD data (B). Original in colour.

3.1.1.7 Thermogravimetric analysis

The derivative thermogravimetric (DTG) curves of the analysed samples are presented in **Figure 3.13**. The presented DTG curves can be divided into four distinct areas corresponding to: the evolution of moisture and volatiles (25–140 °C, T_d ~85 °C); the decomposition of pectinaceous matter (140–270 °C, T_d ~240 °C); the decomposition of cellulose (270–400 °C, T_d ~345–360 °C), and; the residue (400–700 °C, T_d ~500 °C; this should not be confused with the residual char left after sample's pyrolysis).[155,166,217] As already summarised in **Table 3.1**, each of these regions (apart from the last one) were used to calculate the proximate content of moisture, pectin and cellulose in the samples (see corresponding TG mass loss curves in **Figure 3.14**). Hemicellulose decomposition (220–330 °C)[136,137] could not be distinguished from that of cellulose and pectin due to their overlapping bands, besides, previous research confirmed that hemicellulose decomposes simultaneously with cellulose due to strong interactions between these components, leading to a broadening of the corresponding band.[155,168] A decrease in the pectin band (T_d *ca.* 240 °C) of the samples associated with the increasing severity of treatment (therefore the Hy-MASS concept) is observed in **Figure 3.13** and agrees well with the previous discussed results of this thesis and from the literature.[133,176] While the pectin decomposition band gradually decreased in the samples after HMT treatment, on the other hand, the cellulose band increased in intensity, narrowed and became more thermostable. The narrowing of the band is probably due to the decomposition of hemicellulose, which caused the broadening of the band in the first place.[155] The increase in the cellulose thermostability can be observed by the shifting of the band to the right

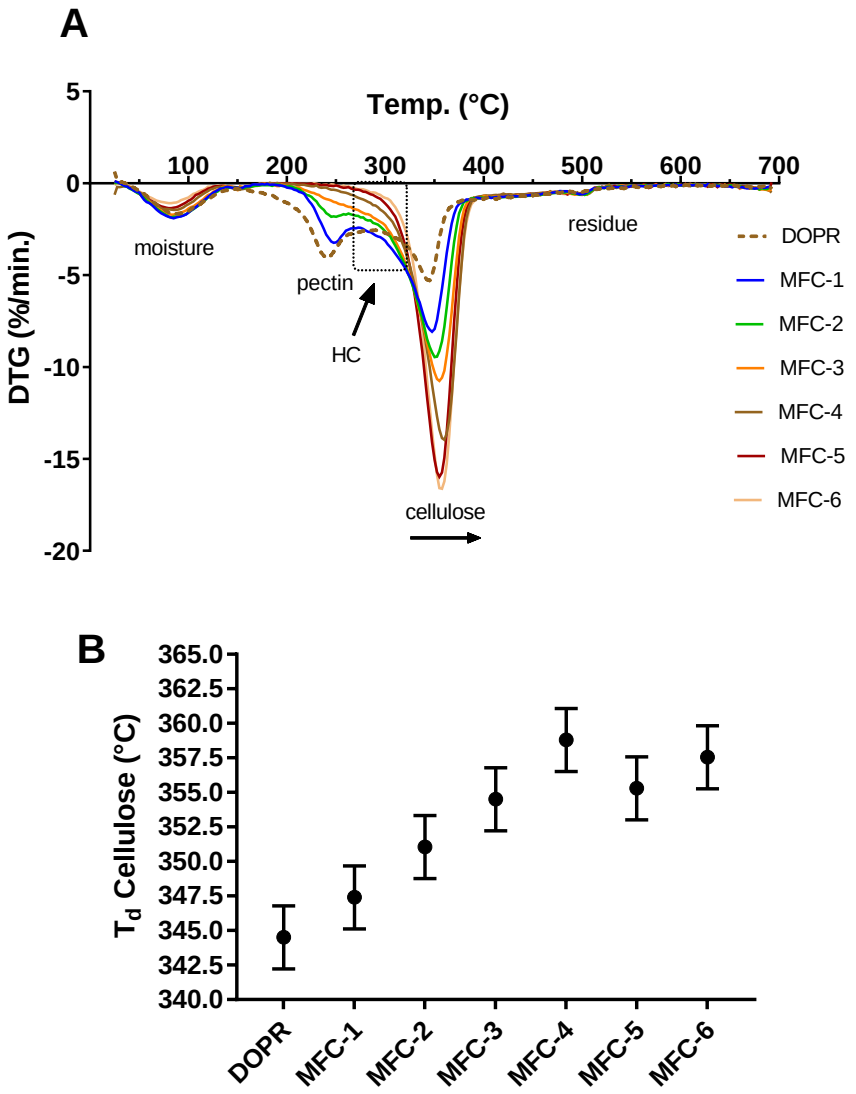

Figure 3.13: DTG curves of DOPR and MFCs (A). Dotted area represents possible region of hemicellulose (HC) decomposition. Arrow indicates the increasing T_d of cellulose (B).

side of the graph (see black arrow under cellulose band in **Figure 3.13A**), where T_d gradually increases from 345 °C in DOPR to a maximum plateau of *ca.* 360 °C in MFC-4 onwards (no significant difference was found among T_d of MFC-4, MFC-5 and MFC-6). This can be linked to the relative increase of crystallinity in the samples, as explained previously, since thermal behaviour of cellulose is also governed by this parameter.[214] The small band with T_d *ca.* 500 °C corresponding to the residue region presented a fixed mass loss of *ca.* 8% in all studied samples, hence it must be associated with some recalcitrant matter present in the biomass.

Based on previously discussed results, one possible candidate is calcium oxalate (CaC_2O_4), since its decomposition to calcium carbonate ($CaCO_3$) with the loss of carbon monoxide occurs at the range 400–530 °C with T_d *ca.* 500 °C.[218] In fact, ATR-FTIR spectra of the residual char was found to be very similar to that of $CaCO_3$ (**Appendix II**). Furthermore, a previous publication[133] showed that in contrast with MFCs produced from acid-free treated DOPR, *biominerals-free* MFCs produced from acid-treated DOPR (called CMC samples in the paper), did not present a decomposition band around 500 °C in their DTG curves, which further supports the hypothesis that this band derives from the decomposition of biominerals. Although the evidences support that biominerals are the main cause of that band, decomposition products arising from other recalcitrant components, such as (*pseudo*-)lignin and char, could also be a source of that degradation band.[155,166,167,219,220]

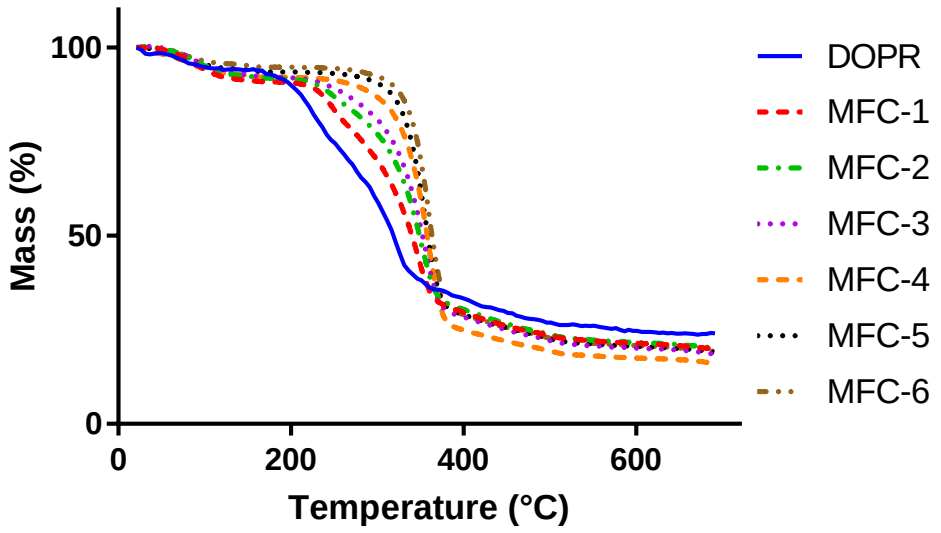

Figure 3.14: TG curves of DOPR and MFCs. Original in colour.

3.1.1.8 Gel permeation chromatography

Gel permeation chromatography (GPC) or size exclusion chromatography (SEC) is used for the separation of polymeric analytes based on their size, where important parameters such as molecular mass distribution (MMD), weight, number, size and viscosity average molecular weight (M_w, M_n, M_z and M_v respectively), dispersity (Đ) and degree of polymerisation (DP) can be obtained.[221–223] GPC coupled with a multi-angle laser light scattering (MALLS) detector was used to analyse the dissolved MFC samples, without any prior cellulose derivatisation. This technique is claimed to be the best available choice for the direct and absolute molar mass measurement of dissolved cellulosic materials.[148,221–223]

Table 3.3 summarises the GPC data of the MFC samples. In general, M_w, and consequently, Đ and DP remained almost unaltered in MFC-1, MFC-2 and MFC-3, which infers that relatively little hydrolysis of the amorphous domains of the cellulose chains occurs up to 160 °C. However, in MFC-4 (produced at 180 °C), a significant decrease in M_w, Đ and DP is observed, implying the onset of hydrolysis of the amorphous cellulosic domains from the lignocellulosic matrix.[133,177,224] Further drastic decrease of M_w, Đ and DP is observed for MFC-5 and MFC-6 (produced at 200 °C and 220 °C, respectively), where, for instance, molecular mass of MFC-6 (0.13 Mg mol^{-1}) is close to 10-fold lower than that of MFC-1 (1.12 Mg mol^{-1}). The much lower M_w, Đ and DP of MFC-5 and MFC-6 (in comparison with the other samples) support the existence of shorter crystalline-rich cellulosic fibrils similar to CNC, as earlier discussed in the TEM analysis. However, since individualized CNC crystals have a much lower DP (60–350)[76,78,225] than that of MFC-5 or MFC-6, it is more likely that under those

conditions aggregates of CNC-like structure were formed rather than single CNC crystals. While native cellulose materials present DP on the range of 10,000–20,000, depending on source, plant tissue and plant cell wall type (primary or secondary),[168,226] MFCs produced here presented comparable DP values to those of processed cellulose materials (chemical and mechanical pulps, MFC and CNF) reported elsewhere (700–4,500).[223,227,228] Moreover, the fact that even at the most severe HMT conditions (220 °C) the DP value found for the respective MFC was considerably higher than the usual level-off degree of polymerization (LODP, *i.e.* limiting DP) of cellulose (100–400)[223,226] was not reached, suggesting that the fibrils and crystalline-rich fibrils fragments (CNC-like structures) could still be further hydrolysed to its most elementary structure, *i.e.* cellulose nanocrystal.

Interestingly, as shown in **Figure 3.15**, samples treated ≤180 °C presented a bimodal MMD (MFC-1 to MFC-4), while MFCs treated above 180 °C (MFC-5 and MFC-6) presented a unimodal MMD. Most probably, the first band appearing in the bimodal distributions corresponds to the lower molecular weight components of MFC, *i.e.* pectin and hemicellulose, which are almost completely hydrolysed at temperatures above 180 °C. In fact, Py-GC/MS data (**Figure 3.4**) further supports this claim since content of furfural, pectin and hemicellulose most common pyrolysis product,[229–232] is much lower in MFC-5 and MFC-6 (1.8%) when compared with the other samples (5–2.8%). The remaining unimodal band (higher molecular mass) must therefore correspond to the cellulose moiety in MFCs. Also, the narrowing of the cellulose band with the increasing temperature of treatment is intimately related to the decreasing dispersity of the samples, as shown in **Table 3.3**. Again, these findings are in good agreement with the previous literature,[133,167,177,224] which shows that above 180 °C amorphous

polysaccharides as well as disordered domains of cellulose chains are hydrolysed from the cellulosic fibrils present in the samples, leaving behind finely fibrillated, shorter and highly-crystalline cellulose fibrils.

Table 3.3: M_w, M_n, Đ and DP of MFC samples calculated from GPC data.

Sample	M_w (Mg mol^{-1})	M_n (Kg mol^{-1})	Đ	DP
MFC-1	1.12±0.05	43.9±2.4	25.7±2.1	6924±282
MFC-2	1.08±0.05	53.6±2.4	20.2±2.1	6663±282
MFC-3	0.99±0.07	53.2±3.4	18.7±3.0	6133±404
MFC-4	0.8±0.05	60.7±2.4	13.2±2.1	4952±282
MFC-5	0.3±0.07	51.9±3.4	5.7±3.0	1829±404
MFC-6	0.13±0.05	38.5±2.4	3.5±2.1	824±282

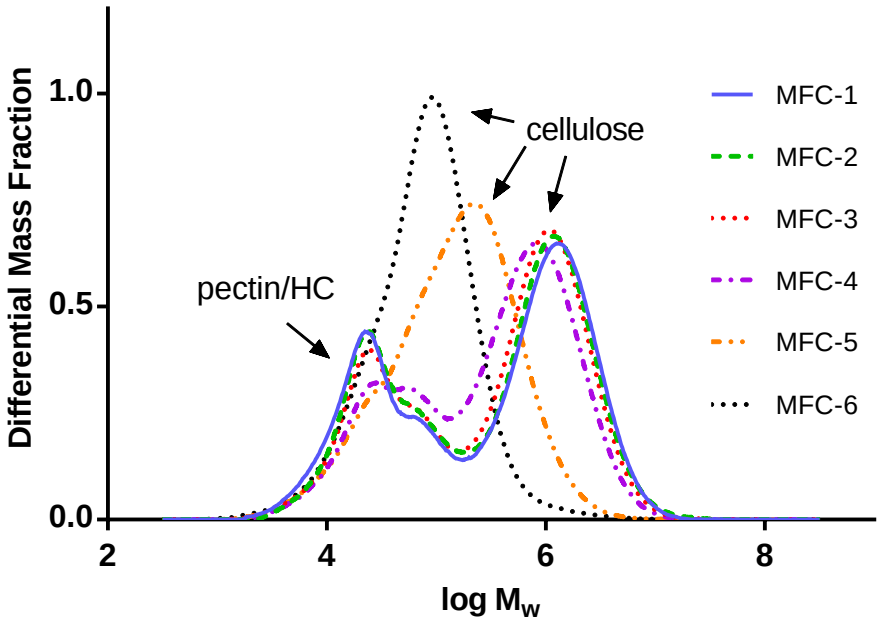

Figure 3.15: Molecular mass distribution (MMD) curves of MFC samples. In the MMDs, when bimodal, the first band corresponds to pectin or/and hemicellulose (HC) and the second band to cellulose. When unimodal, the single band corresponds to cellulose. Original in colour.

3.1.1.9 Porosimetry

It is well known that MFC and other nanocellulose materials usually possess a high specific surface area (SSA) due to its fibrillated nature of high aspect ratio and porous structure.[77,88,91,233,234] The porous structure of MFC can be derived from lumens, pits, nanopores and inter-cellular spaces inherently present in the plant cell structures[63,235,236] (see **Figure 3.16**). The porosity can be artificially formed through changes in the original structure of the feedstock after chemical/mechanical treatment, such as the removal of constituents of the cell wall (subtractive porosity), fibrillation and/or rearrangement of the cellulosic fibrils packing (constitutive porosity).[237–239] Most of the available techniques for the characterisation of porous materials cannot give an absolute value for parameters like SSA, porosity, pore volume (PV) and pore size (PS). Hence, these parameters are dependent on the method and the size of the probe used.[237]

Here, N_2 gas physisorption porosimetry, which is one of the most common technique used for micro-/mesoporous materials, was used for assessing the porosity of MFCs, where BET and BJH approximation models were used to

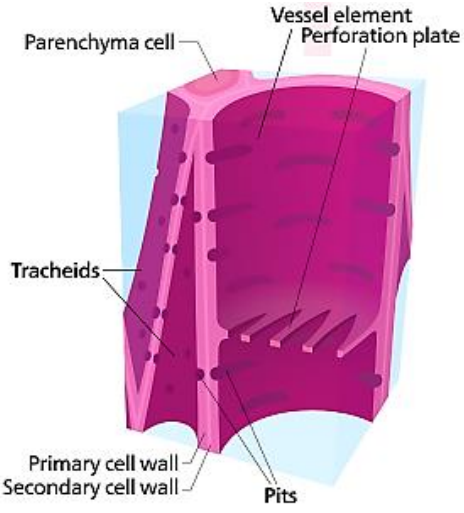

Figure 3.16: Cross-section of xylems cells (ref. 240). Original in colour.

calculate SSA and PV & average PS, respectively, from the physisorption isotherms (see **Table 3.4**).[239,240]

Table 3.4: N_2 physisorption porosimetry results for DOPR and MFC samples.

Sample	BET Surface Area (m^2g^{-1})	Pore Volume (cm^3g^{-1})	Pore Size (nm)
DOPR	0	0	0
MFC-1	10.2±10.9	0.02±0.03	2.9±25.5
MFC-2	3.3±10.9	0±0.03	19.4±25.5
MFC-3	21.1±10.9	0.06±0.03	48.2±25.5
MFC-4	28.8±10.9	0.08±0.03	6.9±25.5
MFC-5	0.1±10.9	0±0.03	0±25.5
MFC-6	22.1±10.9	0.07±0.03	4.5±25.5

In general, an improvement of the porous structure of the material can be observed after HMT at any temperature, since DOPR was found to be a non-porous material while MFCs presented some porous structure. Regarding SSA and PV of the studied MFCs, they both followed the same trend, where mean values increased to a maximum in MFC-4 (29 $m^2\ g^{-1}$ and 0.08 $cm^3\ g^{-1}$, respectively), then sharply decreased to a minimum value in MFC-5 (0.05 $m^2\ g^{-1}$ and 0.003 $cm^3\ g^{-1}$, respectively) and finally increased back in MFC-6 to values close to those found in MFC-3 and MFC-4. Although these values are similar to those found in MFC extracted from wood pulp[241] or orange peel[133], as beforementioned, accessing the absolute value of SSA or PV is a hard task since sample preparation and porosimetry method will influence the results. Therefore, since the MFC samples were oven-dried and afterwards degassed at 90 °C for carrying out the N_2 adsorption experiments, hornification of the fibrils, *i.e.* the irreversible aggregation of the fibrils by interfibrillar hydrogen bonding,[173,174,242] has

inevitably taken place. Besides fibril aggregation, hornification can also lead to the disruption of the pores in the sample, consequentially reducing the surface area and pore volume.[171,234,242] Hence, it might be that more accurate SSA and PV values for MFC can be obtained by changing the sample preparation (drying method) or porosimetry method. For instance, Spence *et al.*[243] obtained SSA values of 40–110 m^2 g^{-1} for (un)bleached pulp MFC by using Congo red dye adsorption as porosimetry method, which does not require the pre-drying of the sample, hence giving more reliable estimations. Osong *et al.*[88] reported that SSA of nanocellulose materials is highly dependent on the drying method used in the sample preparation, *e.g.*, SSA values of 304, 262 and 117 m^2 g^{-1} were found when the material was dried by supercritical CO_2, liquid CO_2 evaporation and *tert*-butanol freeze-drying, respectively. It is also important to note that according to the ANOVA test, the statistical difference among the means of SSA and PV are small (SSA data p-value = 0.047 and PV data p-value = 0.038, for an $\alpha = 0.05$), hence it is difficult to draw any conclusion from that data, apart from the obvious difference between MFC-5 and the other samples, as well as the strong correlation between SSA and PV. However, a possible explanation for this pattern is the fibrillation of the cellulose fibres to microfibrils and the removal of amorphous polysaccharides and other components from the cellulosic matrix surface by means of the HMT treatment up to 180 °C,[133,167] leading respectively to the gradual exposure of the microfibrils surface (increasing SSA) and formation of subtractive and constitutive open pores in MFC structure (increasing PV). Yet, the significant decrease in SSA and PV of MFC-5 (produced at 200 °C) could be due to a total blockage of the open pores with *pseudo*-lignin formed above 180 °C. Interestingly, MFC-6 seems to have recovered the improved surface area and

pore volume, which infers that melting/relocalization of *pseudo*-lignin could have occurred at 220 °C. The average pore size of the MFCs ranged from 0 (MFC-5) to 48 nm (MFC-3), however, no significant difference among the means were found (p-value = 0.382 for an $\alpha = 0.05$).

According to the IUPAC classification of porous materials, most of the MFCs here studied are classified as mesoporous, since its average pore size ranged within 2-50 nm.[240] Bringing together the above presented porosimetry data with the SEM images (see earlier **Figure 3.5**), it is possible to conclude that MFCs present a hierarchical porous structure formed by macropores (observed in the SEM images) and mesopores (confirmed by the porosimetry data) able to provide external/internal pore diffusion and high surface area, which are important features required for most applications, such as adsorbents, filters, membranes, catalysis, supercapacitors, drug delivery agents and carbonaceous materials.[233,244,245] The low statistical significance found for the studied porosimetry of the MFCs (represented by large LDS error values in **Table 3.4**) can be due to the natural heterogeneity of the biomass, *e.g.*, presence of different tissues in the peel (albedo, flavedo, juice sacs, rigs, as shown in **Figure 1.7B**) or biological differences among fruits. Moreover, the obtained values were close to instrument limits of detection.

3.1.1.10 Water holding capacity

Due to the fibrillated nature of MFC, water can be held in the fibril network just like in a sponge, causing the swelling of the fibrils derived from the plant cell wall material.[246,247] Water holding capacity (WHC) values for DOPR and MFCs

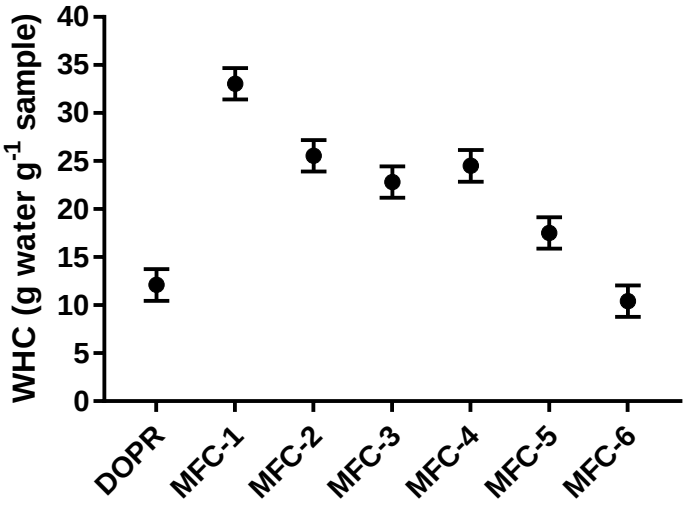

Figure 3.17: WHC of DOPR and MFC samples. Original in colour.

are presented in **Figure 3.17**. In general, all MFC samples presented higher or at least similar WHC values than that of the starting material, DOPR. The WHC increased almost 3-fold from DOPR (12 g water g^{-1} sample) to MFC-1 (33 g water g^{-1} sample), then it gradually decreased from MFC-2 to MFC-4 (*ca*. 23–25 g water g^{-1} sample), MFC-5 (18 g water g^{-1} sample) and eventually reached its minimum value in MFC-6 (10 g water g^{-1} sample). This trend is in good agreement with previous results, showing that WHC is highly influenced by the temperature of the HMT, where higher values are achieved at lower temperatures of treatment.[133,176] Mat Zain *et al.*[147] also showed similar results, where the nanocellulose material derived from citrus waste presented higher WHC than the starting material (13 and 9 g water g^{-1} sample, respectively). Interestingly, although the latter study used conventional treatments (alkali, bleaching and acid hydrolysis of citrus waste) for the preparation of their nanocellulose, the greener approach used in this thesis also produces a nanocellulose material (MFC) with better WHC, independent of the severity of the treatment. The sharp increase in WHC from DOPR to MFC-1 may be related to structural changes in

the cellulosic fibres during the HMT, namely, the removal of pectin and other components and the fibrillation of the macrofibres to its nano- and microfibrils, accompanied by an increase in SSA.[133,147,246]

It is known that the ability of MFC to swell and retain water is closely linked to its improved surface area, porous structure and high aspect ratio. [83,91,248] The exposed surfaces contain numerous free hydroxyl groups (especially those from the amorphous regions) able to form hydrogen bonding and residual soluble structural polysaccharides (pectin and hemicelluloses) which leads to a strong 3D fibril network.[91,238,246,248] The gradual decrease of the WHC of MFCs with increasing treatment temperature, specially above 180 °C, is probably due to the effects related to the already discussed Hy-MASS concept.[133,176] The initial removal of pectin seems to positively influence the WHC of MFC, but the increasing removal of pectin/amorphous matter and the hydrolysis of amorphous regions of cellulose seems to reduce the ability of the fibrils to hold water in its gel-like structure, mainly because above 180 °C the fibrils are much shorter, less hydrophilic and present partially disrupted porous structure. Moreover, with the significant removal of amorphous regions of cellulose fibrils with the increasing of HMT temperature (see the CI data in **Figure 3.12**), much less hydroxyl groups are available for hydrogen-bonding with water. [246,248,249] The presence of recalcitrant *pseudo*-lignin on MFC-5 and MFC-6 surface could also be a cause for their increased hydrophobicity and consequently reduced WHC. Although literature confirms that WHC are intimately linked with the porous structure of a material,[83,91,248] the weak correlation observed between the porosimetry and WHC data of the MFCs studied here implies that the method and sample preparation chosen for assessing porosimetry was not the most

adequate, mainly due to inaccurate estimations driven by hornification effects. WHC is strongly correlated with mechanical strength[77] and rheological properties[147] of MFC, hence, controlling and understanding this property can help to define the most suitable application for these materials.

3.1.2 MFC application: hydrogels and films

As discussed earlier, MFC properties can be tuned to fit the desired application by controlling the parameters of the HMT, such as temperature. These properties reveal MFC as a promising feedstock for producing innumerable functional biomaterials.[96,250,251] Here, an investigation of MFC-based hydrogels and films, two important biomaterials for food, cosmetics and biomedical application, is presented.[91,252] Hydrogels could be formed from some MFC grades, presenting a fine and highly-interconnected 3D fibre network with improved or comparable rheological performance against conventional food and cosmetics rheology modifiers. MFC films presented a lamellar structure of a superimposed fibril network with interesting macroscopic features, *i.e.* flexible, strong and slow-degrading biomaterial.

3.1.2.1 MFC hydrogels

As already discussed, due to its high surface area, aspect ratio and composition (containing pectin and hemicelluloses), MFC can retain lots of water. Hence, when MFC is well-dispersed in water, a fine balance between the steric and volumetric effects due to its high aspect ratio and the non-covalent interactions (hydrogen bonding, ionic, host-guest and hydrophobic interactions) is achieved and a three-dimensional viscous network is formed through the cross-linking and entanglement of the fibrils at relatively low concentrations (0.1–6%).[250,253–257] This system could be regarded as a *hydrogel*,[253,256–258] however, not only neat water,

but also a mixture of water with some polar organic solvents (able to form hydrogen bonding), such as ethanol or acetone, can serve as a dispersion medium to support these structures.[250,258,259]

3.1.2.1.1 Initial characterisation

Samples of DOPR, MFCs and a commercial nanocellulose used as reference (NC) were suspended in water at 2% concentration (w/v), homogenised and tested for hydrogel formation by the inversion test (**Figure 3.18**). Before homogenisation, differences in the macroscopic features among the hydrogel precursors could be observed (**Figure 3.18A**). MFC-1 presented the best swelling and stability (no apparent phase separation or sedimentation) among all gels, followed by the NC and DOPR, which presented a small phase separation but high swelling. From MFC-2 to MFC-6, a clear phase separation was observed, however, samples DOPR, MFC-2, MFC-3 and MFC-4 still presented some swelling, while swelling in MFC-5 and MFC-6 was negligible, even at 3% concentration (**Appendix III**). This is probably related to the presence of residual amorphous polysaccharides or amorphous cellulose domains in samples produced ≤180 °C, which hold most of the available hydroxyl groups for interfibrillar and surrounding medium hydrogen bonding.[246,248] Moreover, the higher content of *pseudo*-lignin in those samples produced above 180 °C explain their higher hydrophobicity, hence phase separation and no swelling.

After the homogenisation of the precursor suspensions (**Figure 3.18B**), hydrogel was formed in some cases, as verified by the gel inversion test (**Figure 3.18C**). Based on this qualitative test, at 2% concentration, "real" gels were formed only

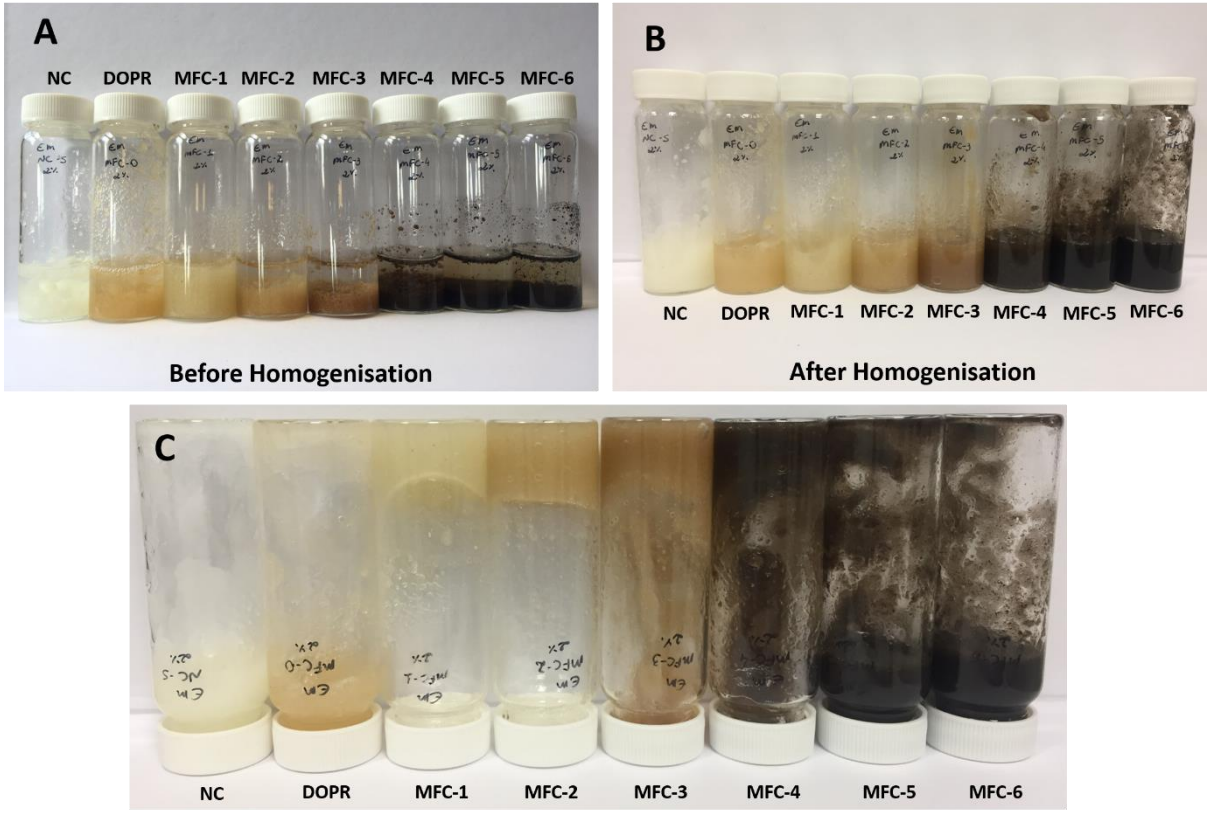

Figure 3.18: Commercial nanocellulose (NC), DOPR and MFCs 2% suspensions before homogenization (A), after homogenisation (B) and after vial inversion test (C). Original in colour.

in MFC-1 and MFC-2. Although all the other samples did not form a "real" gel at that concentration, it does not necessarily mean that they do not have a gel microstructure, but it could mean that, at those conditions, they formed a weaker or fluid gel structure[260–262] with a small yield stress (stress that must be applied to the sample before it starts to flow).[263] In fact, the flowability of a sample during the inversion test does depend on several variables, such as the vial type (size and geometry), sample mass and time of observation.[141,142] Nevertheless, at 3% concentration NC, MFC-3 and MFC-4 also formed strong hydrogels (see **Appendix IV**), meaning that the critical gelator concentration (CGC), *i.e.* minimum gelator concentration to form a gel[141] (the gelator in this case being the cellulose fibrils), was higher in those samples (CGC = 3% at r.t.) than for MFC-1 and MFC-2 (CGC = 2% at r.t., see **Appendix V**). This result also adds to the open debate if the weaker gels formed at 2% concentration is only a "pre-gel" transitional state to a real hydrogel structure, although several biological and artificial materials presenting such physical state also have important properties like stress-induced flowability and self-healing.[261]

3.1.2.1.2 Microstructure characterisation

To further understand the hydrogels' microstructure, SEM analysis was performed on the freeze-dried hydrogels (aerogels)[264] prepared by a liquid nitrogen slush method, which is supposed to keep most of the original material structure intact.[145] The SEM images in **Figure 3.19** show that MFC produced at low temperatures (MFC-1 and MFC-2) yields a strong, fine and highly interconnected 3D network gel of coiled ribbon-like fibrils (100-300 nm wide and several microns long) physically cross-linked. However, for samples prepared above 140 °C their network structure progressively becomes

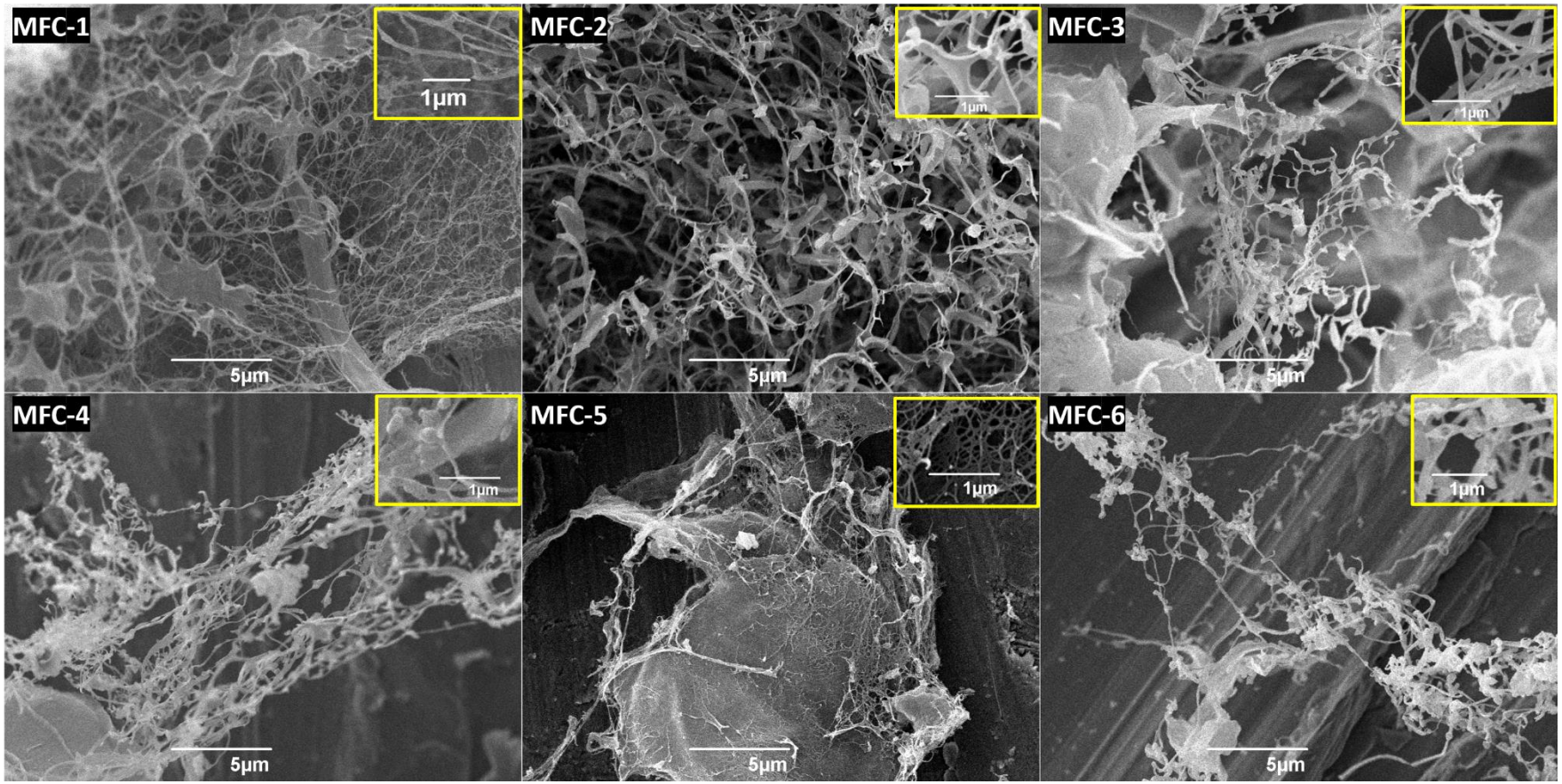

Figure 3.19: SEM images of MFC aerogels. Original in colour.

thicker (100-1000 nm wide) and less cross-linked, eventually leading to a very frail gel structure like that observed in MFC-5 and more drastically on MFC-6, where aggregation overcomes gelation. The weak gel structure of MFC-5 and especially of MFC-6 is probably related with the fact that above 180 °C, virtually all pectin, hemicellulose and most of the amorphous domains of cellulose have been hydrolysed from the fibril matrix. Furthermore, the presence of much shorter nanofibrils and CNC-like agglomerates might also hinder the formation of a fine and strong gel network on the latter samples (see **Figure 3.20**). As discussed in the literature, a stable hydrogel network must be able to hold water and swell, present amorphous and crystalline regions, and present sufficient electrostatic repulsion to avoid aggregation but enough to support gelation.[256,260] These results strongly correlate with the previously discussed qualitative analysis of the hydrogels (visual inspection and inversion test), confirming that MFC physical and chemical aspects tuned by the severity of the microwave treatment, such as presence or not of residual pectin/hemicellulose, *pseudo*-lignin and amorphous domains of the cellulose fibrils, aspect ratio and surface area are the main factors affecting each MFC gelation differently by controlling its ability to cross-link with other fibrils and hydrogen-bonding with surrounding water to form strong three-dimensional gel-like network.[141,253,256,265]

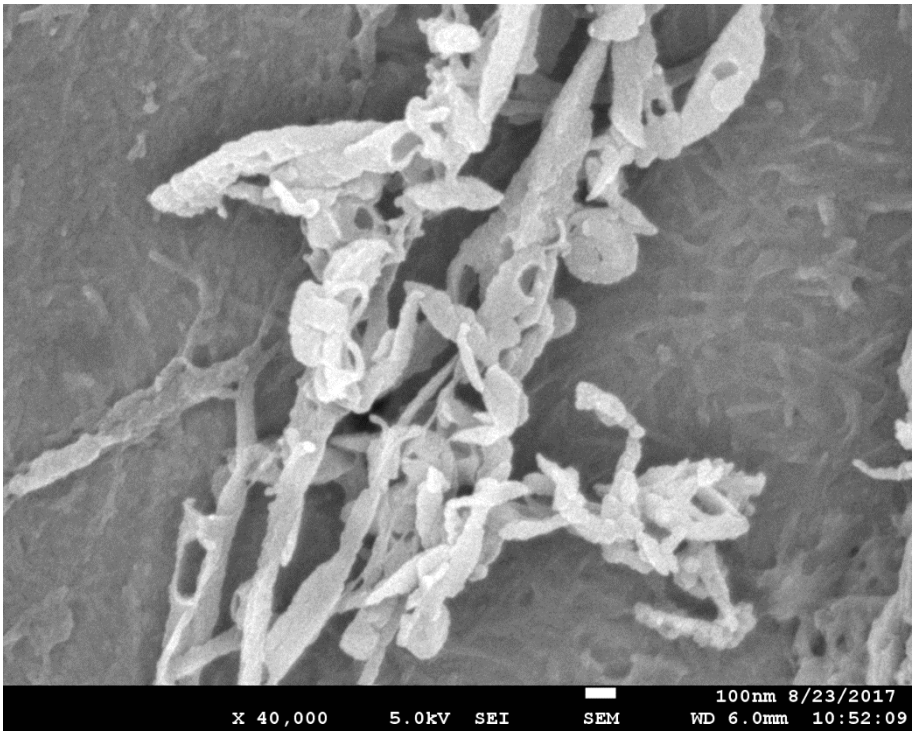

Figure 3.20: SEM image of MFC-6 aerogel showing the aggregation of CNC-like structures. Scale bar = 100 nm.

3.1.2.1.3 Rheological studies

Oscillatory rheology measurements were performed in order to evaluate the rheological behaviour of the most promising MFC hydrogel (MFC-1) on a macroscopic or supramolecular level.[256] The obtained results were compared to those from a commercial nanocellulose material produced from bleached wood pulp (NC) and a conventional food rheology modifier, xanthan gum (XG). Due to its higher sensitivity, oscillatory rheology is commonly preferred over rotational rheology for the characterisation of viscoelastic materials, *i.e.* materials that behaves like solid (elastic component) and liquid (viscous component) in the same time, such as low-viscosity liquids, dispersions, polymer melts, emulsions, gels, pastes, and even stiff solids.[266,267] The most common oscillatory tests are amplitude and frequency sweep. In an amplitude sweep test, shear strain amplitude is varied (γ usually 0.001–1000%) while the angular frequency and

temperature are kept constant (See **Figure 3.21A**)[268], giving insight on the deformation behaviour of a viscoelastic material. In a frequency sweep test, angular frequency is varied (ω usually 0.01–500 s^{-1}) while amplitude and temperature are kept constant (**Figure 3.21B**), giving insight on the time-dependent behaviour (since frequency is the inverse value of time) of a material (shelf-life, sedimentation, flotation, syneresis and phase separation). In this experiment low-frequencies are associated with long-term behaviour and high-frequencies with short-term behaviour.[266]

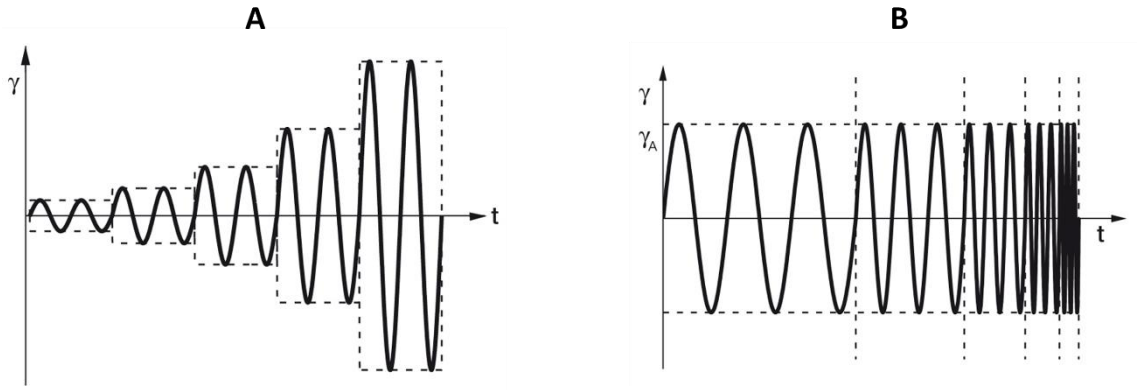

Figure 3.21: Pre-sets of amplitude sweep with constant frequency (A) and frequency sweep with constant amplitude (B). Adapted from ref. 268.

The amplitude sweep of the selected 2% hydrogel samples is shown in **Figure 3.22**, while **Table 3.5** summarises some important rheological parameters extracted from that data. The amplitude sweep (**Figure 3.22**) is composed of two curves, G' (describing the "solid-like" elastic behaviour, storage modulus) and G'' (describing the "liquid-like" viscous behaviour, loss modulus). Considering the whole amplitude range, three main regions can be identified: the linear viscoelastic region (LVE) at low strain values, where G' and G'' values are virtually constant and independent of the strain; the limit of the LVE (γ_L), which corresponds to the point where G' (or G'') starts to deviate from the LVE values

Table 3.5: Important rheological parameters extracted from the amplitude sweep test of MFC-1, xanthan gum (XG) and commercial nanocellulose (NC) 2% (w/v) hydrogels. Those parameters are storage modulus G′ at the LVE region (a measure of gel stiffness), strain (γ) at G''_{max}, yield strain/point (γ_y), flow strain/point (γ_f) and flow transition index (γ_y/γ_f).

Sample (2%)	G' (Pa)	$\gamma_{G''max}$ (%)	γ_y (%)	γ_f (%)	γ_y/γ_f
MFC-1	957	4.6	2.2	147	68.4
NC	122	10	1.5	147	98
XG	22	316	21.5	316	14.7

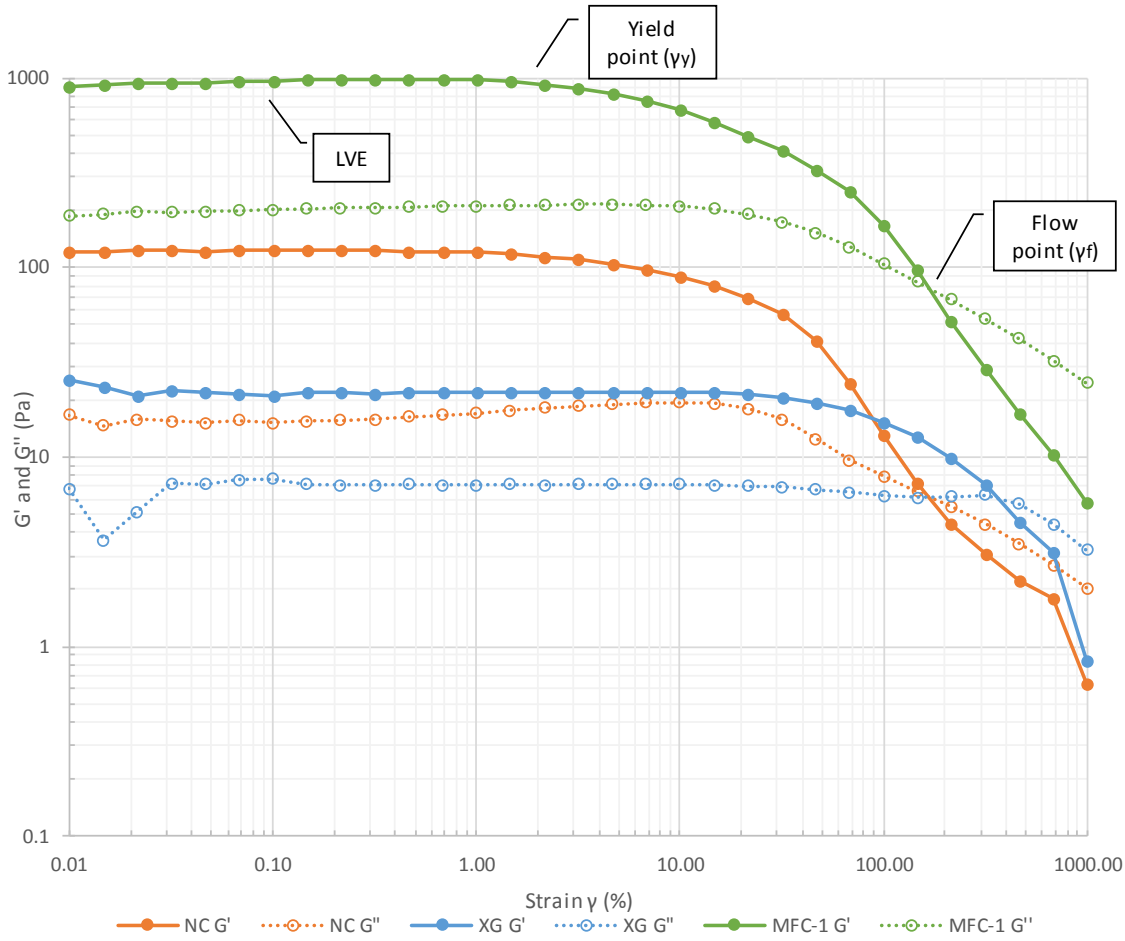

Figure 3.22: Amplitude sweep of NC, XG and MFC-1. Original in colour.

(usually a 5% deviation tolerance is applied), and; the cross-over point, where G′ = G′′ and thereafter G′′ > G′, meaning that the sample starts to flow as a whole.

For all samples, G′ > G′′ in the LVE region, confirming that a gel network structure is present and the samples behave like viscoelastic solids.[261,266] The obtained G′ values in the LVE (**Table 3.5**) can be interpreted as a measure of the gel stiffness or strength at low strain,[266] therefore MFC-1 hydrogel demonstrated excellent gel strength, 8-times higher than NC and 44-times higher than XG, which also supports its high stability at rest. A G′ value similar to that of MFC-1 (~ 1000 Pa) was previously reported for nanofibrillated cellulose gel at 1% concentration.[256] Nevertheless, with increasing strain, G′ and G′′ starts to deviate from the LVE indicating the limit of the LVE range (γ_L), which coincides with the yield of the gel (yield strain, stress or point, γ_y), *i.e.* when the gel starts to flow (irreversible deformation).[266] As shown in **Table 3.5**, the γ_y of MFC-1 (2.2%) is comparable to that of NC (1.5%), however much lower than that of XG (21.5%). According to the literature,[269,270] MFC-1 and NC behave more like a weak gel (where $\gamma_L \equiv \gamma_y < 5\%$) while XG behaves more like an entangled polymer network or structured fluid ($\gamma_L \equiv \gamma_y \approx 25\%$). At the yield strain, G′ starts to decrease while G′′ slightly increases to a maximum (**Table 3.5**). This is due to the increasing entropy of the system (G′′ is the loss modulus, *i.e.* the deformation energy lost by shearing forces) with the increasing strain, where at the cross-over point (γ_f) the whole network collapses and the system starts to flow as whole. MFC-1 and NC presented much lower strains at G''_{max} (4.6% and 10%, respectively) compared to XG (316%), where the strain at G''_{max} of the latter coincided with its flow point. After the cross-over point (G′ = G′′), G′′ > G′ for all samples, meaning that the weak gel-like structure has been disrupted. Interestingly, according to **Table 3.5**, MFC-1 and NC started to flow as a viscoelastic liquid earlier (γ_f at 147%) than XG (γ_f at 316%). One possible explanation is that in the cellulosic materials (MFC-1

and NC), physical interactions among particles are less strong than those found among soluble XG molecules. Moreover, similar flow strain values were found for other cellulosic hydrogels of different biomass (data not shown), which might indicate an inherent rheological property of lignocellulosic materials. Another parameter investigated from the amplitude sweep is the flow transition index (γ_f/ γ_y), which is the ratio between the yield strain and flow strain (called "yield zone" or yield/flow transition range) and indicates the "brittleness" of a gel fracturing.[266] The lower this values is, the more brittle the gel structure will break. In that context, MFC-1 showed much higher value of γ_f/ γ_y (68.4%) than that found for XG (14.7%), meaning that the breakdown of the gel structure in MFC-1 happens more smoothly than in XG. However, NC presented even higher value (98%) than that of MFC. These structural differences between non-cellulosic and cellulosic hydrogels could be related to the fact that XG rheological behaviour is closer to that of an entanglement network than of a weak gel (MFC-1 and NC). Yet, this classification is not absolute, neither is well defined in the literature.[261,269,270]

The frequency sweep results summarised by G', G'' and complex viscosity (η*, also known as dynamic viscosity) curves are presented in **Figure 3.23**. MFC-1, similar to the other studied samples (NC and XG) presented G' > G'' with both curves almost parallel and straight at the lower frequency range (0.05–10 s^{-1}) and a slight slope at the higher frequencies (10–500 s^{-1}). This behaviour, as anticipated by the amplitude sweep results, is typical of gel-like materials, especially regarding the fact that G' > G'' and the independence of G' and G'' at the lower frequency range.[266] Considering that the behaviour of G' (and also G'') at very low frequencies (0.01–0.1 s^{-1}) is an indication of the gel long-term stability,

"consistency-at-rest",[266] it can be said, based on G' values at 0.05 s^{-1}, that MFC-1 (G' = 460 Pa) is 10x more stable at rest than NC (G' = 46 Pa) and 70x more than XG (G' = 7 Pa). Also, while MFC-1 and NC gel structure did not collapse up to 500 s^{-1}, XG gel collapsed at ~232 s^{-1}, which agrees with previous discussed results. Regarding η*, all samples presented a shear-thinning behaviour, *i.e.* decreasing viscosity with increasing shear rate (calculated by $\omega \times \gamma$), however, since at rest (*i.e.* very low frequencies) the hydrogels do not flow, η* value alone has no practical use, independent of how large it is.[266]

To conclude, MFC-1 presented similar rheology performance to that of pulp nanocellulose and, in some aspects, better than xanthan gum. Hence, MFC-1 could be applied as a more sustainable, clean label bio-based alternative to replace conventional rheology modifiers in food, cosmetic and medical products.

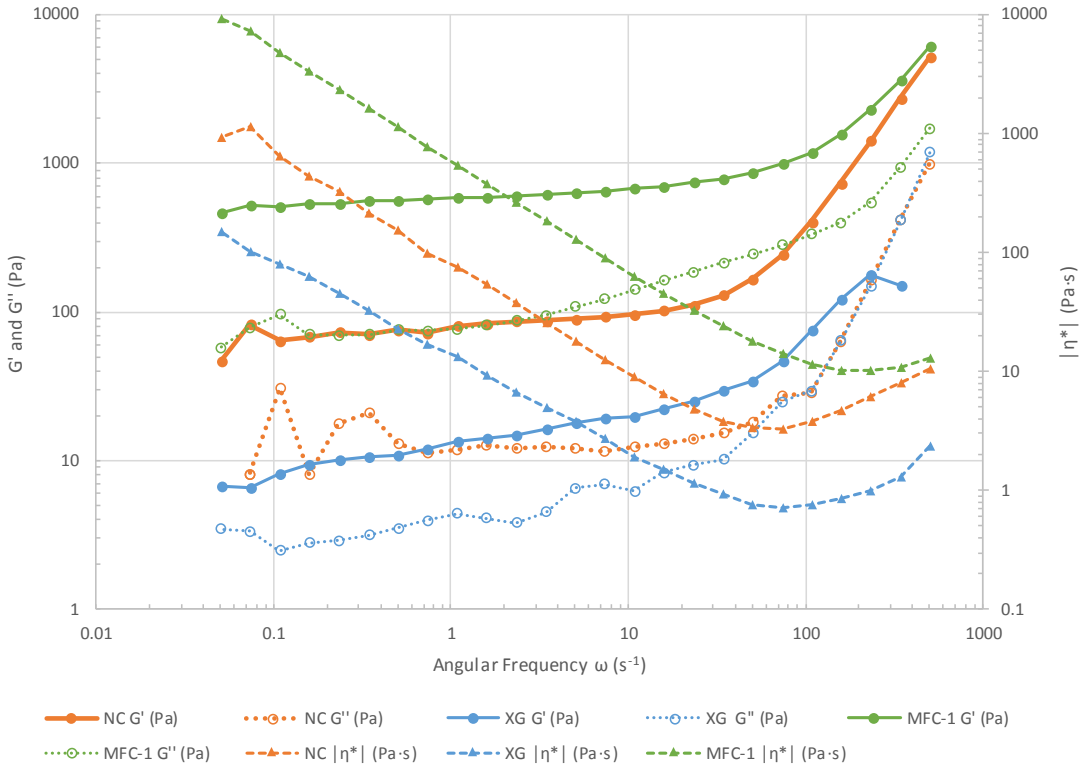

Figure 3.23: Frequency sweep of NC, XG and MFC-1 showing complex viscosity (η*) curves in addition to G' and G'' curves. Original in colour.

3.1.2.2 MFC films

As discussed earlier, hornification is an irreversible process where consecutive drying-wetting cycles on the cellulosic material decrease its ability of water retention and swelling by forming interfibrillar hydrogen bonds and pore collapse (due to capillary forces).[242,264] However, this effect has the advantage of allowing the easy formation of structured films from MFC. Films prepared from 0.2% (w/v) MFC dispersions in neat water are shown in **Figure 3.24**. All films presented high flexibility and strength, due to the high aspect ratio of the fibrils,[138] while transparency gradually reduced with increasing temperature of treatment used to produce the corresponding MFC. This is probably due to the presence of residual degradation products on the cellulose fibrils surface formed at higher temperatures of microwave-assisted hydrolysis (especially above 180 °C), as already discussed. The features presented by these MFC films, especially the ones from low-temperature MFCs, are similar to previously reported (transparent) nanopapers and nanofilms prepared from nanocellulose materials.[138,254,271,272]

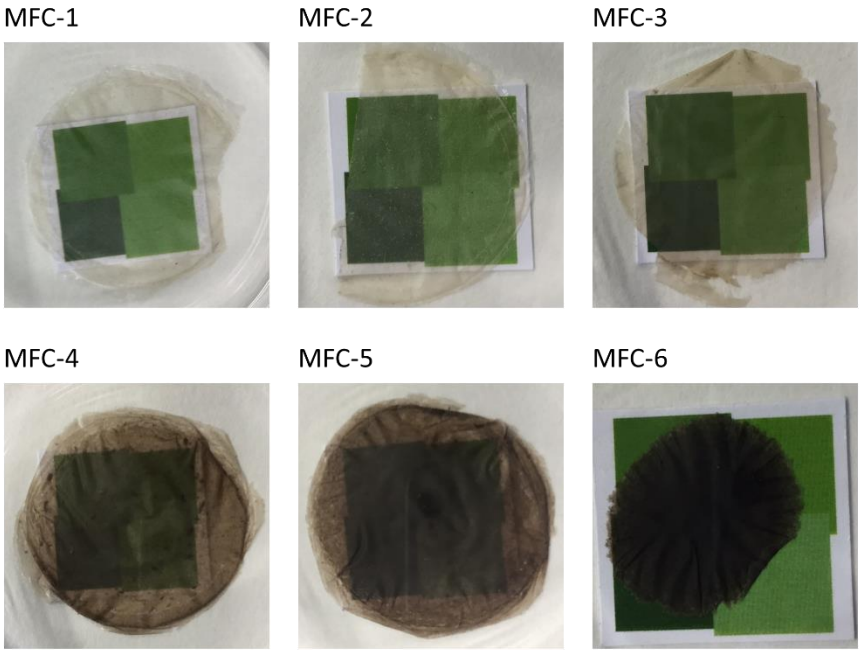

Figure 3.24: MFC films contrasted against a coloured paper background. Original in colour.

3.1.2.2.1 Microstructure characterisation

In order to further understand the film formation and assembly, SEM analysis was carried out and resulting images are presented in **Figure 3.25**. In general, all films seem to have been formed in the same way, meaning by the overlaying and aggregation of MFC fibrils into lamellar layers with considerable mesoporosity (average pore sizes of 10–40 nm) among adjacent fibrils and between layers. The films' surfaces imaged at low magnification (first column in **Figure 3.25**) shows the presence of residual cell wall material that has not been disintegrated (even after sonication), which is a known fact for MFC materials.[273] However, the surface roughness seems to increase with increasing temperature of treatment (see first and second columns in **Figure 3.25**), which could be due to the synergy of the increasing degradation and breakdown of the cellulosic matrix with the increasing hydrophobicity of the material, with the increasing HMT temperature, as confirmed by WHC and previously discussed analyses. The presence of pores at the cross-section of the films (see second column in **Figure 3.25**), can give

interesting mechanical properties to the film for specific application, *e.g.* in flexible devices, where the stress created in the material during bending can be distributed and relieved due to the presence of pores between layers of aggregated fibrils.[138] At high magnification (third column in **Figure 3.25**), the nanostructure of the films becomes more evident, as do the mesopores at the surface. With the increasing of HMT temperature, more of the MFC nanofibrils (10–50 nm wide) become visible due to the increasing removal of amorphous components from the cellulosic matrix. The entanglement and assemble of the nanofibrils are similar to those found in wood-base nanocelluloses.[138,254] Due to the presence of mesopores at the surface these MFC films could also be applied as membranes and filters.[245,271,272]

MFC films are promising green candidates for replacing non-renewable polymers and other materials in several applications, such as: substrate for electronic paper & optoelectronic devices,[138] energy saving & storage devices,[274] food and non-food packaging with improved barrier[275] and antimicrobial properties,[98] (nano)composites,[227,276] membranes for environmental remediation[245] and wound dressing scaffold.[277]

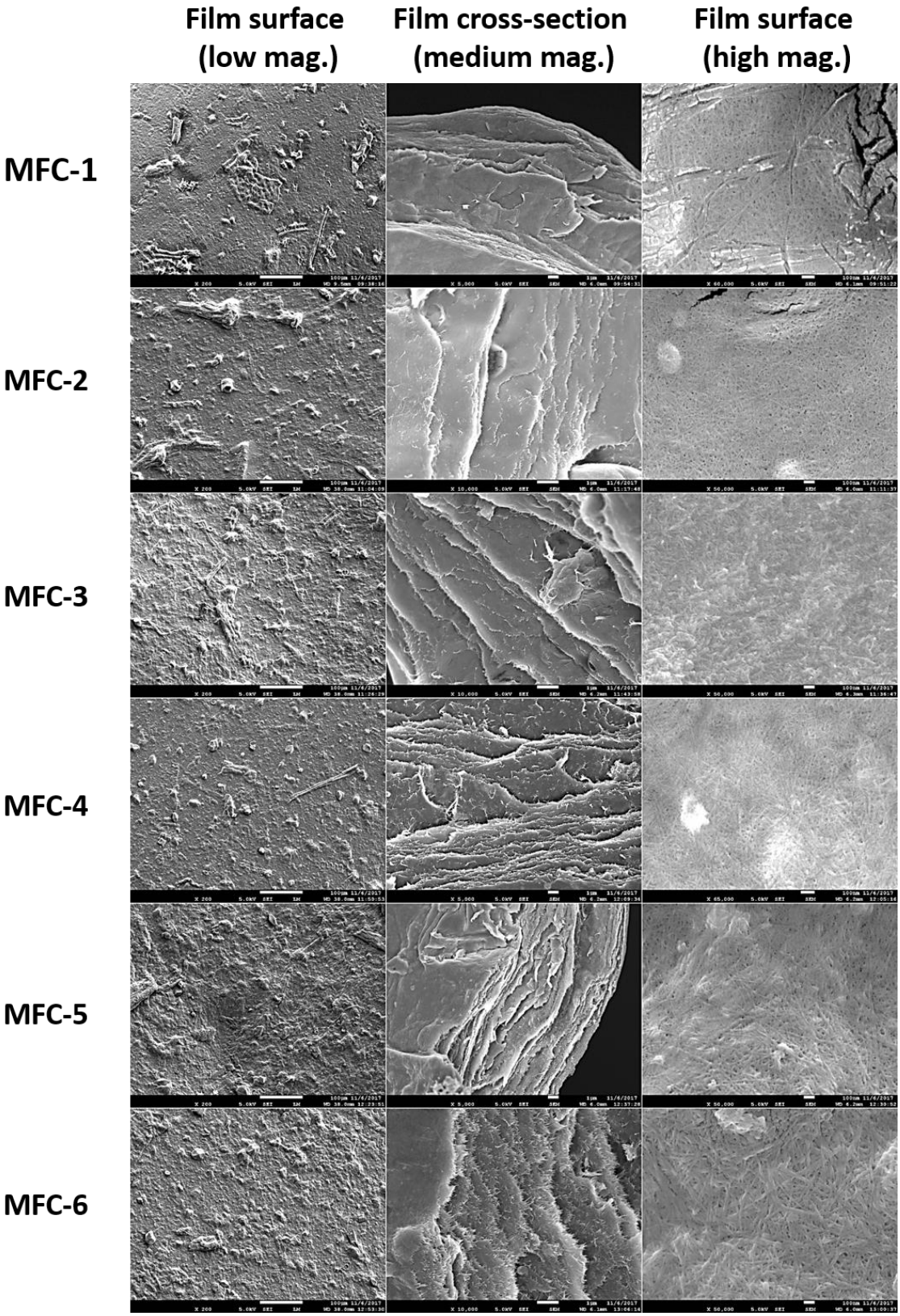

Figure 3.25: SEM images of MFC films showing surface at low magnification (first column, scale bar of 100 µm), cross-section (second column, scale bar of 1 µm) and surface at high magnification (third column, scale bar of 100 nm).

3.2 Part B: Valorisation of Hydrolysates

In order to design a *zero-waste* biorefinery model, all residues must be recovered and valorised as a resource. So here, the valorisation of the hydrolysate (the aqueous filtrate produced after HMT) is achieved by recovering its potentially high-value chemicals: residual pectin; lignin, and; soluble organic molecules (sugars, sugar acids, organic acids and furans).

3.2.1 Residual pectin

The starting material used for the HMT experiments, depectinated orange peel residue (DOPR), is only partially depectinated. That is because even though most of its pectin content is extracted in the first microwave treatment (see **Section 2.1**), some residual pectin is still present on the cellulosic residue (*ca.* 24%, see **Table 3.1**). Therefore, a significant amount of pectin can still be recovered from the second and subsequent microwave treatment(s) of the orange peel biomass (HMT).

3.2.1.1 Pectin characterisation

The DOPR "residual" pectin was successfully extracted from the hydrolysates produced after HMT at 120 °C (P-1), 140 °C (P-2) and 160 °C (P-3). Pectin could not be recovered from hydrolysates produced at and above 180 °C because at those temperatures they undergo complete hydrolysis to sugars and derivatives.[170,278] The pectin yields varied from approximately 15% (120 °C and 140 °C) to 4% (160 °C) as shown in **Figure 3.26**. The significant drop in yield at 160 °C may be attributed to the onset of pectin depolymerisation.[170] The chemical composition of the pectins was very similar to that of commercial citrus pectin, as confirmed by the ATR-FTIR analysis (**Figure 3.27**). All samples presented a characteristic pectin pattern (**Table 3.2**) with strong absorptions at *ca.* 1736 cm^{-1}

(carbonyl of methyl ester and acid from uronic sugar units) and 1607 cm^{-1} (carboxylate from uronic sugar salt units).[279,280] However, with the increasing HMT temperature the relative intensity of the ester absorbance band in contrast to the salt one decreases, indicative of selective ester hydrolysis, hence, directly affecting its degree of esterification.

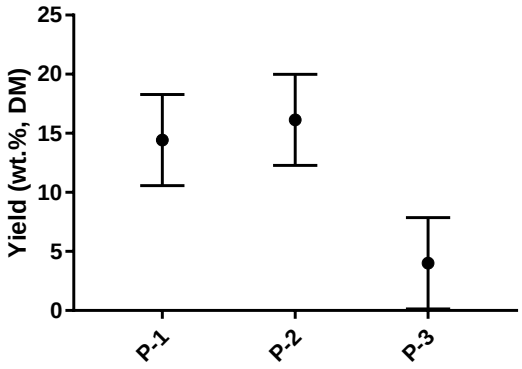

Figure 3.26: Yield for pectin isolated from hydrolysate.

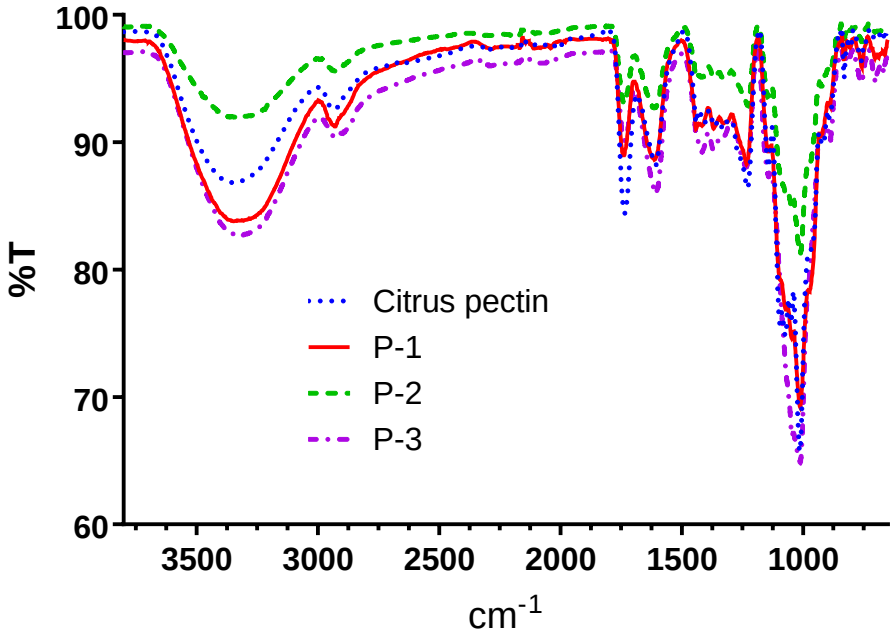

Figure 3.27: Infrared spectra of isolated pectin (P-1, P-2 and P-3) compared to commercial citrus pectin. Original in colour.

Further chemical characterisation of the isolated pectins was carried out by ^{13}C NMR (**Figure 3.28**). As can be observed by the assignments given to the pectin carbons based on literature data,[205,206,281–283] orange peel pectins are mainly composed of galacturonic acid (esterified or not), galactose, arabinose and rhamnose sugar units. The gradual reduction of arabinose (*ca.* C1 at 109, C2/C4 at 87-81, C3 at 78 and C5 at 62.7 ppm) as well as galacturonic acid (*ca.* C1 at 101, C4 at 80, C5 at 72, C2/C3 at 69-70, C6 at 172 and methoxyl at 54 ppm) with the increasing temperature of treatment infers that arabinose-rich side chains (arabinans) present in the "hairy region" (**Figure 1.9**), together with galacturonan regions are hydrolysed to soluble pectin oligomers and monosaccharides, thus yielding an alcohol insoluble pectin (P-3), rich in galactose (galactans).[59] The fact that P-3 also presents rhamnose and some galacturonan signals might be related

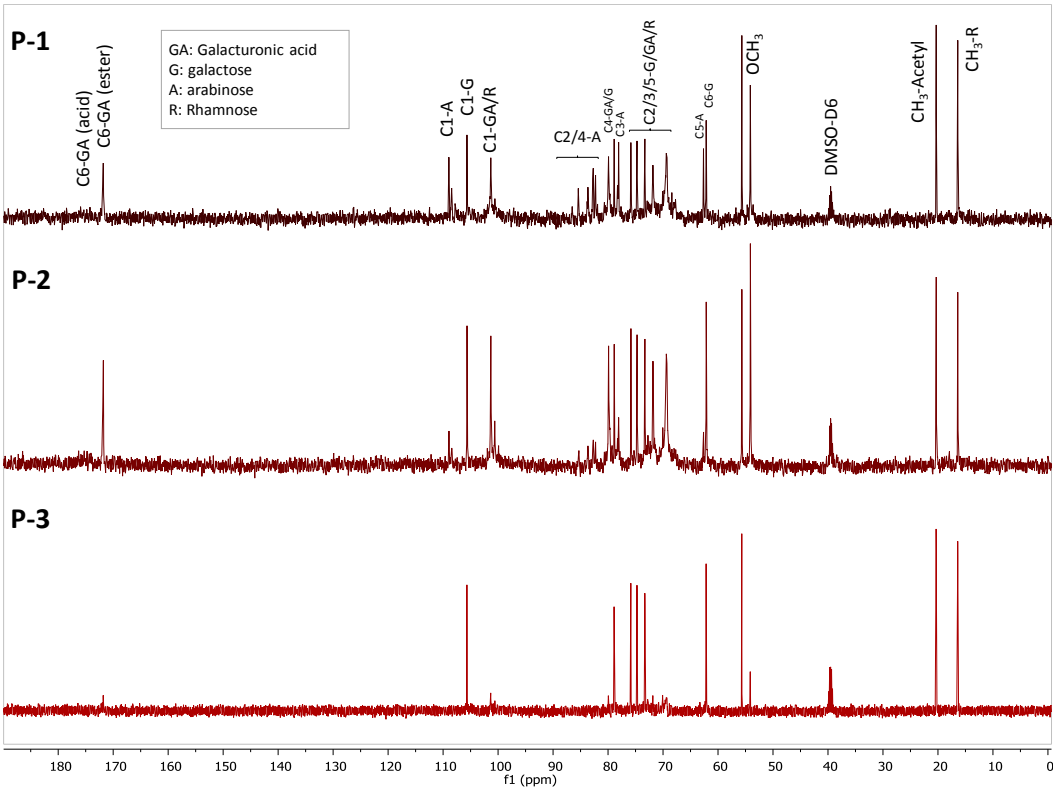

Figure 3.28: ^{13}C NMR spectra of isolated pectins with corresponding attempted assignments. Original in colour.

to residual fragments of the backbone regions close to the galactans that have also survived the hydrolysis at 160 °C. As shown in **Figure 1.9**, galactans side chains are mainly linked to the pectin rhamnogalacturonan backbone at the C4 of rhamnose residues.[59,284]

Thermogravimetric analysis also confirms the partial hydrolysis of pectin above 120 °C shown in **Figure 3.29**. The T_d of P-1 and P-2 (233 °C and 243 °C, respectively) are close to that of commercial citrus pectin (*ca.* 230 °C), while T_d of P-3 is at higher value (*ca.* 290 °C) and its decomposition covers a broader range (*ca.* 200–400 °C), which can indicate the oligomeric character of the sample. It is known that the thermostability of polysaccharides is also related to their molecular weight distribution,[136,285] so the broader decomposition pattern of P-3 may be due to a higher polydispersity of the pectin polymer after being processed at 160 °C, derived from the hydrolysis of arabinan side chains and

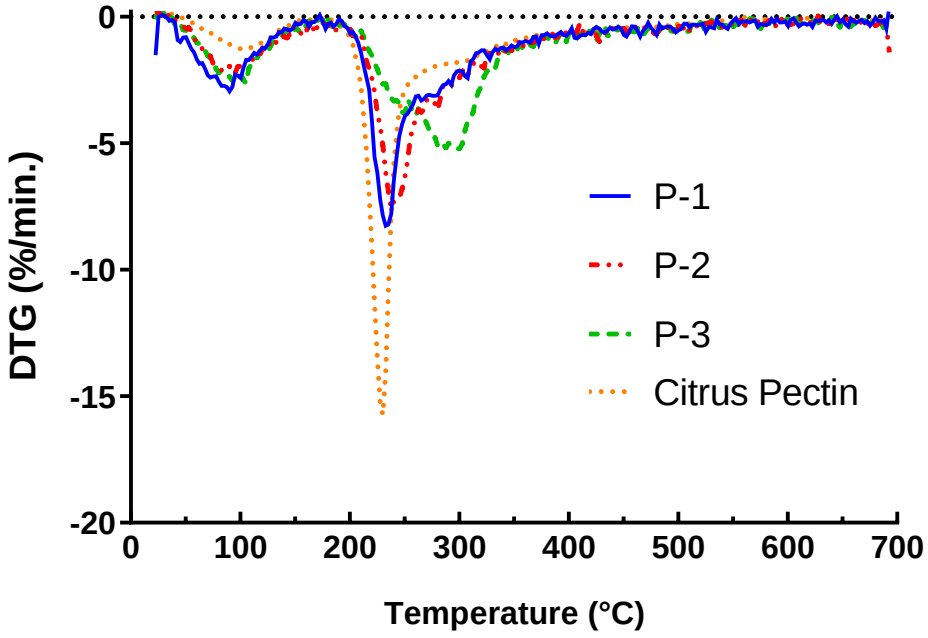

Figure 3.29: DTG thermograms from TGA analysis of the isolated pectins (P-1, P-2 and P-3) against commercial citrus pectin as reference. Original in colour.

homogalacturonan regions. The non-hydrolysed regions like rhamnogalacturonan and galactan seem to be more resilient to the treatment.[286,287]

The calculated DE (see **Section 2.1.4.1.2)** for each pectin sample was found to be 73% (P-1), 62% (P-2) and 54% (P-3). This helps to confirm the hydrolysis of homogalacturonan containing ester functions above 120 °C. In this context, P-1, P-2 and P-3 can be regarded as high-methoxyl pectins, hence they all should be able to form gels in the presence of sugar with solution at low pH.

3.2.1.2 Pectin gels

The gelling property of pectin has been traditionally used by the food & beverage sector in order to improve rheology, nutrition and stability of food products (jams, jellies, yogurts, fruit juices, etc). Recently, even cosmetics and pharmaceutical sectors has shown growing interest for pectin due to its physicochemical and biological properties.[58,60,288,289] As confirmed by the inversion test (**Figure 3.30**), all three pectin samples (P-1, P-2 and P-3) formed strong clear gels, comparable to the reference, in the presence of sucrose at low pH (3.0), which, as anticipated above, is directly related to their high DE values. Probably for having a DE close to 50%, P-3 showed a slight yielding of the gel in comparison with the other gels (see top view of gels in **Figure 3.30**), however, it was enough to prevent the gel from flowing during a large period of time (several months). The slightly browning of the pectin gels with the increasing HMT temperature can be related to the increasing formation of trace degradation products which has remained in (or derives from) the pectin samples. The mechanism behind the gel formation is based on hydrophobic interactions among highly-esterified pectin molecules. Upon addition of sucrose, a highly hygroscopic agent, water is displaced from the polymer network to interact with

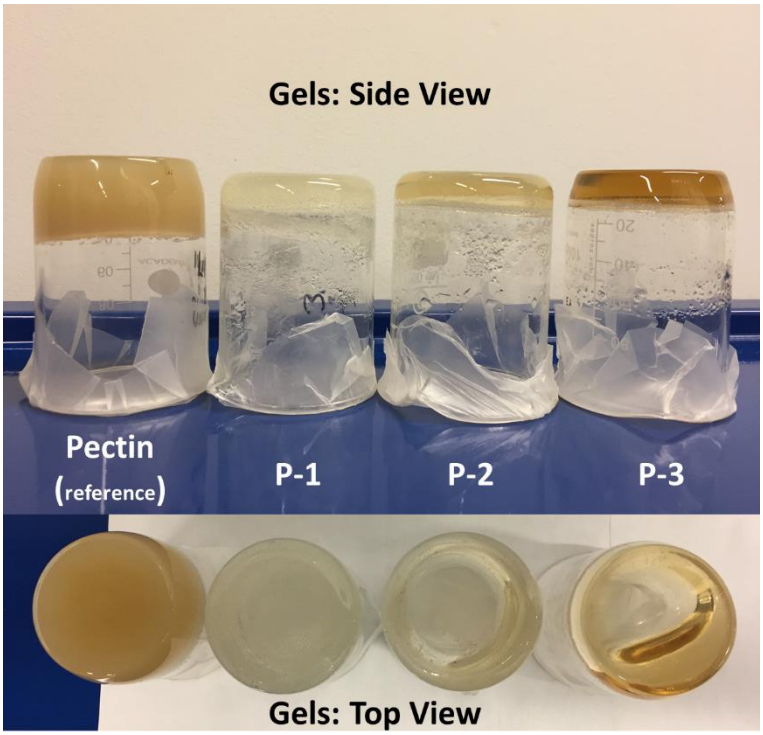

Figure 3.30: Inversion test for isolated pectins (P-1, P-2 and P-3) and pectin reference with side and top views of the samples. Original in colour.

sucrose molecules, where pectin-water interactions are overcome by pectin-pectin interactions (dehydration). The low pH of the solution maintain free carboxylate groups of galacturonic acid units protonated, preventing the electrostatic repulsion between negatively charged pectin molecules.[58] This simple test shows the potential of high-value residual pectin being recovered and used to produce gels useful for several applications and in the same time improve the overall sustainability and greenness of the suggested orange peel biorefinery process.

3.1.1 Lignin microparticles

Lignin is the second most abundant plant-derived biopolymer on Earth, after cellulose.[290] It is ubiquitous in plant secondary cell wall and presents a highly branched and heterogenous aromatic structure based on three phenylpropanoids units (*p*-hydroxyphenyl, guaiacyl, and syringyl), which are ultimately derived by

biosynthetic polymerisation of *p*-coumaryl, coniferyl, and sinapyl alcohols (**Figure 3.31**).[291]

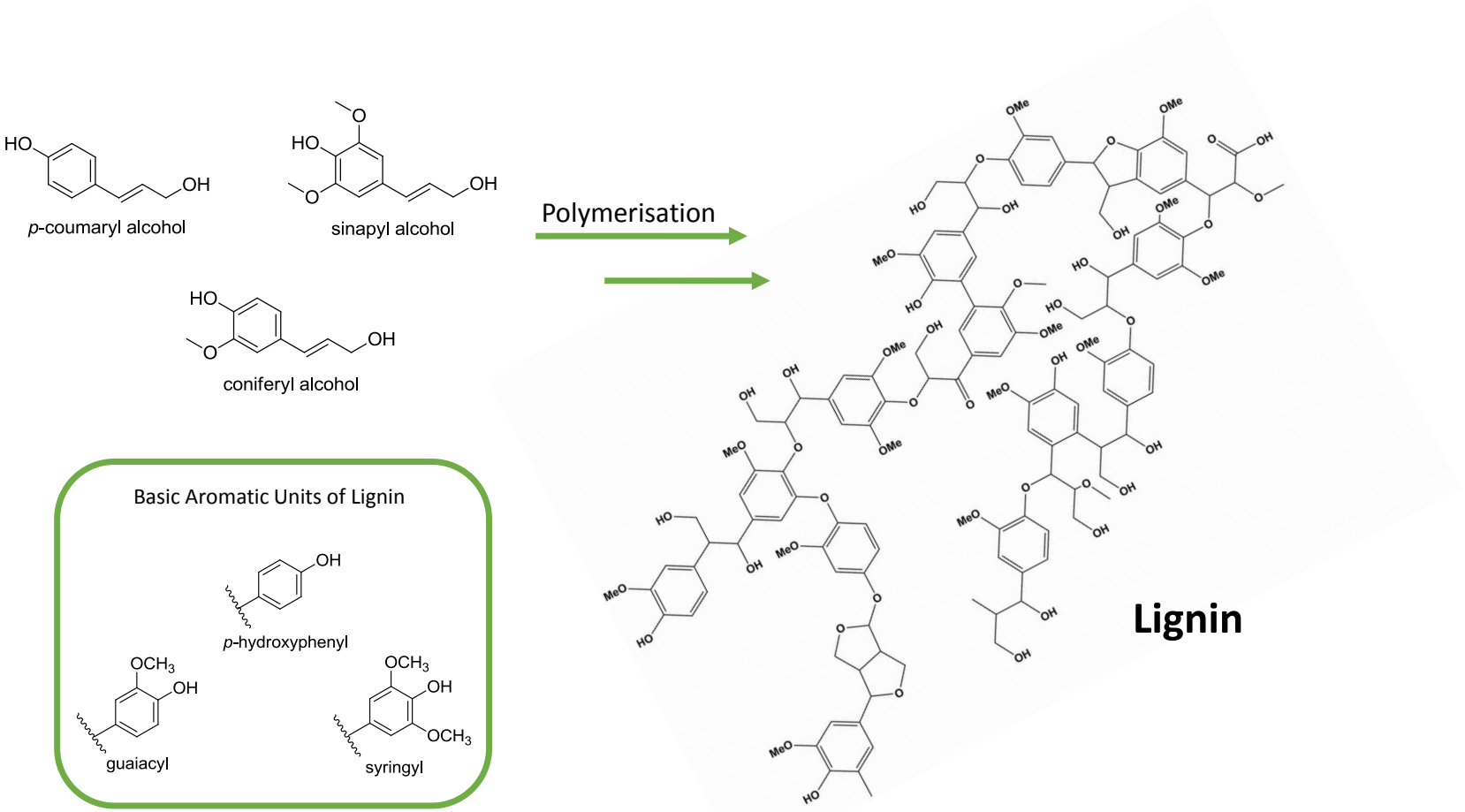

Figure 3.31: Lignin structure, its most common aromatic units and precursors (phenylpropanoids).

Although lignin is not a major component of orange peel (see **Table 3.1**), it could be recovered from some hydrolysates after HMT. After the separation of the MFC fraction from the hydrolysates processed at temperatures ≥180 °C, the latter were refrigerated overnight (4 °C) and a dark precipitate was observed. Those precipitates (L-4 from 180 °C, L-5 from 200 °C and L-6 from 220 °C) were analysed and characterised as a lignin-like compounds.

The ATR-FTIR spectra of those precipitates were compared against a lignin sample extracted from orange peel (L-OP) by the Klason method[139] and are shown in **Figure 3.32**. The spectra of L-4, L-5 and L-6 showed strong similarity with the orange peel lignin, especially regarding the aromatic region (1600–1400 cm^{-1}), and also presented other absorptions typical of lignin characterised elsewhere (see **Table 3.2**).[162,168,199,200]

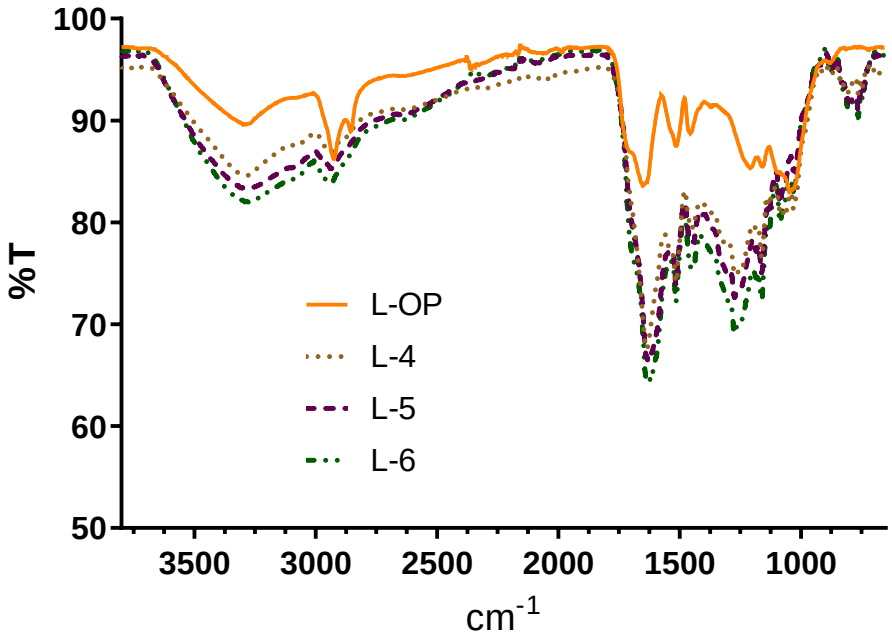

Figure 3.32: Infrared spectra of isolated lignins (L-4, L-5 and L-6) and reference lignin (L-OP) extracted from orange peel using the Klason method. Original in colour.

The ^{13}C SSNMR spectra (**Figure 3.33**) of L-5 and L-6 confirmed the presence of carbonyl carbons (210–165 ppm), aromatic carbons (160–100 ppm), aliphatic carbons from the phenylpropyl and β-O-4 linkages units of lignin (90–10 ppm).[204,212,292]

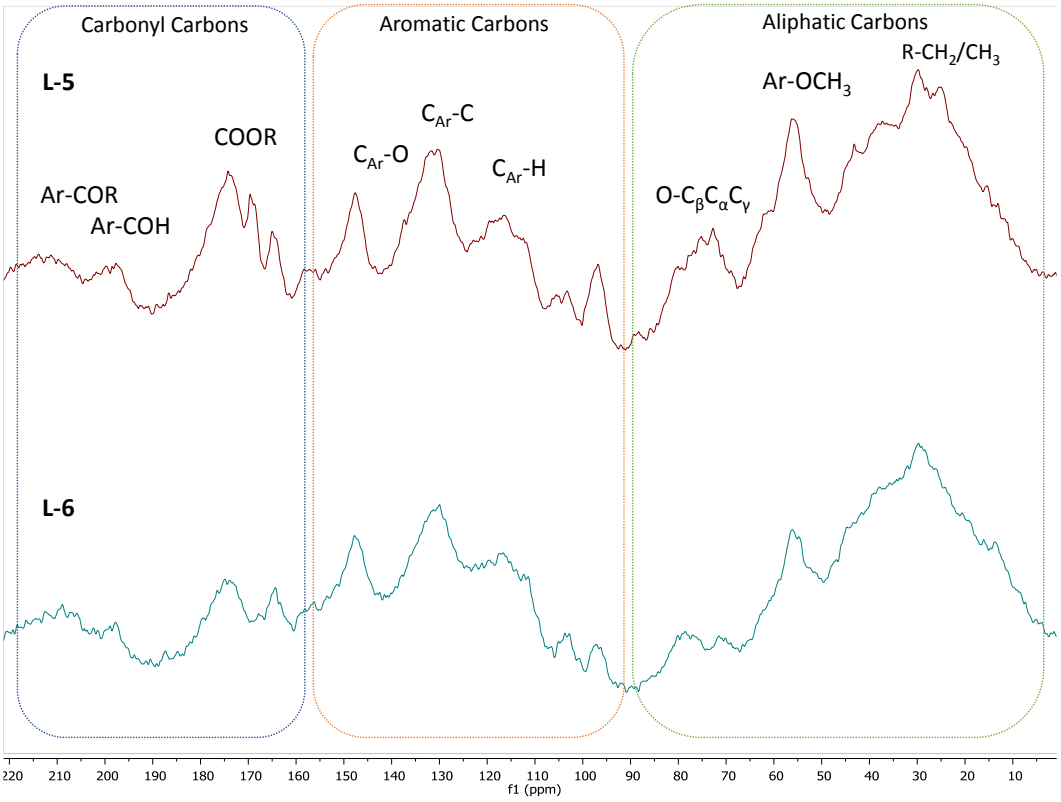

Figure 3.33: Solid state ^{13}C CP-MAS NMR of isolated lignins L-5 and L-6. Original in colour.

The spectroscopic analyses presented above indicate that residual carbohydrate could be present in those lignin-like samples. The carbohydrate moiety could be derived from the decomposition of hemicelluloses and pectins, which were linked to lignin structure in the lignin-carbohydrate complex.[63,123,293]

Thermogravimetric analysis (**Figure 3.34**) further confirmed the lignin character of the studied samples, where the decomposition trace was found to be quite similar to that of orange peel Klason lignin (L-OP). The broad and slow-rate decomposition pattern (200–600 °C) with T_d *ca.* 350–400 °C is characteristic of

lignin extracted from lignocellulosic biomass.[155,166,167] The first mass loss band (50–120 °C) corresponds to moisture loss.[166]

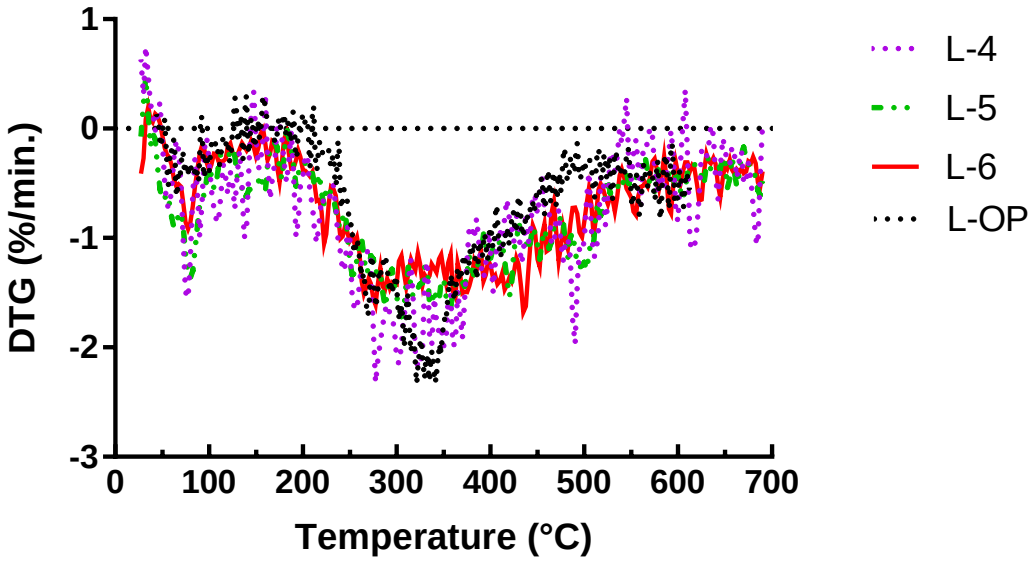

Figure 3.34: DTG thermograms of isolated lignins (L-4, L-5 and L-6) and reference orange peel extracted lignin (L-OP). Original in colour.

The recovered lignins microstructures were investigated by SEM, TEM and CLSM as shown in **Figure 3.35**. The SEM and TEM images show that lignin aggregates into discrete or "fused" spherical microparticles where each sample presents a slightly different average diameter. The average microparticle diameter for L-4, L-5 and L-6 are *ca.* 500 nm, 1000 nm and 800 nm, respectively. In all cases, some of these discrete microspheres seem to have fused together to give larger ellipsoid-like particles of *ca.* 500–3000 nm wide. A few rhomboidal shapes could also be observed in some samples (yellow arrows in **Figure 3.35**), which is probably impurities of calcium oxalate crystals, as previously discussed and identified in orange peel biomass.[133] In plants, these crystals can be found under different morphologies,[294] including rhomboidal.[295] The CLSM images further confirmed that those microparticles are mainly composed of lignin (based

on the emission spectrum referenced from Klason lignin extracted from orange peel).

The formation of lignin particles has been previously discussed in the literature[278,296] and one of the suggested mechanism considers that at temperatures above lignin glass transition (*ca.* 180 °C), biomass lignin melts, coalesces into larger molten lignin "spheres" (**Figure 3.36**), migrates through the cell wall fibres and when the temperature of the system decreases it is either re-deposited on the surface of the biomass fibres or precipitated in the aqueous phase of the studied system through extrusion from the biomass matrix.[158,297,298]

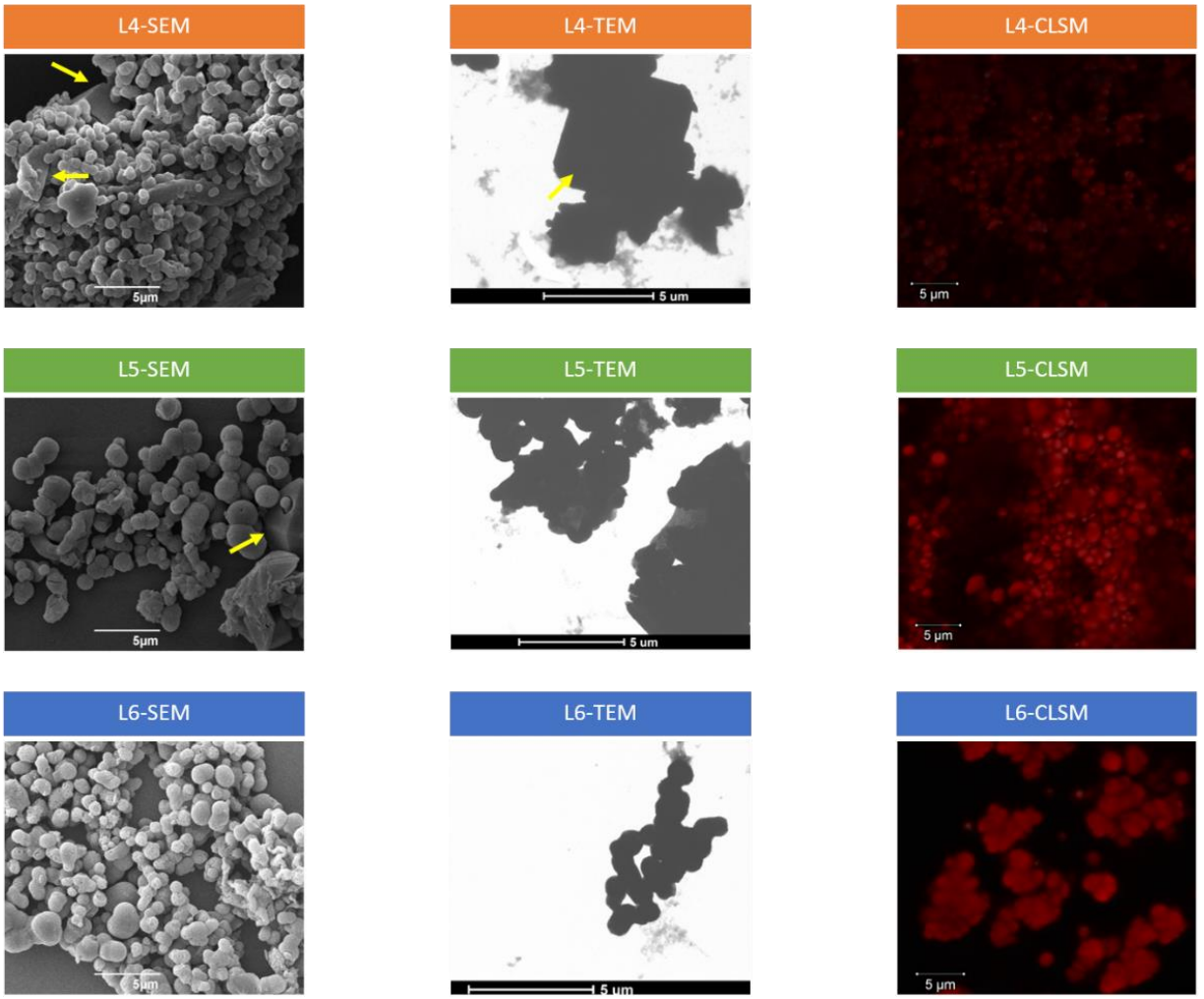

Figure 3.35: SEM, TEM and CLSM images of the isolated lignins. Scale bar = 5 µm. Yellow arrows indicate, probably, calcium oxalate crystals. Original in colour.

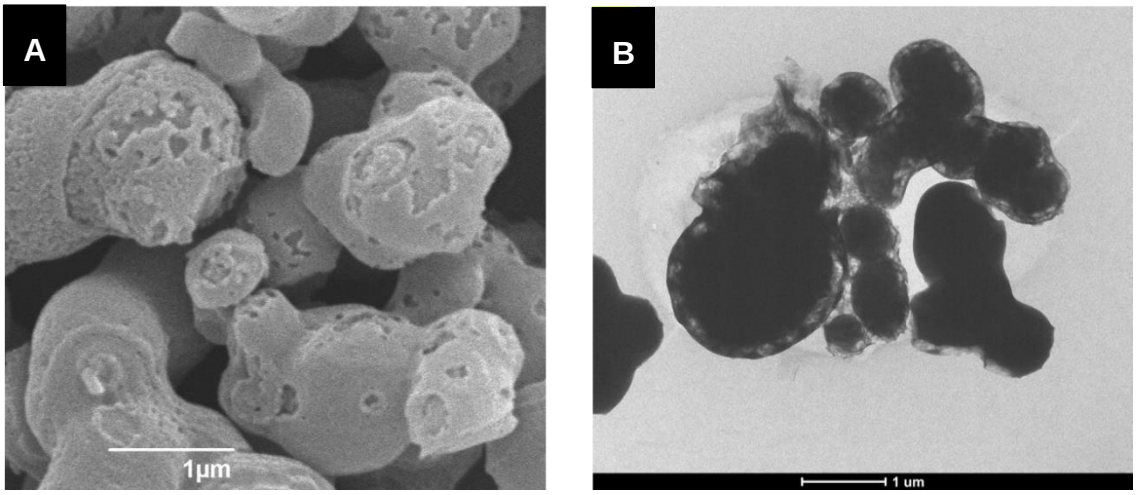

Figure 3.36: High magnification of SEM (A) and TEM (B) images of L-6 showing *coalesced spheric lignin* structures. Scale bar = 1 µm.

3.1.2 Sugars and other small molecules

Another promising fraction of the hydrolysate are the soluble sugars (monosaccharides mainly), organic acids and furans. The HPLC analysis of the filtered hydrolysates are summarised in **Figure 3.37**. The presence of different monosaccharides and a disaccharide (cellobiose), which are all derived from the hydrolysis of polysaccharides originally present in the biomass (pectin, cellulose and hemicellulose), as well as their decomposition products (furans and organic

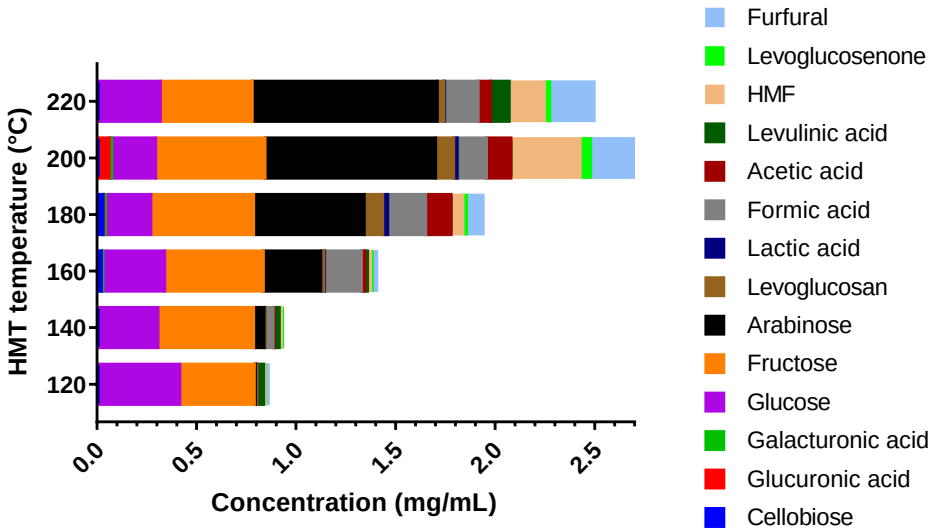

Figure 3.37: Sugars, small organic acids and furans present in the HMT hydrolysates identified by HPLC. Original in colour.

acids), could be observed.[229] Fructose and xylose could not be separated by the HPLC method used, but we assume that relatively little xylose is present since it is not a major carbohydrate in citrus.[39,288,299]

Seven sugar types were detected and separated by HPLC, namely: three neutral monosaccharides (glucose, fructose and arabinose); two sugar acids (galacturonic acid and glucuronic acid); one disaccharide (cellobiose), and; one anhydrosugar (levoglucosan). These sugars account for the majority of the total soluble components present in the hydrolysates, where higher temperatures (above 180 °C) gave up higher yields of sugars, up to a total of 1.8 mg/mL (at 200 °C). Up to a treatment temperature of 160 °C, glucose and fructose are the major monosaccharides present in the hydrolysate at *ca.* 0.30 and 0.45 mg/mL, respectively. These sugars occur naturally in orange/citrus fruits and peel but could also be derived from the hydrolysis of sucrose (naturally present in citrus as well).[39,53,55] In addition, glucose could have been converted into fructose via isomerisation.[177] Above 160 °C, although glucose and fructose content remained almost unaltered, arabinose became the major sugar component of the hydrolysate, with values up to *ca.* 1.0 mg/mL (at 220 °C). The rapid increase in arabinose content above 160 °C can be explained by the previously discussed hydrolysis of arabinan regions from pectin structure (see **Section 3.2.1**), which are then further hydrolysed to free arabinose monosaccharides at those temperatures.[170] The two sugar acids, galacturonic acid and glucuronic acid, respectively derived from hydrolysis of pectin and hemicellulose,[167,300,301] were detected only at 180 °C (at negligible quantities) and 200 °C (at 0.01 and 0.06 mg/mL, respectively). The very low content of those species in those hydrolysates may infer that the complete hydrolysis (saccharification) of pectin and

hemicellulose is not achieved under those conditions, yielding more oligomers than monosaccharides. Cellobiose, most probably derived from the partial hydrolysis of amorphous domains of cellulose, was detected at 160 °C and 180 °C also in low concentrations (*ca.* 0.02 mg/mL). Its absence at higher temperatures than 180 °C may indicate its hydrolysis to glucose has occurred. Levoglucosan, also derived from cellulose hydrolysis,[137,177] was detected in all hydrolysates, but significant concentration was found only at 180 °C and 200 °C (0.1 mg/mL). At 220 °C its concentration declines to 0.03 mg/mL, which may indicate its conversion to glucose.[177]

Apart from sugars, four species of organic acids (lactic, formic, acetic and levulinic acid) and three degradation products of sugars (HMF and furfural, levoglucosenone) were also detected. Significant concentrations of the organic acids (*ca*. 0.02-0.2 mg/mL) started to appear from 160 °C up to 220 °C, but with maximum concentrations at 180 °C for most acids. These acids may have been present inherently in the biomass, since orange peel is composed of up to 9% of free organic acids,[302] or originated from the hydrolysis of polysaccharides present in the biomass. More specifically, acetic acid may have been produced from ester hydrolysis of hemicellulose and pectin acetyl groups or decomposition reactions of sugars, formic acid from the decomposition of furans (HMF and furfural), while levulinic acid and formic acid from HMF decomposition. [167,177,229,303] Above 180 °C, a significant increase of furfural, HMF and levoglucosenone was observed (*eg.*, HMF increased from *ca.* 0.06 mg/mL at 180 °C to 0.4 mg/mL at 200 °C). This can be related to the increasing severity of the treatment with increasing temperature, leading to further degradation of pentoses (like xylose and arabinose) to furfural and hexoses (mainly glucose and galactose) to

levoglucosenone or HMF.[229,304,305] In order to summarise all this complex data related to the conversion of orange peel polysaccharides all the way down to monosaccharides and its derivatives,[177,229,305,306] a scheme representing the possible hydrolytic pathways taken during HMT is shown in **Figure 3.38**.

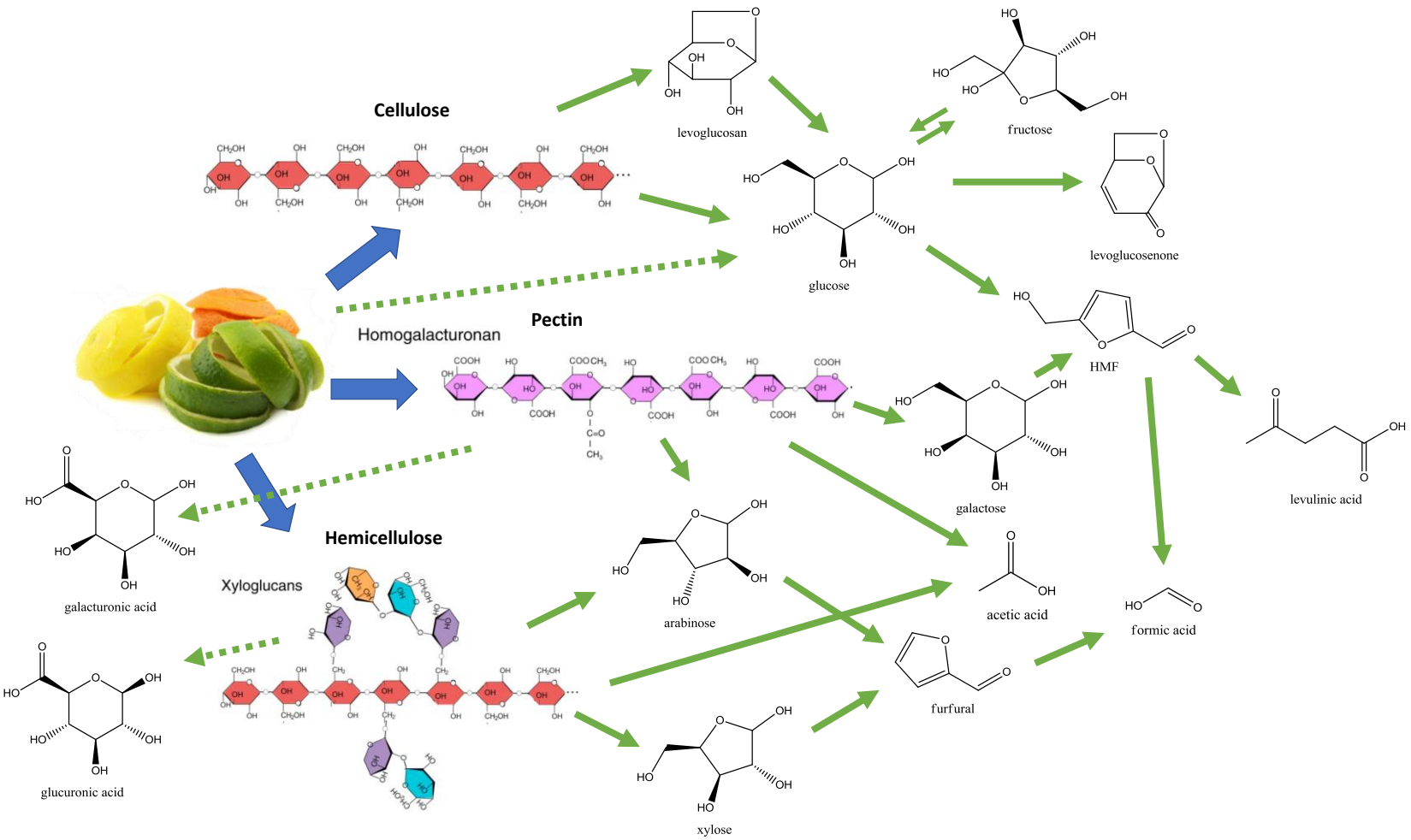

Figure 3.38: Scheme representing the possible hydrolytic pathways of citrus peel main polysaccharides (cellulose, hemicellulose and pectin) down to sugar degradation products (organic acids, furfural and HMF) during hydrothermal microwave treatment. Original in colour.

3.3 Part C: Process Greenness Assessment

In order to evaluate the total greenness and the environmental impact of the technological process for the production of MFC suggested in this thesis (HMT), some useful metrics were used, namely, energy efficiency, E-factor and green star.[129,307,308] Interestingly, microwave-based hydrothermal process at lab-scale was found to be *ca.* 50–30% more energy-efficient than using a conventional hydrothermal system (hot plate and pressurised reactor). In addition, CHT experiments presented E-factor up to 2-fold higher than HMT, meaning that HMT is a more environmentally-friendly approach, at least in the studied scale. Based on the green star results, the overall greenness of the HMT process was higher than that of a conventional process scenario for MFC production. Nevertheless, its greenness can be greatly improved by removing the solvent washes from the MFC work-up.

3.1.3 Process energy efficiency analysis

For several chemical processes, energy efficiency (*i.e.* less energy consumption with high product yield) is the most important economic and environmental aspect to be considered, especially regarding the process feasibility at large-scale.[129,132,309] It is well known in the literature that MFC production at large-scale is strongly hindered by process energy consumption and the consequential high energy costs.[99,243,310] Hence, the search for more energy-efficient technologies has rocketed lately and microwave has been on the spotlight for its fast and efficient heating delivery for chemical processes, in particular for water-based ones and treatment of biomass.[119,120,123,130,131]

Energy efficiency (as energy consumption during process heating) and approximated electricity cost of the hydrothermal microwave treatment (HMT) were assessed and compared against conventional hydrothermal treatment (CHT) of the same biomass (orange peel residue). Energy consumption per kilo of MFC produced (kWh/kg) and electricity cost (£/kg of MFC) of both systems (HMT and CHT) were measured by using a power-meter (Energenie, model ENE007) directly connected to the equipment (microwave or heating plate) during the experiments. The cost of electricity was set to £0.14/kWh, which is the average UK energy cost (2018).[311]

In **Figure 3.39**, the energy consumption (as a measure of energy efficiency) and electricity cost of MFC production based on the microwave-heating hydrothermal system used in this thesis (HMT) was compared with a conventional-heating hydrothermal system using a hotplate (CHT). It can be observed that HMT is *ca.* 50% more energy-efficient (consumes *ca.* 50% less energy) than CHT at lower temperatures (120–160 °C) and *ca*. 35% more efficient at higher temperatures (180–220 °C). That trend is probably related to the reduced time necessary to achieve the desired temperature using microwave heating, as previously reported in the literature.[123,132,309] For example, while in HMT the ramping time (a controllable parameter) to the desired temperature was set to 15 minutes, in CHT, the time required to achieve the desired temperature varied from 20–35 minutes, depending on the selected temperature. Logically, with increasing temperature, more energy is required to achieve that temperature and less solid product is recovered from the process (due of leaching and hydrolysis to aqueous fraction), hence, production of MFC at 120 °C using HMT would be the most energy-efficient, with an energy consumption of 69

kWh/kg MFC. Another possible reason for the high energy efficiency of microwave-heating is due to the low temperature of the reactor vessel in comparison to conventional-heating.[129] In a similar way, the higher energy efficiency of microwave over conventional-heating of meso-scale (1-3 L) organic reactions at low-temperatures (<200 °C) has also been previously reported in the literature.[130,132] However, due to the limited scale of the studied systems, the

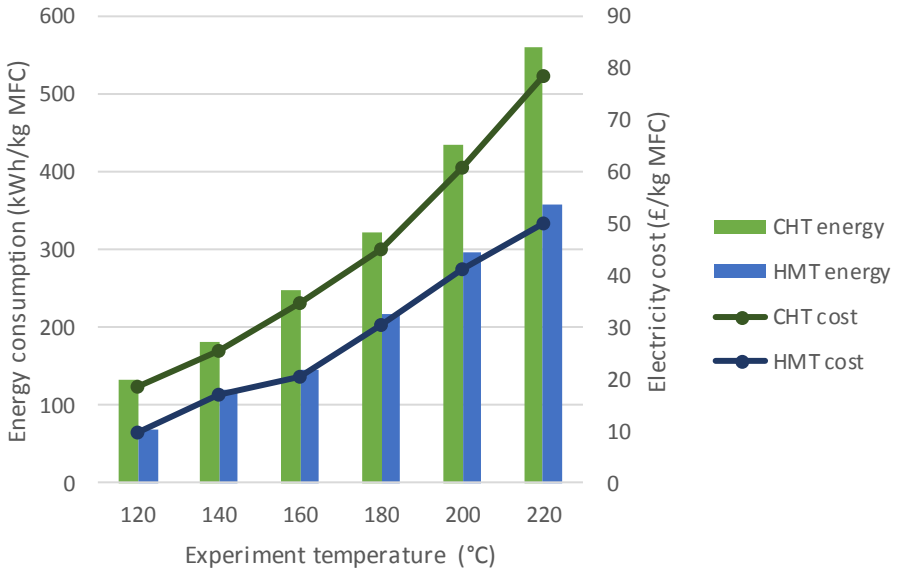

Figure 3.39: Energy consumption and electricity cost for running HMT or CHT experiments at lab-scale (1 L and 0.25 L, respective) at different temperatures. Original in colour.

energy consumption values presented in **Figure 3.39** is still very high (hundreds of times higher) compared to industrial- or pilot-scale MFC production reported elsewhere.[99,243,312] Therefore, these values are not representative of or comparative to an industrial-scale MFC manufacturing.

Since the electricity cost is directly proportional to the energy consumption, the same trend was observed (**Figure 3.39**), meaning that HMT electricity cost (£10–50/kg MFC) was *ca.* 50–40% cheaper than for CHT (£19–79/kg MFC). Again, the costs here reported are not representative of a "real-world" manufacturing, since

even the lowest electricity cost calculated from HMT at 120 °C (*ca.* £10/kg MFC) is still 100–5 times higher than those values found for MFC production at pilot-scale using conventional technologies and processing methodologies (£0.1–2/kg MFC).[99,243] Nevertheless, these figures give an idea of the economic impact of the process technology and temperature for MFC production, which can be used as guidelines for future scalability studies.

3.3.1 E-factor analysis

E-factors from both processes (HMT and CHT) were calculated from the total amount (g) of waste generated in the process divided by the yield of product (g), in this case MFC, of each experiment. The amounts of MFC, solvent waste and hydrolysate generated in each experiment is summarised in **Table 3.6**. Here, hydrolysate (aqueous fraction) was not considered as waste, because it can be valorised for the production of chemicals and materials.

Table 3.6: MFC yields and waste volumes of the hydrothermal experiments.

Process	MFC yield (g)	Solvent waste (g)	Hydrolysate (g)
HMT-120	5.8	945	711
HMT-140	4.0		
HMT-160	3.8		
HMT-180	3.0		
HMT-200	2.5		
HMT-220	2.3		
CHT-120	1.4	292	377
CHT-140	1.2		
CHT-160	1.1		
CHT-180	0.9		
CHT-200	0.8		
CHT-220	0.7		

Table 3.7 summarises MFC yield and E-factor of both hydrothermal systems. E-factor (*environmental factor*) is a simple metric which gives a quantitative indication of the impact of the waste in a process mass balance. The closer to zero an E-factor is, lesser waste is generated and greener the process will be.[308] Overall, E-factor of HMT was 20–2% lower than that of CHT. This must be due to the higher yield of solid product (MFC) from HMT in comparison to CHT, once, even if the reactor volumes where different for each system (1 L for HMT and 250 mL for CHT), the same solid-to-liquid ratio and washing steps were applied in both systems. For both cases E-factor rapidly increases with temperature, due to the gradual decrease of MFC yield. Regarding processing temperature, at 220 °C, the process can become as much as 2.5-times more wasteful than running an experiment at 120 °C. Hence, HMT at 120 °C would be most preferable conditions to produce MFC by means of hydrothermal processing, due to its lower cost, higher energy efficiency and higher greenness. It is important to note that E-factor values are highly influenced by product volumes, *i.e.* the higher the product tonnage/scale of production, the lower the E-factor for that process will be due to process intensification.[308]

Table 3.7: MFC yields and E-factor of the studied hydrothermal experiments. In this case, the aqueous fractions (hydrolysates) is not considered as waste as it can be recycled for pectin, lignin and sugars recovery.

Process	MFC yield (%)	E-factor ($g_{waste}/g_{product}$)
HMT-120	69	163
HMT-140	48	237
HMT-160	45	250
HMT-180	36	317
HMT-200	30	380
HMT-220	27	414
CHT-120	48	204
CHT-140	39	254
CHT-160	38	260
CHT-180	29	335
CHT-200	26	371
CHT-220	23	425

3.1.4 Green star analysis

Since neither E-factor or energy assessment gives an indication of the health and environmental hazards of a chemical process or product, an additional metric covering this matter was necessary to complete the greenness assessment of the process studied in this thesis. *Green star* is a greenness metric initially developed for the dissemination of green chemistry education, which can be easily applied to assess and compare the greenness of chemical syntheses and processes.[307,308] The assessment of a green star gives insights of the aspects of a process/reaction where sustainability, safety and greenness can be improved.[307,313]

The green star is represented by a radar-type chart (found in Excel®), where each tip of the "star" correspond to one of the seven principles of green chemistry[128] (see **Figure 1.14**) selected for analysis (P1, P3, P5, P6, P7, P10 and P12). A score is then given for each star tip depending on the fulfilment of the corresponding principle. The score is based on the Globally Harmonized System of

Classification and Labelling of Chemicals (GHS), and varies from 1 (lowest fulfilment/greenness) to 3 (highest fulfilment/greenness). For the full list of criteria, please see Ribeiro *et al.* (2010).[307] For the purpose of comparison, besides the HMT process scenario used in this thesis, three other scenarios were imagined (a conventional MFC processing using TEMPO oxidation and/or bleached wood pulp), HMT without acetone washes and HMT using only water washes). Green star index (GSI; %) of each process scenario was calculated as the sum of the total green star score of each scenario divided by the maximum score value (21) and finally multiplied by 100.

Figure 3.40 shows the green star charts (based on seven of the green chemistry principles) of four different MFC manufacturing scenarios, where scenario A is the base-case (the studied process of this thesis, *i.e.* HMT including solvent wash work-up) and other three are possible imaginary scenarios. The overall fulfilment of the principles for each green star is represented by the *green star index* (GSI). Generally, all scenarios present some considerable greenness (GSI varying from 48–90%), however, the conventional scenario for MFC production (B), based on the use of bleached wood pulp as starting material and TEMPO oxidation as pre-treatment before disintegration of fibres to MFC, presented the lowest overall greenness (GSI = 48%) in comparison to the three HMT scenarios. The conventional production of MFC fails to comply with several of the selected principles, hence the minimum score is given for P1 (waste prevention), P3 (less hazardous chemical processing), P5 (use of auxiliary substances/solvents), P6 (energy efficiency), and P12 (design of safer process for accident prevention). In comparison to the scenario B, the base-case scenario A presented improved

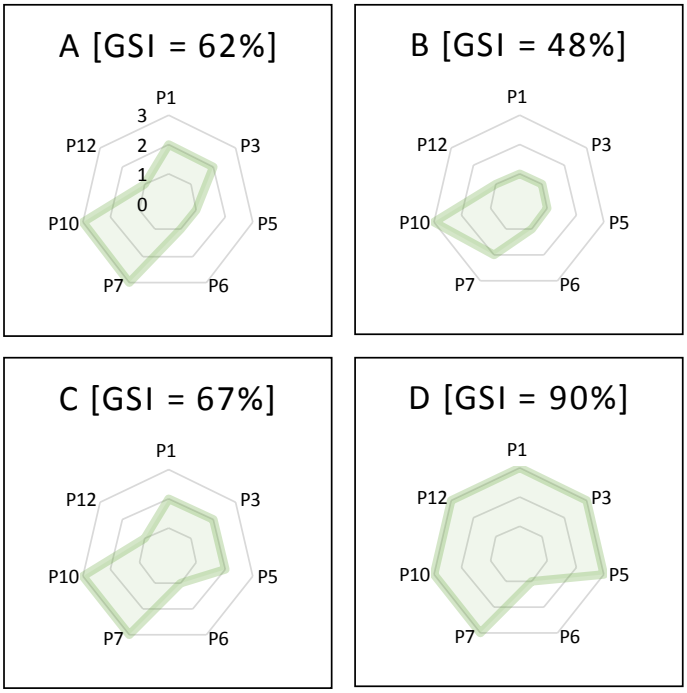

Figure 3.40: Green star charts for base-case HMT scenario (A), conventional scenario (B), acetone-free HMT scenario (C) and water-only HMT scenario (D), each with their respective GSI. Original in colour.

greenness (GSI = 62%), especially regarding principles P1, P3 and P7 (use of renewable resources). That is mainly because while the conventional manufacturing of MFC depends on the use of bleach pulp (which has passed through several chemical treatments) and catalysts like TEMPO, which present some health hazards (caustic and toxic) and is not renewable,[88,312] the HMT process is 100% renewable and additive-free, only based on water and orange peel, an innocuous feedstock. Although scenario A presented improved greenness over scenario B, its overall greenness can be further improved by reducing the amount of solvent washes during the work-up of MFC (scenario C: HMT without acetone wash) or remove it altogether (scenario D: water washes only, no ethanol or acetone washes). By removing acetone from the work-up, P5 score improved, rising the process GSI in 5% (from 62% in A to 67% in C). That is mainly because acetone is more toxic than ethanol, presenting four GHS

hazards codes (H225, H319, H336, H373).[f] However, as ethanol is not completely innocuous (presents two GHS codes: H225, H319), when its use is also removed from the work-up, the HMT process greenness greatly improves (GSI of 90% for scenario D) to an almost complete fulfilment of the green chemistry principles selected. In fact, this scenario (water-only) can be easily applied in the process by washing the solid fraction yield after HMT with hot water, which might remove most of soluble sugars and other substances from the final product, MFC. In all scenarios, the only principle which remained with the lowest score was P6, which regards to the energy efficiency of the process. That is because the maximum score criteria of that principle required conducting the reaction at room temperature and atmospheric pressure,[307] which makes senses in synthesis but it is hard to be fulfilled when treating biomass.

[f] More information on GHS hazards codes can be found in: https://en.wikipedia.org/wiki/GHS_hazard_statements

Chapter 4

4 CONCLUSIONS

4.1 Regarding the Obtained Results

As presented in the introduction (Chapter 1), few prior works have been undertaken on the design of scalable, microwave-based approaches for the valorisation of orange peel waste.[49,126,127] However, these studies neither considered a fully-integrated ("zero-waste") process nor were done with in-depth research. In this work, a new approach based on *acid-free* hydrothermal microwave treatment was designed, with focus on the valorisation of the orange peel cellulosic residue. This valorisation approach resulted in the production of MFC, a state-of-the-art nanomaterial, besides other valuable biomolecules extracted from the hydrolysate (pectin, lignin, sugars and other small molecules). MFC, in particular, was successfully characterised as a nanostructure material with outstanding physicochemical properties, such as hydrogel formation at low concentrations. MFC hydrogels presented competitive performance against conventional rheology modifiers for food and cosmetic applications, as well as the ability to form strong flexible films, which can find applications in cutting-edge areas, such as regenerative medicine or flexible electronics. Residual pectin remaining in DOPR was concomitantly extracted with MFC (but from the hydrolysate) up to 160 °C. According to its NMR and TGA characterisation, it presented some degradation of the "hairy" regions (arabinans) above 140 °C, however, this did not affect its gel formation. Lignin microparticles were successfully isolated from the hydrolysates generated from high-temperature HMT experiments (180–220 °C), where several characterisation techniques confirmed their lignin-like composition and core-shell structure. These lignin particles can be applied, for instance, as dispersion stabilisers (Pickering particles), antioxidants, or in composite formulations.[297,314] Sugars were the most

abundant fraction of soluble molecules identified in the hydrolysates with important economic value as bioresource, since by means of synthesis or biotechnology they can be converted into several platform molecules, bio-based polymers, biofuels and biomaterials.[34,39,42]

In summary, the hydrothermal microwave treatment applied to the production of MFC was comparably more energy-efficient than using conventional-heating. But since current commercial scale of microwave reactors are not optimised for energy efficiency and scalability,[130] the energy consumption values found were much higher than it would be in an industrial-scale. Also, microwave-heating presented lower E-factor values than conventional-heating treatment, meaning, less environmental impact of generated waste per mass of product (MFC). The overall greenness of the HMT process was found to be higher than that of a conventional process used in MFC manufacturing, however it could be further improved by removing the solvent wash steps, which are the main source of human and environment hazards derived from the HMT process.

In contrast to previous works on this matter,[49,126,127] this thesis expands the acid-free hydrothermal microwave treatment of orange peel waste by including the valorisation of the overlooked cellulosic residue produced after pectin extraction. This novel approach offers a more sustainable, scalable and fully-integrated orange peel biorefinery model, where all by-products are transformed into valuable materials and biomolecules. This *zero-waste* biorefinery model is also in line with the concept of circular-bioeconomy to its fullness, due to increased circularity of the bio-based resources and products within the economy and the reduction of waste generation. Another important aspect of this biorefinery

model is its *feedstock-insensitivity*, meaning that it can be applied to other lignocellulosic biomass besides orange/citrus peel. This study has also greatly contributed to the nanocellulose research field by presenting a greener and cleaner alternative methodology for MFC production, which currently is driven by expensive and not-as-green approaches.[1,99,312]

4.2 Limitations and Future Work

Although this work was carried out thoroughly, a few limitations were identified with the purpose to direct and motivate future work.

4.2.1 Regarding MFC characterisation and application

Although a proximate composition analysis of the DOPR and MFC samples was carried out (**Table 3.1**), this was based on mixture of indirect data from instrumental techniques such as TGA, ICP-OES and CHN, which can give a good approximation of the molecular composition of the material but not as accurate as it would be using conventional wet chemistry techniques. Therefore, in future work, proximate composition and analysis should also be carried out by recommended methodologies, such as the proximate detergent method[249] and other consecutive biomass fractionation methods.[315–317] That should also give clearer separation of biomolecules like pectin and hemicellulose, which cannot be easily differentiated by TGA for instance.

The assessment of the SEM images of the MFC was slightly affected by the cellulose fibrils hornification caused mainly by air or oven drying of the sample prior imaging. Hornification causes the aggregation of the fibrils, which complicates the dimension measurements of individuals and can alter the original porous structure of the material. Therefore, for better assessment and

accuracy of SEM images, freeze-drying the sample, instead of over or air-drying, prior to its imaging is recommended. As shown in (**Appendix V**), the structure of MFC is better preserved when lyophilised. The concentration of the suspension should also be kept to a minimum (0.05–0.2%) to avoid overlapping and aggregation of the fibrils during drying. While TEM is the best available technique to identify and classify a nanocellulose material as CNF, MFC or CNC,[174,217] other complementary techniques such as (ultra)centrifugation[81–83], mechanical fractionation[84] and foam filtration[85] should also be explored for the fractionation of mixed nanocellulose materials (*eg.* separation of CNF from MFC).

The porous structure of MFC (surface area, pore volume and pore area) analysed by means of N_2 physisorption porosimetry presented some limitations due to the sample preparation, *i.e*, the sample had to be dried before the analysis, which most probably led to hornification, hence the results were not precise. Hence, an alternative porosimetry method, such as thermoporosimetry (DSC), radiation scattering and Congo red dye adsorption, that do not require the prior drying of the sample should be considered in the future.[237,240,243]

Due to equipment and time limitations, other important characterisation analyses of MFC, such as surface charge and mechanical properties, were not investigated in this work, but it is highly recommended for future work, since these are important properties regarding MFC performance in many applications, such as dispersions and emulsions stabilizer, composites, packaging, electronics, etc.[77,258]

Regarding MFC hydrogels, additional work can be done on its rheological characterisation, including flow curves (determines the viscosity of the sample at

varied shear rates), temperature sweep and structure recovery test (to determine the rate and extent of viscosity recovery of the sample after shear).[266] Moreover, other application tests should be carried out to test MFC performance in a "real" product. For example, initial food and cosmetic formulation tests and antimicrobial activity tests for medical applications.[318,319]

Although physicochemical analysis and application tests of the MFC films were beyond the scope of this thesis, the study of its oxygen and other gases barrier properties, water retention capacity, porosimetry, mechanical properties, antimicrobial activity, packaging and biomedical applications (*i.e.* the potential use of MFC as scaffold for wound dressings) should be explored.

4.2.2 Regarding hydrolysate valorisation

Several valuable products initially identified and extracted from the hydrolysate in this work can be further characterised and explored for potential applications. For instance, the GPC analysis of the pectin will add valuable information regarding the implications of the process temperature (or other parameters) in its molecular weight, while further testing its gel properties and performance can give some indication of its potential use in food formulations. Further important characterisation of lignin microparticles includes GPC, DLS (for particle size), DSC (thermostability), antioxidant and antimicrobial activity tests. Also, exploring the performance of lignin microparticles as stabilizer in emulsions and dispersions, as well as its use in composite formulations (as functional filler, antimicrobial/antioxidant/hydrophobic agent) is recommended. Lastly, new research opportunities could be explored by an in-depth analysis of the sugars and small molecules present in the hydrolysate by LC-MS and GC-MS, as well as

the potential of using the extracted sugars in biotechnology for the production of platform molecules or biofuels (*eg.* bioethanol).

4.2.3 Regarding the HMT process

Despite the approach presented in this thesis greatly improving and extending the technical, environmental and economic aspects of previously studied microwave-based orange peel biorefinery models, there is still room for improvement.

Starting with the pre-treatment of the feedstock, at lab scale, the biomass should not be dried (specially oven-dried) prior to any treatment to avoid hornification of the fibres. Also, particle size should be kept to a minimum (ideally <1 mm) for better diffusion and extraction of the biomolecules during the microwave treatment.

Regarding treatment of the feedstock, before the HMT, the extraction of the essential oil (or d-limonene) by microwave-assisted distillation[56] is recommended, unless the feedstock is coming from an industrial plant which has already extracted the essential oil as part of their process. That will mimic the process used in industry but using a cleaner technology (microwave) and should also reduce the amount of degradation products originating from the presence of oil residues during the subsequent hydrothermal microwave treatment of orange peel. The separation of the oil will also add value to the process and its full characterisation will greatly contribute to the advance of citrus waste valorisation research. Another step which may be incorporated in the biorefinery model is the extraction of pigments from orange peel (*eg.* carotenoids). That could be done by solvent extraction (Soxhlet or microwave-assisted), however, as the use of

solvents like ethanol and acetone has a great impact in the total greenness of the process (as seen in **Section 3.1.4**), an organic solvent-free extraction could be carried out by means of supercritical CO_2 for instance, which is a green scalable technology able to extract less polar compound from biomass feedstocks.[111,320] An integrated pectin and MFC extraction at 120 °C should be carried out in one step instead of two (as done in this thesis). That should be a better approach regarding scalability of the process and energy efficiency. In a batch system, increasing residence time of the sludge in the microwave reactor or/and performing cyclic re-extractions with new solvent should maximize pectin and sugars extraction while keeping the cellulosic residue "cleaner". The extraction temperature of 120 °C is recommend because it: allows the reaction to reach hydrothermal conditions (autohydrolysis), which might not be achieved at lower temperatures, while reducing formation of degradation products (such as *pseudo*-lignin); gives the best yields for MFC and pectin making the process more profitable; keeps pectin structure intact with high DE and excellent gel formation and produces an MFC with most suitable properties for posterior applications (light colour, high WHC, excellent hydrogel formation with promising rheology behaviour and ability to form semi-transparent, flexible films).

Regarding the work-up steps for the products isolation (washing and drying), for MFC, considering that oil, pigments, pectin, sugars and other soluble molecules has been extracted from the cellulosic matrix, instead of using solvent washes (which is a major environmental drawback of the process), a better and greener approach would be repeatedly wash the solid cellulosic residue with hot water until complete wash of all solubles or using a more reproducible and robust method, such as membrane ultrafiltration system (also known as tangential flow

filtration or cross-flow filtration)[41,321], which is a promising green scalable technology suitable for aqueous systems.[120] Finally, for a better performance of MFC into dispersions and other formulations, the hornification of the cellulose fibres should be avoided. For that, instead of air- or oven-drying the material after its isolation and purification, a better drying method would be lyophilisation (freeze-drying), which should reduce hornification effects, maintain the porous structure of the material as good as prior drying and improve its dispersibility in water or other liquids. For the hydrolysate work-up, cross-flow filtration should be able to successfully separate high-Mw retentate (pectin) from low-Mw solubles (sugars, oligomers and other small molecules) and freeze-drying would also be recommended as drying method. Following these guidelines, a more integrated, greener and efficient biorefinery model for the orange peel waste valorisation can be designed (**Figure 4.1**).

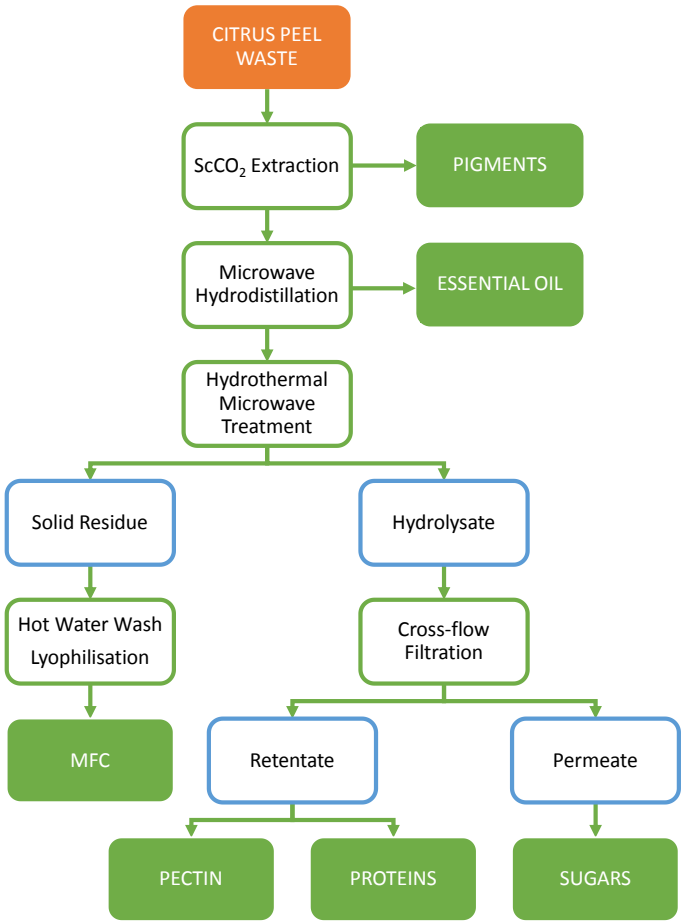

Figure 4.1: Proposed model for a *zero-waste* orange peel biorefinery generating five high-value products. Original in colour.

4.3 Final Remarks

In a broader context, while food waste is still considered an environmental burden in many countries, due to the lack of incentive from the government body to support research and technology advancements towards food waste/agroindustrial biomass valorisation for chemicals and materials, as well as the lack of technology & knowledge transfer and unviable operational costs, microwave technology applied to the valorisation of food waste biomass can bring innumerable benefits for the local economy, environment and scientific development. Investing in a local microwave-based biorefinery for processing food waste biomass can drastically reduce operational and logistical costs while promoting income for food producers and local community, especially in

developing nations like Brazil, in which the economy is highly dependent on agriculture. Furthermore, by using an acid-free, water-based process to produce a high-tech product such as MFC makes the process very competitive and cost-effective. This approach complies with several of the Sustainable Development Goals by helping reduce poverty & inequality, creating new job opportunities, promoting the sustainable use of resources & responsible innovation, reducing environment & climate impact and promoting circular bioeconomy.

REFERENCES

1 Q. Li, S. McGinnis, C. Sydnor, A. Wong and S. Renneckar, *ACS Sustain. Chem. Eng.*, 2013, **1**, 919–928.

2 United Nations, in *Climate Change 2013 - The Physical Science Basis*, ed. Intergovernmental Panel on Climate Change, Cambridge University Press, Cambridge, 2015, pp. 1–30.

3 OECD, Material Resources, Productivity and the Environment, https://goo.gl/tRhD3z, (accessed 4 April 2018).

4 H. Corvellec, New directions for management and organization studies on waste, https://bit.ly/2H7WHnO, (accessed 9 November 2018).

5 Plastic Oceans Foundation, The facts, https://bit.ly/2pLpExi, (accessed 17 January 2018).

6 FAO and OECD, OECD-FAO Agricultural Outlook 2015, https://bit.ly/2BUyJsE, (accessed 9 November 2018).

7 U.S. Energy Information Administration, International Energy Outlook 2017, www.eia.gov/ieo, (accessed 9 January 2018).

8 J. B. Binder and R. T. Raines, *J. Am. Chem. Soc.*, 2009, **131**, 1979–1985.

9 Our World in Data (University of Oxford), How long before we run out of fossil fuels? - Our World in Data, https://bit.ly/2H5pDN3, (accessed 12 January 2018).

10 BP, BP Statistical Review of World Energy 2016, https://on.bp.com/2VwB3O1, (accessed 12 January 2018).

11 United Nations, Adoption of the Paris Agreement, https://bit.ly/1YbayHO, (accessed 9 November 2018).

12 C. McGlade and P. Ekins, *Nature*, 2015, **517**, 187–190.

13 Carbon Tracker, Unburnable Carbon 2013: Wasted capital and stranded assets, https://bit.ly/2deTQMB, (accessed 12 January 2018).

14 IPCC, Special Report on Global Warming of 1.5 °C, https://bit.ly/2pA6aKo, (accessed 17 October 2018).

15 CICERO, Carbon budget for dummies, https://bit.ly/2tFld7P, (accessed 12 January 2018).

16 A. S. Matharu, E. M. de Melo and J. A. Houghton, *Bioresour. Technol.*, 2016, **215**, 123–130.

17 S. Liu, *Biotechnol. Adv.*, 2010, **28**, 563–582.

18 United Nations, Transforming Our World: The 2030 Agenda for Sustainable Development, sustainabledevelopment.un.org, (accessed 9 November 2018).

19 FAO, Food wastage footprint. Impacts on natural resources - Summary Report, https://bit.ly/1kMi2QN, (accessed 9 November 2018).

20 FAO, IFAD, UNICEF, WFP and WHO, The State of Food Security and Nutrition in the World 2017, https://bit.ly/2jubGOu, (accessed 12 March 2018).

21 D. J. Garcia and F. You, *Comput. Chem. Eng.*, 2016, **91**, 49–67.

22 FAO, Global initiative on food loss and food waste reduction, http://www.fao.org/save-food/en/, (accessed 22 March 2018).

23 M. Bond, T. Meacham, R. Bhunnoo and T. G. Benton, Food waste within global food systems, www.foodsecurity.ac.uk, (accessed 9 November 2018).

24 E. Vandamme, T. Anthonis and S. Dobbelaere, Industrial Biomass: Source of Chemicals, Materials, and Energy!

25 A. S. Matharu, E. M. de Melo and J. A. Houghton, in *Routledge Handbook of the Resource Nexus*, eds. R. Bleischwitz, H. Hoff, C. Spataru, E. van der Voet and S. D. VanDeveer, Routledge, 2017, pp. 457–467.

26 B. Bilska, M. Wrzosek, D. Kołożyn-Krajewska and K. Krajewski, *Waste Manag.*, 2016, **52**, 269–277.

27 J. Hargreaves, I. Pulford, M. Balakrishnan and V. Batra, *Conversion of Large Scale Wastes into Value-added Products*, CRC Press, 2013.

28 M. Z. Jacobson, *J. Geophys. Res. Atmos.*, 2014, **119**, 8980–9002.

29 C. O. Tuck, E. Pérez, I. T. Horváth, R. a Sheldon and M. Poliakoff, *Science*, 2012, **337**, 695–9.

30 E. Scott, F. Peter and J. Sanders, *Appl. Microbiol. Biotechnol.*, 2007, **75**, 751–762.

31 M. Carus and L. Dammer, The " Circular Bioeconomy " – Concepts,

Opportunities and Limitations, www.bio-based.eu/nova-papers, (accessed 15 November 2018).

32 MIT, The dirty secret of biomass waste, https://bit.ly/2Tm8zc1, (accessed 9 November 2018).

33 Q. Xu, L.-L. Chen, X. Ruan, D. Chen, A. Zhu, C. Chen, D. Bertrand, W.-B. Jiao, B.-H. Hao, M. P. Lyon, J. Chen, S. Gao, F. Xing, H. Lan, J.-W. Chang, X. Ge, Y. Lei, Q. Hu, Y. Miao, L. Wang, S. Xiao, M. K. Biswas, W. Zeng, F. Guo, H. Cao, X. Yang, X.-W. Xu, Y.-J. Cheng, J. Xu, J.-H. Liu, O. J. Luo, Z. Tang, W.-W. Guo, H. Kuang, H.-Y. Zhang, M. L. Roose, N. Nagarajan, X.-X. Deng and Y. Ruan, *Nat. Genet.*, 2013, **45**, 59–66.

34 P. Putnik, D. Bursać Kovačević, A. Režek Jambrak, F. Barba, G. Cravotto, A. Binello, J. Lorenzo and A. Shpigelman, *Molecules*, 2017, **22**, 680–703.

35 FAO, Citrus Fruit Fresh and Processed Statistical Bulletin 2016, https://bit.ly/2tGIpSS, (accessed 9 November 2018).

36 FAO, FAO Statistics, http://faostat.fao.org, (accessed 9 November 2018).

37 C. Chen, *Pigments in fruits and vegetables: Genomics and dietetics*, Springer, Lake Alfred, USA, 2015.

38 U. Ringblom, *The Orange Book*, Tetra Pak Processing Systems, Lund, Sweden, 3rd edn., 2017.

39 D. Mamma and P. Christakopoulos, *Waste and Biomass Valorization*, 2014, **5**, 529–549.

40 I. John, K. Muthukumar and A. Arunagiri, *Int. J. Green Energy*, 2017, **14**, 599–612.

41 J. A. Houghton, PhD Thesis, University of York, 2017.

42 C. S. K. Lin, L. A. Pfaltzgraff, L. Herrero-Davila, E. B. Mubofu, S. Abderrahim, J. H. Clark, A. A. Koutinas, N. Kopsahelis, K. Stamatelatou, F. Dickson, S. Thankappan, Z. Mohamed, R. Brocklesby and R. Luque, *Energy Environ. Sci.*, 2013, **6**, 426–464.

43 J. Á. S. López, Q. Li and I. P. Thompson, *Crit. Rev. Biotechnol.*, 2010, **30**, 63–69.

44 V. Heuzé, G. Tran, P. Hassoun and F. Lebas, Feedpedia - Citrus pulp, fresh, https://www.feedipedia.org/node/679, (accessed 15 November 2018).

45 V. Negro, G. Mancini, B. Ruggeri and D. Fino, *Bioresour. Technol.*, 2016, **214**, 806–815.

46 R. Wikandari, H. Nguyen, R. Millati, C. Niklasson and M. J. Taherzadeh, *Biomed Res. Int.*, 2015, **2015**, 1–6.

47 C. M. Santos, J. Dweck, R. S. Viotto, A. H. Rosa and L. C. de Morais, *Bioresour. Technol.*, 2015, **196**, 469–479.

48 L. Aguiar, F. Márquez-Montesinos, A. Gonzalo, J. L. Sánchez and J. Arauzo, *J. Anal. Appl. Pyrolysis*, 2008, **83**, 124–130.

49 L. A. Pfaltzgraff, PhD Thesis, University of York, 2014.

50 Brazil, Política Nacional de Resíduos Sólidos, https://bit.ly/2J0A7MJ, (accessed 14 June 2018).

51 T. L. H. Treuer, J. J. Choi, D. H. Janzen, W. Hallwachs, D. Peréz-Aviles, A. P. Dobson, J. S. Powers, L. C. Shanks, L. K. Werden and D. S. Wilcove, *Restor. Ecol.*, 2018, **26**, 275–283.

52 A. S. Matharu, E. M. de Melo and J. A. Houghton, in *Waste biorefinery: potential and perspectives*, eds. T. Bhaskar, A. Pandey, S. V. Mohan, D. J. Lee and S. K. Khanal, Elsevier, 1st edn., 2018, pp. 219–233.

53 L. A. Pfaltzgraff, M. De bruyn, E. C. Cooper, V. Budarin and J. H. Clark, *Green Chem.*, 2013, **15**, 307–314.

54 F. R. Marín, C. Soler-Rivas, O. Benavente-García, J. Castillo and J. a. Pérez-Alvarez, *Food Chem.*, 2007, **100**, 736–741.

55 G. Dugo and A. Di Giacomo, *Citrus: The Genus Citrus*, Taylor & Francis Group, 1st edn., 2002.

56 J. Bustamante, S. van Stempvoort, M. García-Gallarreta, J. A. Houghton, H. K. Briers, V. L. Budarin, A. S. Matharu and J. H. Clark, *J. Clean. Prod.*, 2016, **137**, 598–605.

57 Intracen, Price information of conventional essential oils, https://bit.ly/2VsLwdg, (accessed 15 November 2018).

58 R. Ciriminna, N. Chavarría-Hernández, A. Inés Rodríguez Hernández and M. Pagliaro, *Biofuels, Bioprod. Biorefining*, 2015, **9**, 368–377.

59 J. Harholt, A. Suttangkakul and H. Vibe Scheller, *Plant Physiol.*, 2010, **153**, 384–395.

60 Global Info Research, Global Pectin Market by Manufacturers, Regions, Type and Application, Forecast to 2021, https://bit.ly/2VrN0nM, (accessed 15 November 2018).

61 R. Ciriminna, A. Fidalgo, R. Delisi, A. Tamburino, D. Carnaroglio, G. Cravotto, L. M. Ilharco and M. Pagliaro, *ACS Omega*, 2017, **2**, 7991–7995.

62 R. Ciriminna, A. Fidalgo, R. Delisi, I. M. Ilharco and M. Pagliaro, *Agro Food Ind. Hi Tech*, 2016, **27(5)**, 17–20.

63 B. H. Davison, J. Parks, M. F. Davis and B. S. Donohoe, in *Aqueous Pretreatment of Plant Biomass for Biological and Chemical Conversion to Fuels and Chemicals*, John Wiley & Sons, Ltd, Chichester, UK, 2013, pp. 23–38.

64 G. Costa and I. Plazanet, *Adv. Biol. Chem.*, 2016, **6**, 70–105.

65 M. A. C. M. Haniffa, Y. Ching, L. Abdullah, S. Poh and C. Chuah, *Polymers (Basel).*, 2016, **8**, 246.

66 E. F. Lessa, M. S. Gularte, E. S. Garcia and A. R. Fajardo, *Carbohydr. Polym.*, 2017, **157**, 660–668.

67 P. D. Pathak, S. A. Mandavgane and B. D. Kulkarni, *Rev. Chem. Eng.*, 2015, **31**, 361–381.

68 O. Pezoti, A. L. Cazetta, K. C. Bedin, L. S. Souza, R. P. Souza, S. R. Melo and V. C. Almeida, *Chem. Eng. J.*, 2016, **283**, 1305–1314.

69 USPTO, US20080193590, 2008.

70 USPTO, US 7094317 B2, 2006.

71 USPTO, US 2014/0356463 A1, 2014.

72 USPTO, WO2001017376A1, 2000.

73 USPTO, WO1994027451 A1, 1994.

74 Internet, Nanocellulose for tires: something new in performance and sustainability : Biofuels Digest, https://goo.gl/47VeNO, (accessed 9 March 2017).

75 M. Mariano and A. Dufresne, in *Nanocelluloses: Their Preparation, Properties, and Applications - ACS Symposium Series*, American Chemical Society, Washington, USA, 2017, pp. 203–225.

76 H. Kargarzadeh, M. Ioelovich, I. Ahmad, S. Thomas and A. Dufresne, in

Handbook of Nanocellulose and Cellulose Nanocomposites, Wiley-VCH Verlag GmbH & Co. KGaA, Weinheim, Germany, 2017, pp. 1–49.

77 D. Klemm, F. Kramer, S. Moritz, T. Lindström, M. Ankerfors, D. Gray and A. Dorris, *Angew. Chemie Int. Ed.*, 2011, **50**, 5438–5466.

78 W. Y. Hamad, *Cellulose Nanocrystals: Properties, production and applications*, John Wiley & Sons, Chichester, UK, 2017.

79 G. Chinga-Carrasco, *Nanoscale Res. Lett.*, 2011, **6**, 417.

80 N. Lavoine, I. Desloges, A. Dufresne and J. Bras, *Carbohydr. Polym.*, 2012, **90**, 735–764.

81 S. Alila, I. Besbes, M. R. Vilar, P. Mutjé and S. Boufi, *Ind. Crops Prod.*, 2013, **41**, 250–259.

82 R. Salminen, M. Reza, T. Pääkkönen, J. Peyre and E. Kontturi, *Cellulose*, 2017, **24**, 1657–1667.

83 H. Bian, L. Chen, R. Gleisner, H. Dai and J. Y. Zhu, *Green Chem.*, 2017, **19**, 3370–3379.

84 A. Tanaka, V. Seppanen, J. Houni, A. Sneck and P. Pirkonen, *Nord. Pulp Pap. Res. J.*, 2012, **27**, 689–694.

85 A. Tanaka, T. Hjelt, A. Sneck and A. Korpela, *Sep. Sci. Technol.*, 2012, **47**, 1771–1776.

86 A. Dufresne, *Philos. Trans. R. Soc. A Math. Phys. Eng. Sci.*, 2018, **376**, 20170040.

87 USPTO, US20150158955 A1, 2015.

88 S. H. Osong, S. Norgren and P. Engstrand, *Cellulose*, 2016, **23**, 93–123.

89 Internet, Nanocellulose State of the Industry, https://goo.gl/Tzz2WV, (accessed 14 November 2018).

90 USPTO, US9187865 B2, 2015.

91 Borregaard, Microfibrillated Cellulose at a glance, https://goo.gl/EJHTo9, (accessed 18 September 2017).

92 A. Dufresne, *Mater. Today*, 2013, **16**, 220–227.

93 Markets and Markets, Global Nanocellulose Market - Forecast until 2019,

https://bit.ly/2EBo6wr, (accessed 11 November 2018).

94 G. Ström, C. Öhgren and M. Ankerfors, Nanocellulose as an additive in foodstuff, https://bit.ly/2Vpl1oT, (accessed 15 November 2018).

95 C. Gómez H., A. Serpa, J. Velásquez-Cock, P. Gañán, C. Castro, L. Vélez and R. Zuluaga, *Food Hydrocoll.*, 2016, **57**, 178–186.

96 T. Abitbol, A. Rivkin, Y. Cao, Y. Nevo, E. Abraham, T. Ben-Shalom, S. Lapidot and O. Shoseyov, *Curr. Opin. Biotechnol.*, 2016, **39**, 76–88.

97 N. Lavoine and L. Bergström, *J. Mater. Chem. A*, 2017, **5**, 16105–16117.

98 H. M. C. Azeredo, M. F. Rosa and L. H. C. Mattoso, *Ind. Crops Prod.*, 2017, **97**, 664–671.

99 C. A. de Assis, C. Houtman, R. Phillips, E. M. T. Bilek, O. J. Rojas, L. Pal, M. S. Peresin, H. Jameel and R. Gonzalez, *Biofuels, Bioprod. Biorefining*, 2017, **11**, 682–700.

100 Internet, Nanocellulose prices, https://www.celluloselab.com/, (accessed 21 September 2017).

101 Y. Mälkki, *MOJ Food Process. Technol.*, 2017, **4**, 1–3.

102 K. Nelson, T. Retsina, M. Iakovlev, A. van Heiningen, Y. Deng, J. A. Shatkin and A. Mulyadi, in *Materials Research for Manufacturing - An Industrial Perspective of Turning Materials into New Products*, eds. L. D. Madsen and E. B. Svedberg, Springer, 2016, pp. 267–302.

103 Fraunhofer, Agri and food waste valorisation co-ops based on flexible multi-feedstocks biorefinery processing technologies for new high added value applications., https://bit.ly/2SwG8Ur, (accessed 14 December 2017).

104 M. Mariño, L. Lopes da Silva, N. Durán and L. Tasic, *Molecules*, 2015, **20**, 5908–5923.

105 A. García, A. Gandini, J. Labidi, N. Belgacem and J. Bras, *Ind. Crops Prod.*, 2016, **93**, 26–38.

106 M. Boukroufa, C. Boutekedjiret, L. Petigny, N. Rakotomanomana and F. Chemat, *Ultrason. Sonochem.*, 2014, **24**, 72–79.

107 A. M. Balu, V. Budarin, P. S. Shuttleworth, L. A. Pfaltzgraff, K. Waldron, R. Luque and J. H. Clark, *ChemSusChem*, 2012, **5**, 1694–1697.

108 J. Tsukamoto, N. Durán and L. Tasic, *J. Braz. Chem. Soc.*, 2013, **24**, 1537–

1543.

109 B. Satari, J. Palhed, K. Karimi, M. Lundin, M. J. Taherzadeh and A. Zamani, *BioResources*, 2017, **12**, 1706–1722.

110 J. S. Van Dyk, R. Gama, D. Morrison, S. Swart and B. I. Pletschke, *Renew. Sustain. Energy Rev.*, 2013, **26**, 521–531.

111 S. R. Shirsath, S. H. Sonawane and P. R. Gogate, *Chem. Eng. Process. Process Intensif.*, 2012, **53**, 10–23.

112 K. Kaderides, A. M. Goula and K. G. Adamopoulos, *Innov. Food Sci. Emerg. Technol.*, 2015, **31**, 204–215.

113 I. John, P. Yaragarla, P. Muthaiah, K. Ponnusamy and A. Appusamy, *Resour. Technol.*, 2017, **3**, 429–433.

114 USPTO, US9169523B2, 2015.

115 SAIREM, Industrial Microwave Systems & Components Manufacturing - SAIREM, https://www.sairem.com/, (accessed 22 June 2018).

116 AMT, Advanced Microwave Technologies, https://bit.ly/2NwnZFi, (accessed 22 June 2018).

117 IDCO, IDCO - Microwave Technology, http://www.idco-france.com/, (accessed 22 June 2018).

118 Y. Li, A.-S. Fabiano-Tixier, M. Abert-Vian and F. Chemat, in *Microwave-assisted Extraction for Bioactive Compounds: Theory and Practice*, eds. F. Chemat and G. Cravotto, Springer US, Boston, MA, 2013, pp. 103–125.

119 E. Destandau, T. Michel and C. Elfakir, in *Natural Product Extraction: Principles and Applications*, eds. M. A. Rostagno and J. M. Prado, The Royal Society of Chemistry, 2013, pp. 113–156.

120 N. Flórez, E. Conde and H. Domínguez, *J. Chem. Technol. Biotechnol.*, 2015, **90**, 590–607.

121 C. O. Kappe, *Angew. Chemie Int. Ed.*, 2004, **43**, 6250–6284.

122 C. O. Kappe, B. Pieber and D. Dallinger, *Angew. Chemie Int. Ed.*, 2013, **52**, 1088–1094.

123 S. Tsubaki and J.-I. Azum, in *Advances in Induction and Microwave Heating of Mineral and Organic Materials*, InTech, 2011, pp. 697–722.

124 D. J. Macquarrie, J. H. Clark and E. Fitzpatrick, *Biofuels, Bioprod. Biorefining*, 2012, **6**, 549–560.

125 J. González-Rivera, A. Spepi, C. Ferrari, C. Duce, I. Longo, D. Falconieri, A. Piras and M. R. Tinè, *Green Chem.*, 2016, **18**, 6482–6492.

126 USPTO, US 2015/0065698 A1, 2015.

127 A. Bagaria, MRes Thesis, University of York, 2014.

128 P. T. Anastas and J. C. Warner, *Green Chemistry: Theory and Practice*, Oxford University Press, Incorporated, 1998.

129 D. Kim, S. K. Seol and W. S. Chang, *Korean J. Chem. Eng.*, 2016, **33**, 527–531.

130 R. Luque, J. A. Menéndez, A. Arenillas and J. Cot, *Energy Environ. Sci.*, 2012, **5**, 5481–5488.

131 J. D. Moseley and C. O. Kappe, *Green Chem.*, 2011, **13**, 794–806.

132 J. D. Moseley and E. K. Woodman, *Energy & Fuels*, 2009, **23**, 5438–5447.

133 E. M. de Melo, J. H. Clark and A. S. Matharu, *Green Chem.*, 2017, **19**, 3408–3417.

134 M. J. Serapiglia, K. D. Cameron, A. J. Stipanovic and L. B. Smart, *BioEnergy Res.*, 2009, **2**, 1–9.

135 M. J. Serapiglia, K. D. Cameron, A. J. Stipanovic and L. B. Smart, *Appl. Biochem. Biotechnol.*, 2008, **145**, 3–11.

136 T.-Q. Yuan, F. Xu, J. He and R.-C. Sun, *Biotechnol. Adv.*, 2010, **28**, 583–593.

137 K. Werner, L. Pommer and M. Broström, *J. Anal. Appl. Pyrolysis*, 2014, **110**, 130–137.

138 H. Zhu, Z. Fang, C. Preston, Y. Li and L. Hu, *Energy Environ. Sci.*, 2014, **7**, 269–287.

139 A. Sluiter, B. Hames, R. Ruiz, C. Scarlata, J. Sluiter, D. Templeton and D. Crocker, *Lab. Anal. Proced.*, 2012, **1**, 1–15.

140 A. M. Magomya, D. Kubmarawa, J. A. Ndahi and G. G. Yebpella, *Int. J. Sci. Technol. Res.*, 2014, **3**, 68–72.

141 J. Zhang, Y. Hu and Y. Li, *Gel Chemistry*, Springer Singapore, Singapore, 2018, vol. 96.

142 S. R. Raghavan and B. H. Cipriano, in *Molecular Gels: Materials with Self-Assembled Fibrillar Networks*, Springer-Verlag, Berlin/Heidelberg, 2005, pp. 241–252.

143 S. Park, J. O. Baker, M. E. Himmel, P. A. Parilla and D. K. Johnson, *Biotechnol. Biofuels*, 2010, **3**, 3–10.

144 L. Segal, J. J. Creely, A. E. Martin and C. M. Conrad, *Text. Res. J.*, 1959, **29**, 786–794.

145 A. K. Pathan, J. Bond and R. E. Gaskin, *Mater. Today*, 2010, **12**, 32–43.

146 S. Lowell, J. E. Shields, M. A. Thomas and M. Thommes, *Characterization of Porous Solids and Powders: Surface Area, Pore Size and Density*, Springer Netherlands, Dordrecht, 2004, vol. 16.

147 N. F. Mat Zain, S. M. Yusop and I. Ahmad, *J. Nutr. Food Sci.*, 2014, **05**, 10–13.

148 R. Berggren, F. Berthold, E. Sjöholm and M. Lindström, *J. Appl. Polym. Sci.*, 2003, **88**, 1170–1179.

149 W. Wang and J.-H. Liu, *Gene*, 2015, **555**, 421–429.

150 H.-D. Belitz, W. Grosch and P. Schieberle, *Food Chemistry*, Springer Berlin Heidelberg, Berlin, Heidelberg, 2009, vol. 107.

151 G. E. Ravilious and J. M. Jez, *Nat. Prod. Rep.*, 2012, **29**, 1138.

152 K. E. M. Hendricks, R. S. Donahoo, P. D. Roberts and M. C. Christman, *Am. J. Plant Sci.*, 2013, **04**, 282–290.

153 E. Rodrigues, I. I. Rockenbach, C. Cataneo, L. V. Gonzaga, E. S. Chaves and R. Fett, *Ciência e Tecnol. Aliment.*, 2009, **29**, 642–645.

154 J. Sidana, V. Saini, S. Dahiya, P. Nain and S. Bala, *Int. J. Pharm. Sci. Rev. Res.*, 2013, **18**, 20–27.

155 Y.-M. Kim, H. W. Lee, S. Kim, C. Watanabe and Y.-K. Park, *BioEnergy Res.*, 2015, **8**, 431–439.

156 F. Hu, S. Jung and A. Ragauskas, *Bioresour. Technol.*, 2012, **117**, 7–12.

157 I. Aarum, H. Devle, D. Ekeberg, S. J. Horn and Y. Stenstrøm, *ACS Omega*, 2018, **3**, 4924–4931.

158 S. D. Shinde, X. Meng, R. Kumar and A. J. Ragauskas, *Green Chem.*, 2018,

20, 2192–2205.

159 K. Yao, Q. Wu, R. An, W. Meng, M. Ding, B. Li and Y. Yuan, *AIChE J.*, 2018, **64**, 1938–1953.

160 P. Sannigrahi, D. H. Kim, S. Jung and A. Ragauskas, *Energy Environ. Sci.*, 2011, **4**, 1306–1310.

161 F. Araya, E. Troncoso, R. T. Mendonça and J. Freer, *Biotechnol. Bioeng.*, 2015, **112**, 1783–1791.

162 L. Moghaddam, J. Rencoret, V. R. Maliger, D. W. Rackemann, M. D. Harrison, A. Gutiérrez, J. C. del Río and W. O. S. Doherty, *ACS Sustain. Chem. Eng.*, 2017, **5**, 4846–4855.

163 L. Zhou, V. Budarin, J. Fan, R. Sloan and D. Macquarrie, *ACS Sustain. Chem. Eng.*, 2017, **5**, 3768–3774.

164 G. van Erven, R. de Visser, D. W. H. Merkx, W. Strolenberg, P. de Gijsel, H. Gruppen and M. A. Kabel, *Anal. Chem.*, 2017, **89**, 10907–10916.

165 A. Duval and M. Lawoko, *React. Funct. Polym.*, 2014, **85**, 78–96.

166 M. Carrier, A. Loppinet-Serani, D. Denux, J.-M. Lasnier, F. Ham-Pichavant, F. Cansell and C. Aymonier, *Biomass and Bioenergy*, 2011, **35**, 298–307.

167 Y. Luo, J. Fan, V. L. Budarin, C. Hu and J. H. Clark, *Green Chem.*, , DOI:10.1039/C7GC02300F.

168 S. Sabiha-Hanim and A. Aziatul-Akma, in *Polymer Science: Research Advances, Practical Applications and Educational Aspects*, eds. A. Méndez-Vilas and A. Solano-Martín, Formatex Research Center, Spain, 2016, pp. 404–411.

169 S. Hiasa, S. Iwamoto, T. Endo and Y. Edashige, *Ind. Crops Prod.*, 2014, **62**, 280–285.

170 A. T. Quitain, T. Kai, M. Sasaki and M. Goto, *Ind. Eng. Chem. Res.*, 2013, **52**, 7940–7946.

171 T. Röder and H. Sixta, *Lenzinger Berichte*, 2004, **83**, 79–83.

172 L.-S. Johansson, T. Tammelin, J. M. Campbell, H. Setälä and M. Österberg, *Soft Matter*, 2011, **7**, 10917.

173 M. V. Zimmermann, C. Borsoi, A. Lavoratti, M. Zanini, A. J. Zattera and R. M. Santana, *J. Reinf. Plast. Compos.*, 2016, **35**, 628–643.

174 M. Kaushik, C. Fraschini, G. Chauve, J.-L. Putaux and A. Moores, in *The Transmission Electron Microscope - Theory and Applications*, InTech, 2015.

175 K. Karimi and M. J. Taherzadeh, *Bioresour. Technol.*, 2016, **200**, 1008–1018.

176 A. S. Matharu, E. M. de Melo, J. Remón, S. Wang, A. Abdulina and E. Kontturi, *ChemSusChem*, 2018, **11**, 1344–1353.

177 J. Fan, M. De bruyn, V. L. Budarin, M. J. Gronnow, P. S. Shuttleworth, S. Breeden, D. J. Macquarrie and J. H. Clark, *J. Am. Chem. Soc.*, 2013, **135**, 11728–11731.

178 M. C. Jarvis, *Philos. Trans. R. Soc. A Math. Phys. Eng. Sci.*, 2018, **376**, 20170045.

179 I. Usov, G. Nyström, J. Adamcik, S. Handschin, C. Schütz, A. Fall, L. Bergström and R. Mezzenga, *Nat. Commun.*, 2015, **6**, 7564.

180 F. Navarro, PhD Thesis, Virginia Polytechnic Institute and State University, 2010.

181 R. H. Atalla, R. S. Atalla and U. P. Agarwal, in *Nanocelluloses: Their Preparation, Properties, and Applications - ACS Symposium Series*, American Chemical Society, Washington, USA, 2017, vol. 23, pp. 1–18.

182 F. W. Herrick, R. L. Caseiber, J. K. Hamilton and K. R. Sandberg, *J. Appl. Polym. Sci. Appl. Polym. Symp.*, 1983, **37**, 797–813.

183 D. J. Cosgrove, *Nat. Rev. Mol. Cell Biol.*, 2005, **6**, 850–861.

184 M. McCann, B. Wells and K. Roberts, *J. Cell Sci.*, 1990, **96**, 323–334.

185 N. Billinton and A. W. Knight, *Anal. Biochem.*, 2001, **291**, 175–197.

186 J. A. Olmstead, J. H. Zhu and D. G. Gray, *Can. J. Chem.*, 1995, **73**, 1955–1959.

187 P. Singh and A. Pandey, *Biotechnology for Agro-Industrial Residues Utilisation*, 2009.

188 S. Singh, G. Cheng, N. Sathitsuksanoh, D. Wu, P. Varanasi, A. George, V. Balan, X. Gao, R. Kumar, B. E. Dale, C. E. Wyman and B. A. Simmons, *Front. Energy Res.*, 2015, **2**, 1–12.

189 T. A. Chimenez, M. H. Gehlen, K. Marabezi and A. A. S. Curvelo, *Cellulose*, 2014, **21**, 653–664.

190 L. Donaldson and A. Vaidya, *Sci. Rep.*, 2017, **7**, 1–14.

191 V. C. Coletta, C. A. Rezende, F. R. da Conceição, I. Polikarpov and F. E. G. Guimarães, *Biotechnol. Biofuels*, 2013, **6**, 1–10.

192 H. Wondraczek, A. Kotiaho, P. Fardim and T. Heinze, *Carbohydr. Polym.*, 2011, **83**, 1048–1061.

193 S. Singh, B. A. Simmons and K. P. Vogel, *Biotechnol. Bioeng.*, 2009, **104**, 68–75.

194 J. Zhuang, X. Wang, J. Xu, Z. Wang and M. Qin, *Wood Sci. Technol.*, 2017, **51**, 165–174.

195 F. Hu, PhD Thesis, Georgia Institute of Technology, 2014.

196 J. A. Olmstead and D. G. Gray, *J. Photochem. Photobiol. A Chem.*, 1993, **73**, 59–65.

197 Y. Wang, *Plant Omics*, 2012, **5**, 508–513.

198 C. Sene, M. C. McCann, R. H. Wilson and R. Grinter, *Plant Physiol.*, 1994, **106**, 1623–1631.

199 M.-J. Chen, X.-Q. Zhang, A. Matharu, E. Melo, R.-M. Li, C.-F. Liu and Q.-S. Shi, *ACS Sustain. Chem. Eng.*, 2017, **5**, 7278–7283.

200 F. Lionetto, R. Del Sole, D. Cannoletta, G. Vasapollo and A. Maffezzoli, *Materials (Basel).*, 2012, **5**, 1910–1922.

201 J. A. Perez-Pimienta, M. G. Lopez-Ortega, J. A. Chavez-Carvayar, P. Varanasi, V. Stavila, G. Cheng, S. Singh and B. A. Simmons, *Biomass and Bioenergy*, 2015, **75**, 180–188.

202 J. A. Perez-Pimienta, H. M. Poggi-Varaldo, T. Ponce-Noyola, A. C. Ramos-Valdivia, J. A. Chavez-Carvayar, V. Stavila and B. A. Simmons, *Biomass and Bioenergy*, 2016, **91**, 48–55.

203 O. N. Friday and M. M. Muhammad, *J. Appl. Sci. Environ. Manag.*, 2015, **19**, 787–792.

204 Y. Pu, B. Hallac and A. J. Ragauskas, in *Aqueous Pretreatment of Plant Biomass for Biological and Chemical Conversion to Fuels and Chemicals*, John Wiley & Sons, Ltd, Chichester, UK, 2013, pp. 369–390.

205 Z. A. Popper, T. J. Bootten, P. J. Harris, L. D. Melton and R. H. Newman, *The Plant Cell Wall*, Humana Press, Totowa, NJ, 2011, vol. 715.

206 R. M. S. Ratnayake, I. M. Sims, R. H. Newman and L. D. Melton, *J. Agric.*

Food Chem., 2011, **59**, 7186–7193.

207 W. Chen, Q. Li, J. Cao, Y. Liu, J. Li, J. Zhang, S. Luo and H. Yu, *Carbohydr. Polym.*, 2015, **117**, 950–956.

208 H. Halonen, PhD Thesis, Royal Institute of Technology, 2012.

209 M. Bardet, M. F. Foray, J. Bourguignon and P. Krajewski, *Magn. Reson. Chem.*, 2001, **39**, 733–738.

210 M. Dick-Perez, T. Wang, A. Salazar, O. A. Zabotina and M. Hong, *Magn. Reson. Chem.*, 2012, **50**, 539–550.

211 H. Tang, P. S. Belton, A. Ng and P. Ryden, *J. Agric. Food Chem.*, 1999, **47**, 510–517.

212 G. D. Love, C. E. Snape and M. C. Jarvis, *Phytochemistry*, 1998, **49**, 1191–1194.

213 O. D. Bernardinelli, M. A. Lima, C. A. Rezende, I. Polikarpov and E. R. DeAzevedo, *Biotechnol. Biofuels*, 2015, **8**, 110.

214 S. Xiao, R. Gao, Y. Lu, J. Li and Q. Sun, *Carbohydr. Polym.*, 2015, **119**, 202–209.

215 X. Ouyang, W. Wang, Q. Yuan, S. Li, Q. Zhang and P. Zhao, *RSC Adv.*, 2015, **5**, 61650–61656.

216 M. Hajir, R. Graf and W. Tremel, *Chem. Commun.*, 2014, **50**, 6534–6536.

217 C. S. Davis, R. J. Moon, S. Ireland, L. Johnston, J. A. Shatkin, K. Nelson, E. J. Foster, A. M. Forster, M. T. Postek, A. Vladar and J. W. Gilman, in *2014 TAPPI International Conference on Nanotechnology for Renewable Materials Report*, National Institute of Standards and Technology, Gaithersburg, MD, 2015, pp. 1–42.

218 Kathryn Lawson-Wood and Ian Robertson, Decomposition of Calcium Oxalate Monohydrate using a Hyphenated TG-IR system, https://bit.ly/2BWtpFh, (accessed 16 September 2017).

219 M. Brebu and C. Vasile, *Cellul. Chem. Technol.*, 2010, **44**, 353–363.

220 R. Sánchez Orozco, P. Balderas Hernández, G. Roa Morales, F. Ureña Núñez, J. Orozco Villafuerte, V. Lugo Lugo, N. Flores Ramírez, C. E. Barrera Díaz and P. Cajero Vázquez, *BioResources*, 2014, **9**, 1873–1885.

221 A. Potthast, S. Radosta, B. Saake, S. Lebioda, T. Heinze, U. Henniges, A.

Isogai, A. Koschella, P. Kosma, T. Rosenau, S. Schiehser, H. Sixta, M. Strlič, G. Strobin, W. Vorwerg and H. Wetzel, *Cellulose*, 2015, **22**, 1591–1613.

222 J. Oberlerchner, T. Rosenau and A. Potthast, *Molecules*, 2015, **20**, 10313–10341.

223 B. B. Hallac and A. J. Ragauskas, *Biofuels, Bioprod. Biorefining*, 2011, **5**, 215–225.

224 V. L. Budarin, J. H. Clark, B. A. Lanigan, P. Shuttleworth and D. J. Macquarrie, *Bioresour. Technol.*, 2010, **101**, 3776–3779.

225 M. Lorenz, S. Sattler, M. Reza, A. Bismarck and E. Kontturi, *Faraday Discuss.*, 2017, **202**, 315–330.

226 Y. Habibi, *Chem. Soc. Rev.*, 2014, **43**, 1519–1542.

227 I. Siró and D. Plackett, *Cellulose*, 2010, **17**, 459–494.

228 A. B. Fall, A. Burman and L. Wågberg, *Spec. Issue Nanocellulose - Nord. Pulp Pap. Res. J.*, 2014, **29**, 176–184.

229 O. Ibraheem and B. K. Ndimba, *Int. J. Biol. Sci.*, 2013, **9**, 598–612.

230 M. Dashtban, A. Gilbert and P. Fatehi, *J. Sci. Technol. For. Prod. Process.*, 2012, **2**, 44–53.

231 Y. Zhao, H. Lin and S. Wang, *Energy Sci. Eng.*, 2017, **5**, 208–216.

232 A. Shafeeq, A. Muhammad, S. Sarfaraz, Z. Akram, H. M. U. Saeed and U. Farooq, *Int. J. Chem. Eng. Appl.*, 2015, **6**, 381–384.

233 J. Nemoto, T. Saito and A. Isogai, *ACS Appl. Mater. Interfaces*, 2015, **7**, 19809–19815.

234 K. Kekäläinen, PhD Thesis, University of Oulu, 2016.

235 H. Chen, in *Biotechnology of Lignocellulose: Theory and Practice*, 2014, pp. 1–511.

236 S. Viamajala, B. S. Donohoe, S. R. Decker, T. B. Vinzant, M. J. Selig, M. E. Himmel and M. P. Tucker, in *Sustainable Biotechnology: Sources of Renewable Energy*, Springer Netherlands, 2010, pp. 1–18.

237 A. Julbe and J. D. F. Ramsay, in *Membrane Science and Technology*, Elsevier, 1996, vol. 4, pp. 67–118.

238 D. Topgaard and O. Söderman, in *Magnetic Resonance in Colloid and Interface Science*, Springer Netherlands, Dordrecht, 2002, pp. 631–635.

239 R. G. Munro, Porosity and Specific Surface Area Measurements for Solid Materials, http://www.ncbi.nlm.nih.gov/pubmed/22544181, (accessed 31 January 2018).

240 L. M. Anovitz and D. R. Cole, *Rev. Mineral. Geochemistry*, 2015, **80**, 61–164.

241 Z. Lu, Z. Su, S. Song, Y. Zhao, S. Ma and M. Zhang, *Cellulose*, 2018, **25**, 619–629.

242 S. F. Santos, G. H. D. Tonoli, J. E. B. Mejia, J. Fiorelli and H. Savastano Jr, *Mater. Construcción*, 2015, **65**, e041.

243 K. L. Spence, R. A. Venditti, O. J. Rojas, Y. Habibi and J. J. Pawlak, *Cellulose*, 2011, **18**, 1097–1111.

244 A. Borisova, M. De Bruyn, V. L. Budarin, P. S. Shuttleworth, J. R. Dodson, M. L. Segatto and J. H. Clark, *Macromol. Rapid Commun.*, 2015, **36**, 774–779.

245 N. Mahfoudhi and S. Boufi, *Cellulose*, 2017, **24**, 1171–1197.

246 S. S. Cho and M. L. Dreher, *Handbook of dietary fiber*, Taylor & Francis, New York, NY, 2001, vol. 113.

247 R. G. M. van der Sman, E. Paudel, A. Voda and S. Khalloufi, *Food Res. Int.*, 2013, **54**, 804–811.

248 Y. Qin, X. Qiu and J. Y. Zhu, *Sci. Rep.*, 2016, **6**, 1–12.

249 P. J. Van Soest, in *Nutritional Ecology of the Ruminant*, Cornell University Press, 2nd., 1994, pp. 140–155.

250 N. Lin, J. Huang and A. Dufresne, *Nanoscale*, 2012, **4**, 3274–3294.

251 R. J. Moon, A. Martini, J. Nairn, J. Simonsen and J. Youngblood, *Chem. Soc. Rev.*, 2011, **40**, 3941.

252 M. Bulota, B. Maasdam and S. Tiekstra, Breakthrough technologies, https://bit.ly/2NxDsF5, (accessed 21 September 2018).

253 K. J. De France, T. Hoare and E. D. Cranston, *Chem. Mater.*, 2017, **29**, 4609–4631.

254 H. Dong, J. F. Snyder, D. T. Tran and J. L. Leadore, *Carbohydr. Polym.*, 2013, **95**, 760–767.

255 K. Abe and H. Yano, *Carbohydr. Polym.*, 2011, **85**, 733–737.

256 M. Chau, S. E. Sriskandha, H. Thérien-Aubin and E. Kumacheva, in *Supramolecular Polymer Networks and Gels*, ed. S. Seiffert, Springer International Publishing, 2015, vol. 268, pp. 167–208.

257 P. Li and R. Liu, in *Supramolecular Polymer Networks and Gels*, ed. S. Seiffert, Springer International Publishing, 2015, vol. 268, pp. 209–251.

258 C. Salas, T. Nypelö, C. Rodriguez-Abreu, C. Carrillo and O. J. Rojas, *Curr. Opin. Colloid Interface Sci.*, 2014, **19**, 383–396.

259 Borregaard, Exilva Solvent Compatibility, https://goo.gl/7Tv5JL, (accessed 6 November 2018).

260 S. Banerjee and S. Bhattacharya, *Crit. Rev. Food Sci. Nutr.*, 2012, **52**, 334–346.

261 J. Douglas, *Gels*, 2018, **4**, 1–14.

262 S. Holland, C. Tuck and T. Foster, *Food Biophys.*, 2018, **13**, 175–185.

263 Malvern Instruments, Understanding Yield Stress, https://bit.ly/2BVNyvc, (accessed 14 November 2018).

264 A. Carlsson, PhD Thesis, Uppsala University, 2014.

265 B. O. Okesola and D. K. Smith, *Chem. Soc. Rev.*, 2016, **45**, 4226–4251.

266 T. G. Mezger, *The Rheology Handbook,* Vincentz Network, 4th edn., 2014.

267 N. Willenbacher and K. Georgieva, in *Product Design and Engineering*, eds. U. Bröckel, W. Meier and G. Wagner, Wiley-VCH Verlag GmbH & Co. KGaA, Weinheim, Germany, 2013, pp. 7–49.

268 Anton Paar, Amplitude sweeps, https://bit.ly/2IIEbEH, (accessed 24 September 2018).

269 D. R. Picout and S. B. Ross-Murphy, *Sci. World J.*, 2003, **3**, 105–121.

270 S. B. Ross-Murphy and K. P. Shatwell, *Biorheology*, 1993, **30**, 217–227.

271 H. Sehaqui, Q. Zhou, O. Ikkala and L. A. Berglund, *Biomacromolecules*, 2011, **12**, 3638–3644.

272 E. Rojo, M. S. Peresin, W. W. Sampson, I. C. Hoeger, J. Vartiainen, J. Laine and O. J. Rojas, *Green Chem.*, 2015, **17**, 1853–1866.

273 G. Chinga-Carrasco, *Micron*, 2013, **48**, 42–48.

274 V. A. Barbash, O. V Yaschenko, S. V Alushkin, A. S. Kondratyuk, O. Y. Posudievsky and V. G. Koshechko, *Nanoscale Res. Lett.*, 2016, **11**, 410.

275 A. Ferrer, L. Pal and M. Hubbe, *Ind. Crops Prod.*, 2017, **95**, 574–582.

276 M. Park, D. Lee, S. Shin, H.-J. Kim and J. Hyun, *Carbohydr. Polym.*, 2016, **140**, 43–50.

277 T. Hakkarainen, R. Koivuniemi, M. Kosonen, C. Escobedo-Lucea, A. Sanz-Garcia, J. Vuola, J. Valtonen, P. Tammela, A. Mäkitie, K. Luukko, M. Yliperttula and H. Kavola, *J. Control. Release*, 2016, **244**, 292–301.

278 S. Fan, P. Zhang, F. Li, S. Jin, S. Wang and S. Zhou, *Curr. Org. Chem.*, 2016, **20**, 2799–2809.

279 A. S. Matharu, J. A. Houghton, C. Lucas-Torres and A. Moreno, *Green Chem.*, 2016, **337**, 695–699.

280 S. S. Hosseini, F. Khodaiyan and M. S. Yarmand, *Carbohydr. Polym.*, 2016, **140**, 59–65.

281 Z. Košťálová, Z. Hromádková, A. Ebringerová, M. Polovka, T. E. Michaelsen and B. S. Paulsen, *Ind. Crops Prod.*, 2013, **41**, 127–133.

282 P. Phyo, T. Wang, C. Xiao, C. T. Anderson and M. Hong, *Biomacromolecules*, 2017, **18**, 2937–2950.

283 C. M. G. C. Renard, M.-J. Crépeau and J.-F. Thibault, *Carbohydr. Res.*, 1995, **275**, 155–165.

284 T. J. Foster, S. Ablett, M. C. McCann and M. J. Gidley, *Biopolymers*, 1996, **39**, 51–66.

285 F. Peng, J.-L. Ren, F. Xu, J. Bian, P. Peng and R.-C. Sun, *J. Agric. Food Chem.*, 2009, **57**, 6305–6317.

286 C. M. G. C. Renard, R. M. Weightman and J. F. Thibault, *Int. J. Biol. Macromol.*, 1997, **21**, 155–162.

287 F. H. Larsen, I. Byg, I. Damager, J. Diaz, S. B. Engelsen and P. Ulvskov, *Biomacromolecules*, 2011, **12**, 1844–1850.

288 N. Babbar, W. Dejonghe, M. Gatti, S. Sforza and K. Elst, *Crit. Rev. Biotechnol.*, 2015, **8551**, 1–13.

289 L. Leclere, P. Van Cutsem and C. Michiels, *Front. Pharmacol.*, 2013, **4**, 128.

290 W. Zhao, B. Simmons, S. Singh, A. Ragauskas and G. Cheng, *Green Chem.*, 2016, **18**, 5693–5700.

291 X. Zhao, F. Qi and D. Liu, in *Nanotechnology for Bioenergy and Biofuel Production, Green Chemistry and Sustainable Technology*, eds. M. Rai and S. S. da Silva, Springer International Publishing, 2017, pp. 117–151.

292 C. Rezende, M. de Lima, P. Maziero, E. DeAzevedo, W. Garcia and I. Polikarpov, *Biotechnol. Biofuels*, 2011, **4**, 54.

293 F. S. Panthapulakkal, PhD Thesis, University of Toronto, 2014.

294 S. Tütüncü Konyar, N. Öztürk and F. Dane, *Bot. Stud.*, 2014, **55**, 1–9.

295 W. P. Hartl, H. Klapper, B. Barbier, H. J. Ensikat, R. Dronskowski, P. Müller, G. Ostendorp, A. Tye, R. Bauer and W. Barthlott, *Can. J. Bot.*, 2007, **85**, 501–517.

296 Y. Zeng, S. Zhao, H. Wei, M. P. Tucker, M. E. Himmel, N. S. Mosier, R. Meilan and S.-Y. Ding, *Biotechnol. Biofuels*, 2015, **8**, 1–12.

297 M. Ago, B. L. Tardy, L. Wang, J. Guo, A. Khakalo and O. J. Rojas, *MRS Bull.*, 2017, **42**, 371–378.

298 B. S. Donohoe, S. R. Decker, M. P. Tucker, M. E. Himmel and T. B. Vinzant, *Biotechnol. Bioeng.*, 2008, **101**, 913–925.

299 I. Prabasari, F. Pettolino, M.-L. Liao and A. Bacic, *Carbohydr. Polym.*, 2011, **84**, 484–494.

300 A. Wikiera, M. Mika, A. Starzyńska-Janiszewska and B. Stodolak, *Food Chem.*, 2015, **172**, 675–680.

301 T. H. Emaga, N. Rabetafika, C. S. Blecker and M. Paquot, *Biotechnol. Agron. Soc. Environ.*, 2012, **16**, 139–147.

302 V. A. Bampidis and P. H. Robinson, *Anim. Feed Sci. Technol.*, 2006, **128**, 175–217.

303 M. Martínez, R. Yáñez, J. L. Alonsó and J. C. Parajó, *Ind. Eng. Chem. Res.*, 2010, **49**, 8470–8476.

304 Z. Zhu, R. Simister, S. Bird, S. J McQueen-Mason, L. D Gomez and D. J Macquarrie, *AIMS Bioeng.*, 2015, **2**, 449–468.

305 V. Reginatto and R. V. Antônio, *Brazilian J. Microbiol.*, 2015, **46**, 323–335.

306 H. Höfte and A. Voxeur, *Curr. Biol.*, 2017, **27**, R865–R870.

307 M. G. T. C. Ribeiro, D. A. Costa and A. A. S. C. Machado, *Green Chem. Lett. Rev.*, 2010, **3**, 149–159.

308 M. Tobiszewski, M. Marć, A. Gałuszka and J. Namieśnik, *Molecules*, 2015, **20**, 10928–10946.

309 T. Razzaq and C. O. Kappe, *ChemSusChem*, 2008, **1**, 123–132.

310 M. Ankerfors, PhD Thesis, KTH Royal Institute of Technology, 2012.

311 UK Power, Gas & electricity prices per kWh, https://www.ukpower.co.uk/home_energy/tariffs-per-unit-kwh, (accessed 30 July 2018).

312 R. Arvidsson, D. Nguyen and M. Svanström, *Environ. Sci. Technol.*, 2015, **49**, 6881–6890.

313 M. G. T. C. Ribeiro, S. F. Yunes and A. A. S. C. Machado, *J. Chem. Educ.*, 2014, **91**, 1901–1908.

314 S. Beisl, A. Miltner and A. Friedl, *Int. J. Mol. Sci.*, 2017, **18**, 1244.

315 D. Brindha, S. Vinodhini, K. Alarmelumangai and N. S. Malathy, *Indian J. Fundam. Appl. Life Sci.*, 2012, **2**, 217–221.

316 G. Aravantinos-Zafiris, V. Oreopoulou, C. Tzia and C. D. Thomopoulos, *LWT - Food Sci. Technol.*, 1994, **27**, 468–471.

317 D. Xavier, F. Emmanuel, G. Philippe and M. Eric, *Cellul. Chem. Technol.*, 2012, **46**, 541–550.

318 N. Lin and A. Dufresne, *Eur. Polym. J.*, 2014, **59**, 302–325.

319 Borregaard, Microfibbrilated Cellulose and Rheology Modification: Characteristics and Application Examples, https://goo.gl/GrFHSS, (accessed 6 November 2018).

320 J. Mart Nez, L. Paulo Sales Silva, by A. Mauricio Rostagno and J. M. Prado, in *Natural Product Extraction: Principles and Applications*, 2013.

321 A. Saxena, B. P. Tripathi, M. Kumar and V. K. Shahi, *Adv. Colloid Interface Sci.*, 2009, **145**, 1–22.

APPENDICES

Appendix I

CHN analysis of DOPR and MFCs. Original in colour.

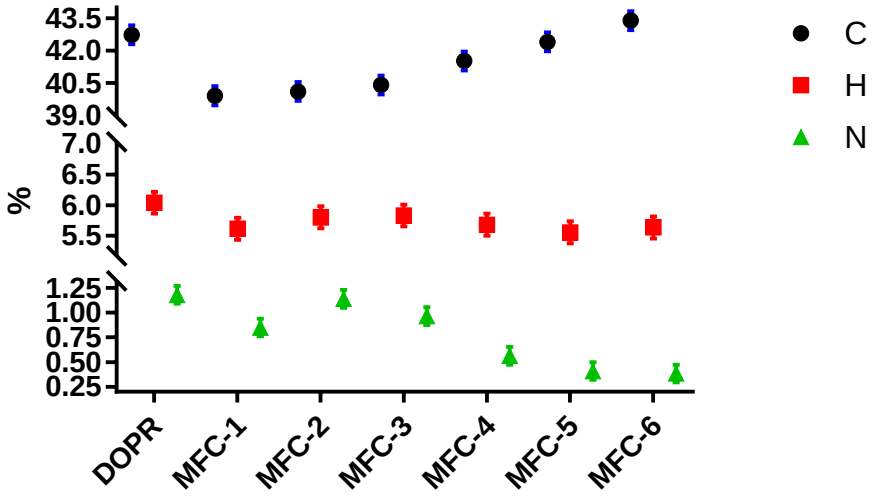

Appendix II

ATR-FTIR spectra of MFC-5 ash (top) and $CaCO_3$ (bottom). Original in colour.

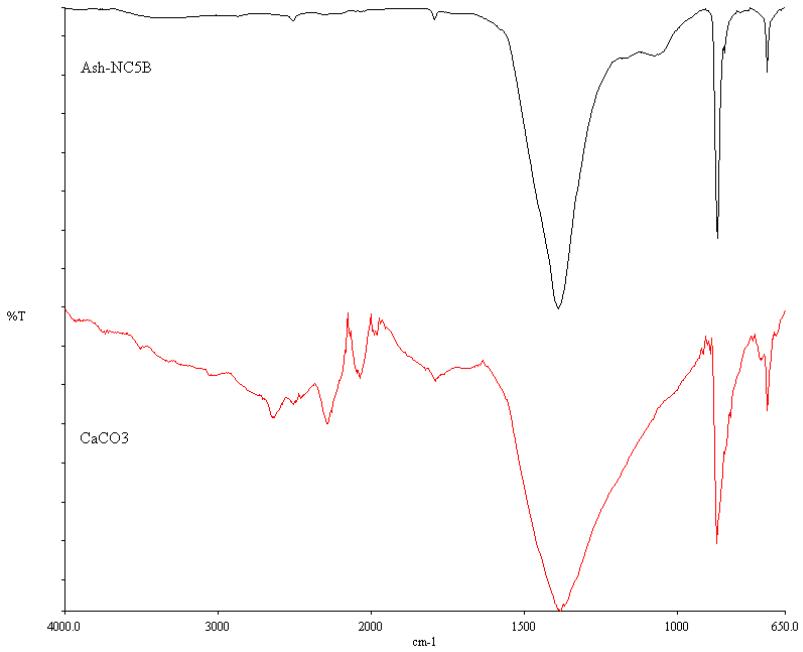

Appendix III

MFC suspensions at 3% concentration before homogenisation (at r.t.). Original in colour.

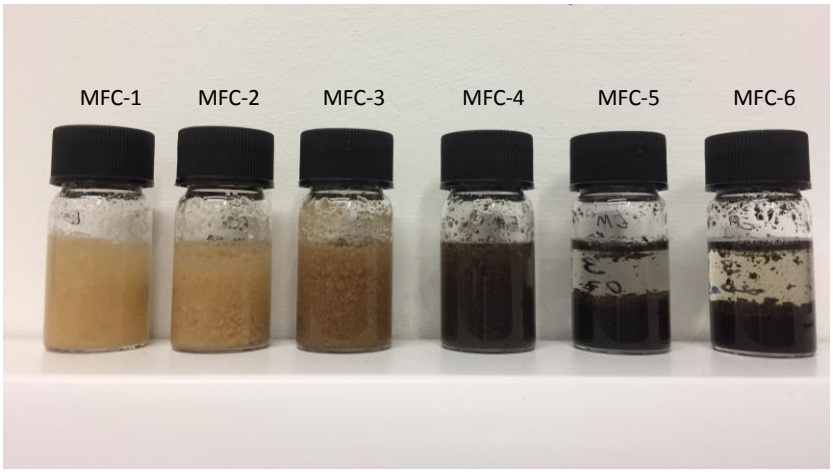

Appendix IV

Inversion test for the selected hydrogel precursors at 3% concentration (at r.t.).

Original in colour.

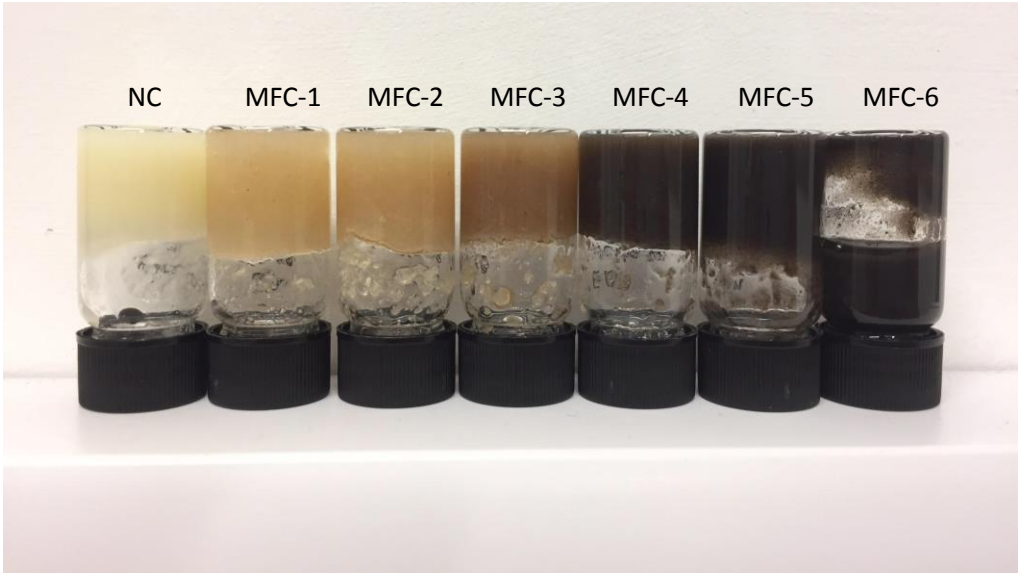

Appendix V

Inversion test for MFC-1 where CGC was found to be 2% (at r.t.). Original in colour.

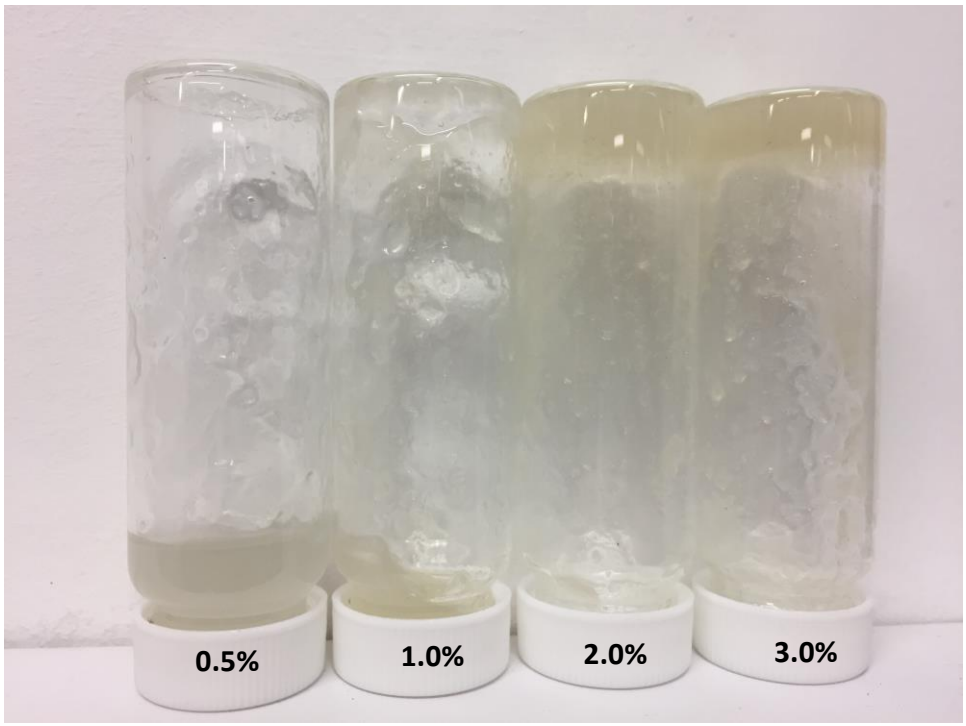

ABBREVIATIONS

ALM — Amidated low-methoxyl (pectin)

ATR-FTIR— Attenuated Total Reflection Fourier-transform Infrared Spectroscopy

BDC — Biorenewables Development Centre (University of York)

BET — Brunauer–Emmett–Teller model for surface area measurements

BJH — Barrett–Joyner–Halenda model for pore structure measurements

CGC — Critical gelator concentration (minimum concentration of a gelator to form a gel)

CHN — Carbon, hydrogen and nitrogen analysis

CHT — Conventional hydrothermal treatment

CI — Crystallinity Index

CICERO — Centre for International Climate Research

CLSM — Confocal Laser Scattering Microscopy

CNC — Cellulose Nanocrystals

CNF — Cellulose Nanofibrils

DE — Degree of Esterification

DM — Dry matter

DOPR — Depectinated Orange Peel Residue

DTG — Derivative Thermogravimetric (curves)

EIA — U.S. Energy Information Administration

EU — European Union

FAO — Food and Agriculture Organization

FSC— Food Supply Chain

GDP — Gross Domestic Product

GHS — Globally Harmonized System of Classification and Labelling of Chemicals

GPC — Gel Permeation Chromatography

GSI — Green Star Index

HM — High-methoxyl (pectin)

HMT — Hydrothermal Microwave Treatment

HPLC — High-performance Liquid Chromatography

ICP—OES — Inductively Coupled Plasma Atomic Emission Spectroscopy

IPCC — International Panel on Climate Change

LM — Low-methoxyl (pectin)

LVE — Linear Viscoelastic region

MFC — Microfibrillated Cellulose

OPEC — Orange Peel Exploitation Company

OPW — Orange peel Waste

Py-GC/MS — Pyrolysis Gas Chromatography coupled with Mass Spectroscopy

PS — Pore size

PV — Pore volume

r.t. — room temperature

SDG — Sustainable Development Goals

SEC — Size Exclusion Chromatography

SSA— Specific Surface Area

(SS)NMR — (Solid State) Nuclear Magnetic Resonance

Td — Temperature of maximum mass loss rate (TGA)

TEMPO — 2,2,6,6-Tetramethylpiperidine-1-oxyl radical

TGA — Thermogravimetric Analysis

UN — United Nations

UFSCW — Unavoidable Food Supply Chain Waste